THESIS FOR THE DEGREE OF DOCTOR OF PHILOSOPHY

Optimizing Enzyme Immobilization in Mesoporous Silica

- A Spectroscopic Study of the Dynamics and Spatial Distribution of the Confined Enzymes

PEGAH S. NABAVI ZADEH

CHALMERS

Department of Chemistry and Chemical Engineering

CHALMERS UNIVERSITY OF TECHNOLOGY

Gothenburg, Sweden 2018

Optimizing Enzyme Immobilization in Mesoporous Silica

- A Spectroscopic Study of the Dynamics and Spatial Distribution of the Confined Enzymes

PEGAH S. NABAVI ZADEH

ISBN: 978-91-7597-718-8

Doktorsavhandlingar vid Chalmers tekniska högskola

Ny serie nr: 4399

ISSN: 0346-718X

Department of Chemistry and Chemical Engineering

Chalmers University of Technology

SE-412 96 Gothenburg

Sweden

Telephone + 46 (0)31-772 1000

Cover:

Front: A graphical illustration of six types of proteins immobilized in two different mesoporous silica particles;

To the left: a schematic illustration of mesostructured cellular foams (MCF) with non-uniform particle size and spherical pore morphology, a TEM image of an immobilized enzyme (black dots indication of enzymes) in MCF.

To the right: a schematic illustration of Santa Barbara amorphous (SBA-15) with uniform particle size and hexagonally structured pores, a TEM image of an immobilized enzyme (black dots indication of enzymes) in SBA-15.

Back: Photograph by Adrian Sanati

Printed by Chalmers Reproservice
Gothenburg, Sweden 2018

"And now here is my secret, a very simple secret: It is only with the heart that one can see rightly; what is essential is invisible to the eye." The fox said to the little prince.

-The Little Prince by Antoine de Saint-Exupéry.

To

My parents

&

those who have the courage to see with their hearts, follow their dreams

and make the world a better place.

Optimizing Enzyme Immobilization in Mesoporous Silica

- A Spectroscopic Study of the Dynamics and Spatial Distribution of the Confined Enzymes

Pegah S. Nabavi Zadeh

Department of Chemistry and Chemical Engineering

Chalmers University of Technology

Abstract

Enzymes as biological catalysts are immobilized in porous materials to improve the enzyme activity and simplify their purification from the reaction media in biocatalytic applications. Mesoporous silica (MPS) particles are used as a promising support material for the immobilization of enzymes. The focus of this thesis is placed on the dynamics and distribution of enzymes in confining environments, to gain further understanding of the immobilization mechanism. The work is mainly based on various spectroscopy techniques using enzyme-attached fluorescent probes.

To elucidate the mechanistic steps of the immobilization process, high time resolutions methods are essential. In this thesis, a fluorescence spectroscopy assay is developed to monitor the translational dynamics of the enzymes in real time while immobilization occurs. It is shown that the size of enzyme for a given pore size can strongly affect the kinetics of enzyme immobilization. The rotational dynamics of the confined enzymes is studied using fluorescence anisotropy and it is shown that the rotation of the enzymes is slower inside the pores compared to the enzymes in free solution. In order to investigate if protein-protein or protein-wall hydrodynamic interactions have an impact on retarding the dynamics of the confined enzymes, the microenvironment inside the MPS particles needs to be studied. In this thesis, the microviscosity inside the MPS particles is measured using enzyme-attached carbocyanine dyes. The results show that the effective microviscosity is about ten times higher inside the MPS particles than in bulk water. The increase is stronger with smaller pores and higher enzyme concentration, and it is concluded that protein-wall hydrodynamic interactions probably have a more significant effect in retarding the confined enzymes.

The distribution of two co-immobilized enzymes in a cascade reaction which converts carbon dioxide (CO_2) to formaldehyde (CH_2O) is studied. The effect of the distance between the enzymes on the catalytic efficiency is investigated using Förster resonance energy transfer spectroscopy. The results demonstrate that the two immobilized enzymes are in close enough proximity resulting in substrate channeling between the active sites and four times more efficient conversion of CO_2 to CH_2O. Finally the location of the immobilized enzymes is visualized using transmission electron microscopy and immunogold staining. Two types of MPS particles are used with different pore morphology, spherical and hexagonal. The results show that not only the size of the pores in the MPS particles is an important factor, but the morphology of the pores also plays a crucial role in optimizing the enzyme immobilization.

Keywords: Enzyme immobilization, mesoporous silica, fluorescence spectroscopy, anisotropy, real-time monitoring, dynamics, microviscosity, Förster resonance energy transfer, Transmission electron microscopy, Immunogold staining, Cy3, Cy5.

List of Publications

This thesis is based on the work presented in the following papers:

I. **A Fluorescence Spectroscopy Assay for Real-Time Monitoring of Enzyme Immobilization into Mesoporous Silica Particles**

Pegah S. Nabavi Zadeh, Kassam Abdel Mallak, Nils Carlsson, Björn Åkerman*

Analytical Biochemistry, ***2015,*** *476, 51–58*

II. **Immobilization of Enzymes in Mesoporous Silica Particles: Protein Concentration and Rotational Mobility in the Pores**

Pegah S. Nabavi Zadeh, Björn Åkerman*

Journal of Physical Chemistry B, ***2017****, 121, 2575-2583*

III. **Measuring Viscosity inside Mesoporous Silica Using Protein-Bound Molecular Rotor Probe**

Pegah S. Nabavi Zadeh*, Milene Zezzi do Valle Gomes, Maria Abrahamsson, Anders E.C. Palmqvist, Björn Åkerman

*Submitted to Physical Chemistry Chemical Physics journal, RSC, 14-Feb-****2018***

IV. **Förster resonance energy transfer study of the improved biocatalytic conversion of CO2 to formaldehyde by co-immobilization of enzymes in siliceous mesostructured cellular foams**

Pegah S. Nabavi Zadeh#*, Milene Zezzi do Valle Gomes#, Björn Åkerman, Anders E.C. Palmqvist

*Submitted to ACS Catalysis journal, 16-Feb-****2018,*** *under revision.*

#: Equally contributed as first authors

V. **The spatial distribution of enzyme immobilized in mesoporous silica of SBA-15 and MCF-types visualized by TEM and immunogold staining.**

Pegah S. Nabavi Zadeh*, Milene Zezzi do Valle Gomes, Anders E.C. Palmqvist,

Björn Åkerman,

Manuscript, January ***2018***

Contribution Report

Details of my personal scientific contribution to each of the papers in the thesis:

I. Performed the spectroscopic experimental work with GOX, analyzed the data and wrote the paper.
Synthesis and characterization of mesoporous silica were done by Hanna Gustafsson.

II. Designed the study and performed all the experimental work, analyzed the data and wrote the paper.
Synthesis and characterization of mesoporous silica were done by Hanna Gustafsson.

III. Designed the study and performed all the experimental work, analyzed the data and wrote the paper.
Synthesis and characterization of mesoporous silica done were done by Milene Zezzi.

IV. Designed the study together with Milene Zezzi, performed and analyzed all the experimental work related to enzyme labelling and FRET, wrote the paper together with Milene Zezzi.
Synthesis and characterization of mesoporous silica as well as measuring the enzymes activity were done by Milene Zezzi.

V. Designed the study and performed all the experimental work, analyzed the data and wrote the paper.
Synthesis and characterization of mesoporous silica were done by Milene Zezzi.

Abbreviation List

BSA	Bovine serum albumin
ADH	Alcohol dehydrogenase
Cy3	Sulfo-Cyanine3 NHS ester
Cy5	Sulfo-Cyanine5 NHS ester
DNA	Deoxyribonucleic acid
DOL	Degree of labeling
FaldDH	Formaldehyde dehydrogenase
FateDH	Formate dehydrogenase
FRET	Förster resonance energy trasnfer
GOX	Glucose oxidase
HMM	Hiroshima mesoporous materials
IGS	Immunogold staining
MCF	siliceous mesostructured cellular foams
MCF-MP	MCF functionalized with 3-mercaptopropyltrimethoxysilane
MCF-OC	MCF functionalized with octyltriethoxysilane
MML	Mucor miehei lipase
MPS	Mesoporous silica
NADH	nicotinamide adenine dinucleotide (NAD) + hydrogen (H)
NIR	Near infrared
Phe	Phenylalanine
SBA-15	Santa Barbara amorphous-15
SEM	Scanning electron microscopy
TEM	Transmission electron microscopy
TEOS	Tetraethyl orthosilicate
Trp	Tryptophan
Tyr	Tyrosine
UV-visible	Ultraviolet–visible

Preface

The work described in this thesis was carried out between June 2013 and May 2018 at Chalmers University of Technology, under the supervision of Professor Björn Åkerman. This research was performed from within the Linnaeus Center for Bio-inspired Supramolecular Function and Design (SUPRA), which was funded by the Swedish Research Council (Vetenskapsrådet; Project no. 21220093). The "Enzyme Cluster" within the framework of SUPRA has been formed since 2007 to bring together expertise from different groups and using interdisciplinary collaboration to answer questions about enzyme immobilization through new approaches. Milene Zezzi do Valle Gomes (Current PhD student), Dr. Hanna Gustafsson (Former PhD student) and Prof. Anders E.C. Palmqvist from the division of Applied Chemistry joined different projects with expertise on synthesis and development of different types of mesoporous silica.

Pegah S. Nabavi Zadeh

May 2018

Table of Contents

Introduction

"So many of the chemical reactions occurring in living systems have been shown to be catalytic processes occurring isothermally on the surface of specific proteins, referred to as enzymes, that it seems fairly safe to assume that all are of this nature and that the proteins are the necessary basis for carrying out the processes that we call life."

- John D. Bernal

The above quote is taken from "*The Physical Basis of Life*", a lecture given by the sage of science, John D. Bernal at 32nd Guthrie Lecture in 1947 [1]. A scientist who was one of the pioneers to exploit his knowledge in physics for molecular biology in order to identify the structure of enzymes [2]. Over 100 years before Bernal beautifully described the importance of enzymes in life, the enzyme diastase had been discovered by Payen for the first time [3]. In the early 1960s, the structure of enzymes were determined by x-ray crystallography, which paved the way for understanding the function of enzymes at an atomic level [4]. Today, we know that what Bernal called "*the surface of specific proteins*", is described as the active site of enzymes, which is mainly in charge of the catalytic process.

Our knowledge of enzymes has progressed a long way since those days. Enzymes are referred to as macromolecular biological catalysts. They speed up chemical reactions in all living cells. Almost all metabolic processes in the cell require enzyme catalysis in order to occur at rates fast enough to sustain life. Enzymes are functioning under mild conditions and are also biodegradable which makes them the most environmentally-friendly catalysts [5, 6].

In the identification of these advantages, it has been noted that enzymes make life happen in living cells. Furthermore, they can enhance our standard of living due to their application in *e.g.* medicine. Enzymes seem to be a suitable alternative to the use of conventional synthetic catalysts in different industries [7, 8]. However, there are some limitations for the use of enzymes in large-scale production. For example, enzymes have a low long-term stability and are also difficult to separate from the reaction media. The latter limits the recovery of enzymes and may lead to contamination of the final product [9, 10]. One approach to minimize these limitations is to immobilize enzymes on/into a support material [11].

The term "immobilized enzymes" refers to "enzymes physically confined or localized in a certain defined region of space with retention of their catalytic activities, and which can be used repeatedly and continuously" [11]. The history of enzyme immobilization goes back to the 1960s and since the early 1990s, immobilization techniques have been significantly developed for complex systems. The main components of an immobilized enzyme system are the enzyme, the support, and the mode of attachment. The enzymes can be attached to the support by different interactions including entrapment, physical adsorption and covalent binding [11, 12].

Immobilization of enzymes can facilitate enzyme reusability and product purification. However, the catalytic activity and stability of the immobilized enzymes can be altered either positively or negatively [13, 14]. The activity and stability effects need to be investigated based on the immobilized enzyme system which is intended to be used for a specific application. Since there are a large number of biocatalysts and very different support materials available today, the design of immobilization processes involves a trial-and-error approach. In other words, a universal method for enzyme immobilization has yet to be developed. Therefore, it is crucial to have a better understanding of how enzyme function is affected by its interaction with the support material. This knowledge certainly leads scientists to optimize the enzyme immobilization for a desired application.

Enzyme immobilization is considered to be an interdisciplinary research area which can be studied from various perspectives, such as molecular biology and physical chemistry using

different techniques employed in these fields. Sometimes it is necessary to combine the techniques and develop a new method in order to design an optimal enzyme immobilization.

The study of interaction between light and matter (*i.e* molecules) is at the heart of physical chemistry and can be applied to different fields such as biology and biotechnology. Optical spectroscopy is a broad and diverse technique, both regarding the type of radiation used (from UV to X-ray radiation) and the type of interactions studied (absorption, emission, scattering). During the last few decades, spectroscopic techniques, especially fluorescence spectroscopy, has emerged as an essential technique in the biochemical, biotechnology and biology sciences. As in all scientific disciplines, the development of modern fluorescence spectroscopy has benefited from the contributions of many scientists. However, Gregorio Weber, undeniably, can be singled out for his outstanding contributions to this field [15]. He developed the use of fluorescence polarization for studying macromolecular dynamics. Furthermore, Weber could demonstrate that proteins can be labeled with fluorophores, which in turn reveal information about the proteins and their interactions through fluorescence spectroscopy [15, 16]. Weber, indeed, is counted as one of the pioneers who could combine "science and art"; as Norman Horowitz is quoted below as saying [17]:

> *"The older I get, the more I appreciate the difference between the results of scientific investigations and the methods by which the results are obtained. The results constitute the body of scientific knowledge- they are science. But, as has been noted by others, the facts of science exist in nature and are waiting to be discovered; if not found by one investigator, they will be found by another. The methods, however, are the creations of individual scientists; they are more art than science. For this reason, and depending on one's mood, they may be even more admirable than the science they make possible"*

Weber's far-reaching efforts to improve the fluorescence spectroscopy have aided a large amount of research in biology and physical chemistry sciences, including this thesis. The focus here is placed on the physical chemistry perspective of enzyme immobilization in the support mesoporous silica particles, aiming to answer two questions: *"What is the mechanism of the enzyme immobilization?"* and *"Where are the enzymes localized after immobilization?"*.

A considerable amount of research has been performed to answer these two questions, however, despite a large number of techniques available, there is still a need for developing high time resolution methods to monitor the immobilization of enzymes directly. A major limitation of our understanding of the immobilization process might be the gap of knowledge

about the microenvironment that immobilized enzymes can experience in mesoporous silica compared to free enzymes in solution. Microenvironmental changes can also affect the mobility and stability of the confined enzymes. Achieving all this information about the enzyme immobilized system can be a step forward to solve the mechanism of the enzyme immobilization. Furthermore, the evaluation of the catalytic efficiency of immobilized enzymes together with physical chemistry characterization of the system can lead to an optimal immobilization design

The main objective of this thesis is to gain a deeper knowledge of the immobilization process as it proceeds, and also how the immobilized enzymes are distributed in the mesoporous particles. In order to achieve these objectives, spectroscopy, especially fluorescence spectroscopy was highly exploited in all appended papers of this thesis, together with different enzymes and mesoporous silica particles synthesized in various pore size and morphology.

The first part of this thesis strives to elucidate the underlying mechanism of enzyme immobilization by proposing a fluorescence assay for real-time monitoring of enzyme binding in mesoporous silica particles. The kinetics of the immobilization process was quantified using the fluorescence of the enzyme-bound dye. In addition to translational dynamics, the rotational dynamics of the confined enzymes were analyzed in mesoporous silica with various pore size and particle diameter. Afterwards, the microenvironment changes that enzymes sense in mesoporous silica particles were characterized by the same strategy. The effect of the pore morphology and diameter of the mesoporous silica on the effective microviscosity sensed by enzymes were evaluated (**Papers I-III described in Chapter 4 and Chapter 5**).

The second part of this thesis is focused on answering the question regarding the localization of enzymes after immobilization using spectroscopy and microscopy techniques. The distribution of two enzymes after immobilization inside mesoporous silica was analyzed by using Förster resonance energy transfer (FRET). Additionally, the effect of the protein concentration on the average distance between the two co-immobilized enzymes was investigated. The location of the immobilized enzymes was visualized in order to understand if the enzymes are mainly located inside the porous structure or adsorbed to the external surface of the support. The visualization method was based on transmission electron microscopy in combination with immunogold staining (TEM-IGS). The influence of the pore morphology on the radial distribution was studied in order to optimize the enzyme immobilization based on choosing suitable mesoporous silica particles for biocatalytic applications (**Papers IV-V discussed in Chapter 6**).

Background

In the first part of the thesis, a background on the structure of enzymes and mesoporous silica, is provided including the enzyme immobilization process. Chapter 1 is an introduction to enzymes, with a special focus on the physico-chemical and structural properties of enzymes used in this thesis. Chapter 2 outlines a literature summary of the historical and recent progress in developing the enzyme immobilization together with an introduction on mesoporous silica particles. Chapter 3 focuses on a brief theoretical background, as well as a methodological description of concepts and techniques used in the experimental work.

1 Enzymes

Enzymes are the biological foundation of this thesis; as they are “the molecular machines of life” Therefore, the first chapter provides an overview of proteins and their structures; also the function of the enzymes used in this thesis is described.

1.1 Proteins

Proteins are comprised of a series of amino acid residues and are typically more than 300 amino acid long. Each amino acid consists of an amine group (-NH_2), a carboxyl group (-*COOH*) and a functional group (called *R* group) attached to the alpha carbon. The functional groups are different in each amino acid and play the main role to give amino acids different chemical properties, such as polarity and charges (Figure 1.1) [18].

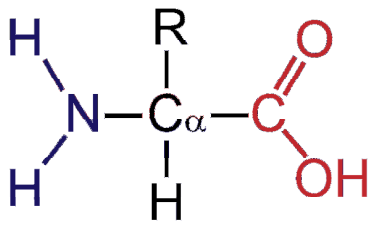

Figure 1.1. General chemical structure of an amino acid

Amino acids can be coupled together to form a peptide. The coupling of 10 or more amino acids to each other results in the formation of a polypeptide. A protein consists of a large polypeptide chain that can be folded into a specific conformation, which determines its function [19].

The structure of proteins can be broken to four levels; primary, secondary, tertiary and quaternary. The primary structure of a protein refers to the sequence of amino acids that make up the backbone of the polypeptide. The secondary protein structure describes localized conformations of the polypeptide backbone or the folding pattern of the protein over a short sequence of amino acid residues. A protein chain can fold into a rigid α-helix, forming a regular pattern of hydrogen bonds between the backbone atoms of nearby amino acids (3.6 residues per turn) [20]. Additionally, backbone atoms of the chain can interact side by side to form beta pleated sheets. These two motifs (α-helix and β-sheet) are the most commonly occurring secondary structure elements in proteins. It is noteworthy that at this level the polypeptide backbone begins to form shapes entirely dependent on the lowest energy conformation through the formation of dipole-dipole interactions [20]. As these structures are comprised of a large number of amino acids, for practical purposes they are depicted as colored strips rather than conventional molecular structures (See Figures in section 1.2.1). In the context of this thesis, the secondary structure of the proteins was monitored in order to detect conformational changes.

Protein tertiary structure is the complete folding pattern of an entire polypeptide chain to produce the overall 3D structure. This folding is not random and it is specific to the protein, giving rise to the protein's function. Factors that influence the tertiary structure include, (*i*) the presence of hydrophobic residues in the interior of the protein and are therefore not in contact with the aqueous environment, and (*ii*) residues with hydrophilic properties tend to be on the exterior of the protein and be involved in dipole-dipole or ion-dipole interactions with water molecules.

Quaternary structure occurs for those proteins which consist of multiple polypeptide subunits. These subunits are not covalently bound together. Mostly weak interactions, such as hydrogen bonding or strong electrostatic interactions between them allow the subunits to arrange themselves in an optimal way for being in close proximity to each other [19].

1.2 Enzymes and function of enzymes

Enzymes in most cases are proteins that function as biological catalysts. A catalyst is a substance that can increase the rate of a chemical reaction without itself being consumed or altered. Therefore, enzymes can accelerate and regulate metabolic reactions in living cells with high chemo-, stereo- and regioselectivity. Without biocatalysts the chemical reactions in life processes, such as digestion of food and synthesis of DNA, could last forever. Moreover, the enzymes can function under very mild conditions in terms of pH and temperature in aqueous solutions. The chemical transformation of a substrate (*S*) into the desired product (*P*) occurs at the active site of the enzyme (*E*). This active site is a region of the enzyme with specific amino acid residues that can bind to the substrate molecule [21]. As substrate selectivity of enzymes is dependent on interactions between the enzyme and substrate, enzymes take advantage of a number of intermolecular forces including hydrogen bonding, van der Waals interactions, as well as polar and hydrophobic interactions, to align the substrate in an optimal orientation so that the reaction can occur. Enzymes increase the rate of the reaction by decreasing the activation energy ($\Delta G^{\neq}$). Activation energy is the difference between the energy levels of the ground state and the transition state of the substrate. By contrast, the energy of the reaction ($\Delta_r G$) is referred to the difference in free energy between the ground states of substrate and product; an energy difference which the catalyst cannot affect (Figure 1.2) [21].

Enzymes achieve the highest catalytic activity at an optimum pH and temperature. The pH can influence the ionization states of amino acid residues, while the temperature influences the chances of a successful collision between enzyme and substrate. The optimum temperature for enzymes is generally around human body temperature, 37 °C [22].

Enzymes are considered as environmentally-friendly catalysts compared to conventional synthetic catalysts employed in different industries such as distillation of crude oil [23]. Conventional catalysts often require high amounts of energy and toxic waste might be generated during the preparation procedure of synthetic catalysts [24].

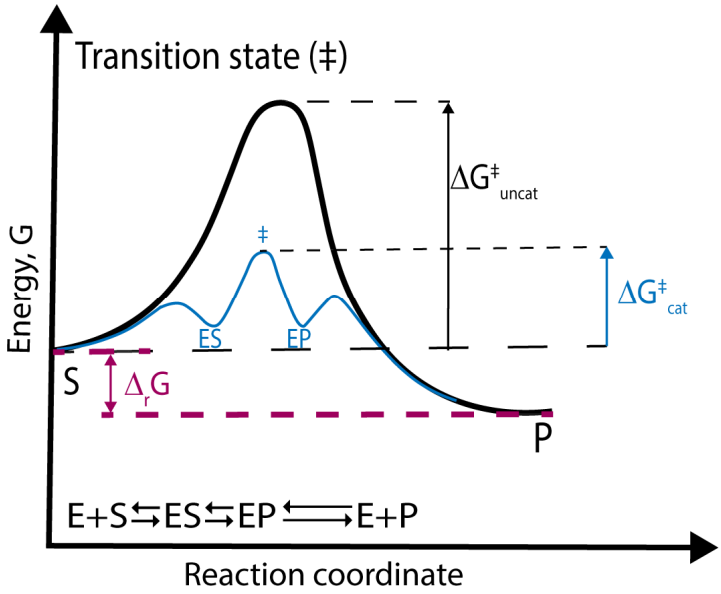

Figure 1.2. Reaction coordinate diagram comparing an un-catalyzed and a catalyzed reaction. ES and EP are reaction intermediates of the enzyme with the substrate and product, respectively. Redrawn from Principles of Biochemistry by Lehninger et al.: 5th edition [21]

Moreover, some of them such as organometallic catalysts, can affect the final products of reactions containing high levels of metal contamination which can be considered as a serious drawback if the metal is toxic for pharmaceutical and food applications [25, 26]. Naturally-occurring microorganisms (fungi and bacteria) are the most productive sources of enzymes as they are easy to handle, can be grown in huge tanks without light, and have a very high growth rate [22]. After the purification process, which might be costly, enzymes are ready to be used in various industrial processes *e.g.* biofuel cells [6, 27], detergent formulations [5], biosensors [7, 28], food (*i.e.* bread, cheese, butter, beer) [29, 30] and pharmaceuticals [5, 31].

1.2.1 Enzymes used in the thesis

This study is about enzyme immobilization from a physical chemistry perspective aiming to probe the behavior of the different enzymes during or after the immobilization into the support materials. Six different proteins are used here, of which five are enzymes. All six proteins were chosen based on their physico-chemical properties including molecular weight, charge and hydrodynamic radius (the effective radius of a given molecule in a solution). The five enzymes were preferred based on their biocatalytic applications. A brief summary of each protein is outlined here and Table 1.1 represents their physico-chemical properties in detail.

Lipase

Lipase (triacylglycerol acylhydrolase) is a group of water-soluble enzymes that can be found in different bacterial strains and play a main role in the metabolism and the digestion of fat. It is recognized as one of the most important groups of enzymes in biotechnology, with applications in food, detergent, pharmaceutical, cosmetic and paper industries. Lipase catalyze the hydrolysis of triacylglycerol to glycerol and free fatty acids in aqueous media [32].

Hydrolysis: $RCOOR' + H_2O \rightarrow RCOOH + R'OH$

Lipase is fairly surface active and hydrophilic and the enzymatic activity is usually increased when interacting with an interface. This is largely due to the fact that the active site of a lipase is covered with a hydrophobic α-helical unit, called the "lid", which adjusts the conformation of the active site to an open state in the presence of a hydrophobic surface [33, 34]. Therefore, immobilizing lipases on an interface can be very useful. In the first three Papers (I, II and III), lipase from *Mucor miehei*, (MML) has been used (Figure 1.3) and compared with different proteins in terms of size and isoelectric point (pI) (Table 1.1) [35, 36].

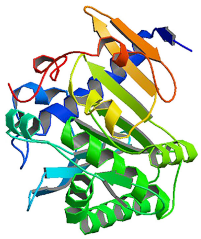

Figure 1.3 Structure of MML [36]

Glucose oxidase

Glucose oxidase (GOX) is found in some fungi and insects where it shows its antibacterial activity by producing hydrogen peroxide. It is an oxidoreductase that catalyzes the oxidation of glucose to hydrogen peroxide and D-gluconolactone [37-39].

β-D-glucose + $O_2 \rightarrow$ D-gluconolactone + H_2O_2

There are many industrial applications for GOX, *i.e.* food processing as a preservative, biofuel cells during conversion of biochemical energy into electrical energy used as biocatalyst [37]. GOX is also used as a biosensor for the determination of blood glucose [40, 41].

Glucose oxidase from *Aspergillus niger* (Figure 1.4) used in paper I is a dimer consisting of 2 equal subunits with a molecular mass of 80 kDa each. The hydrodynamic radius (R_H) of the dimer is 4.5 nm [39, 42].

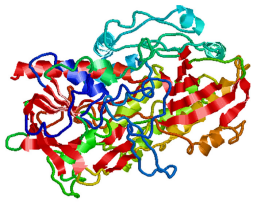

Figure 1.4 Structure of GOX [42]

Bovine serum albumin

Bovine serum albumin (BSA) cannot be listed as an enzyme due to the lack of the active site in its structure [43, 44]. However, it is a well-known protein, which is commonly used as a protein concentration standard in laboratory experiments. BSA also has a number of biochemical applications, including ELISA (Enzyme-Linked Immunosorbent Assay) and immunohistochemistry. BSA is often used as a blocker in immunohistochemistry by binding to nonspecific binding sites and in turn increases the chance that the antibodies will bind only to the antigens of interest [43, 45].

Serum albumin from *Bovine* blood (Figure 1.5) was used besides other enzymes in Paper I, II due to its small size (R_H: 3.5 nm) and high stability [44, 46].

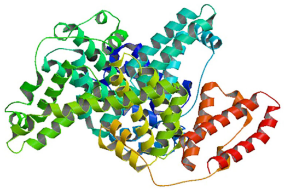

Figure 1.5 Structure of BSA [46]

Formate dehydrogenase

Formate dehydrogenase (FateDH) as an oxidoreductase can be used to convert carbon dioxide (CO_2) to formate using NADH as a cofactor ($CO_2 \rightarrow$ formate). This reaction is the reverse of the pathway in nature and is thermodynamically unfavorable [47, 48]. Therefore, in order to drive the reaction towards the production of formate, high concentrations of the substrate and cofactor are required, along with the rapid removal of the product.

Formate dehydrogenase from *Candida bondini* (Figure 1.6) was used in Paper IV and consists of a homodimer of 84 kDa with an independent active site on each subunit [48].

Figure 1.6 Structure of FateDH [48]

Formaldehyde dehydrogenase

Formaldehyde dehydrogenase (FaldDH) catalyzes the conversion of formic acid to formaldehyde requiring NADH as a cofactor (formic acid → formaldehyde). As this enzyme is very sensitive to substrate concentration and pH, it requires high concentrations of formic acid. However, in high concentrations of the substrate, the pH of the solution becomes lower and the enzyme activity drops significantly as a result. In order to improve the use of this enzyme for the reduction reaction a pressurized reactor can be used [49]. In Paper IV, FaldDH from *Pseudomonas* (Figure 1.7) was used. This enzyme consists of a complex structure formed a homotetramer with the total molecular weight of 170 kDa [50, 51]. FaldDH was co-immobilized with FateDH to catalyze the overall reduction of CO_2 to formaldehyde efficiently by consuming the formate (the anion derived from formic acid) produced by FateDH and converting it to formaldehyde.

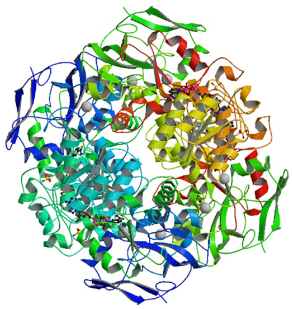

Figure 1.7 Structure of FaldDH [51]

Alcohol dehydrogenase

Alcohol dehydrogenase (ADH) as an oxidoreductase can efficiently reduce formaldehyde to methanol using NADH as a cofactor (formaldehyde → methanol). Unlike FateDH and FaldDH, this reaction is thermodynamically favored. ADH is typically used as the last enzyme in a three-enzymatic cascade reaction to convert CO_2 to methanol under mild conditions [49].

Paper V describes the use of ADH from *Saccharomyces cerevisiae* (Figure 1.8) in order to visualize the location of the immobilized enzyme in different mesostructured silica. This enzyme has a homotetramer structure which has a calculated mass of about 141 kDa [52].

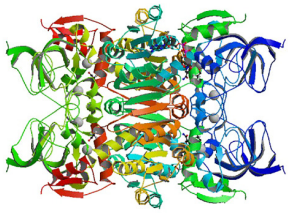

Figure 1.8 Structure of ADH [52]

Table 1.1. The physico-chemical properties of the enzymes used in this thesis

Enzyme [a]	M_w [b] (kDa)	R_H [c] (nm)	pI [d]	ε_{280} [e] ($M^{-1}cm^{-1}$)	Optimum pH and T [f]	Paper
MML	32	2.25	3.8	42800	7 and 37 °C	I, II, III
GOX	160	4.5	4.2	308000	5.5 and 35 °C	I
BSA	66	3.5	4.7	43824	----------	I, II
FateDH	84	3.5	5.3	142000	6.5 and 37 °C	IV
FaldDH	170	8.6·8.6·19	5.4	188000	6.5 and 37 °C	IV
ADH	141	4.5	5.6	205860	6.5 and 25 °C	V

a. MML- Mucor Miehei Lipase, BSA- Bovine Serum Albumin, GOX- Glucose Oxidase, FateDH- Formate DH, FaldDH- Formaldehyde DH, ADH- Alcohol DH
b. Molecular weight [49, 51, 53-56]
c. Hydrodynamic radius, for FaldDH the molecular size from crystal structure reported [49, 51, 53, 56, 57]
d. Isoelectric point, the pH where a molecule has no net charge [53, 55, 57-59]
e. Extinction coefficient [53, 57-60]
f. Optimum pH and temperature [49, 51, 56]

2 Immobilization of Enzymes

One of the main focus of this thesis is to further our understanding of the immobilization mechanisms and in turn optimize the immobilization process for a biocatalytic application. This chapter provides a background about enzyme immobilization as well as an introduction into the support materials which were used as the host for immobilized enzymes.

Today enzymes are used daily in our life through *e.g.* medicines, food, detergents, textiles and biofuels since most of the industries prefer to apply enzymes as eco-friendly catalysts instead of synthetic catalysts. However, the use of enzymes is rather limited due to a low long-term operational stability and costly purification process. Additionally, there are difficulties in recycling enzymes from the reaction media, limiting their reuse as a result. In efforts to overcome these limitations and improve the use of enzymes in biocatalytic applications, enzyme immobilization was introduced in the 1960s [11]. The main motivations for the use of enzyme immobilization in the beginning were improvement of enzyme stability and simplification of biocatalyst recycling. However, higher catalytic activity and high product yield can now be achieved by optimizing the immobilization process [61, 62].

There are several immobilization methods, including (*i*) the covalent binding of enzymes on a solid support such as agarose gels, cellulose and nanoparticles [62, 63], (*ii*) enzyme entrapment inside a material like sol-gel materials and polymers [62, 64], (*iii*) enzyme cross-linking by the addition of salts, organic solvents, acids or non-ionic polymers [65], and (*iv*) the method employed in this thesis, the physical adsorption of the enzyme to a support material such as mesoporous materials [53, 61].

Each method presents a number of advantages and disadvantages, giving us the opportunity to select a proper strategy for gaining the immobilization benefits to the fullest. There is no universal approach to immobilize a given enzyme whilst maintaining its activity and stability, despite extensive research over the past few decades, [66-71]. Therefore, a trial-and-error approach is still necessary in order to develop the immobilization process for a new biocatalyst. Establishing the right immobilization condition is not always straightforward, since so many factors can affect the quality of immobilization such as physico-chemical properties of a given enzyme and support materials.

2.1 Mesoporous silica as support for enzyme immobilization

Mesoporous materials are defined as inorganic materials with a pore diameter between 2 nm and 50 nm. Porous materials with a pore diameter less than 2 nm are called microporous, and if the pores are larger than 50 nm in diameter the materials are named macroporous [72, 73]. Mesoporous solid materials mostly are made of oxides, such as silica (SiO_2) [74], alumina (Al_2O_3) [75] or titania (TiO_2) [76].

This thesis focuses on mesoporous silica (MPS) materials which serve as a promising solid support for enzymes. The main reason is that the pore size, pore structure and particle morphology of MPS materials can be tailored with a high degree of accuracy. Moreover, the MPS materials are made of inexpensive silica precursors *i.e.* Tetraethyl orthosilicate (TEOS) and different structure-direct agents (*i.e.* amphiphilic surfactants). The MPS materials have high mechanical and thermal stability, and due to a large surface area and pore volume, a large quantity of enzymes can be immobilized, thus higher enzyme loadings can be achieved compared to non-porous materials [74, 77]. Furthermore, the porous structure provides a protective environment in which the enzymes often can tolerate extreme pH, higher temperatures and salt concentrations [53, 78, 79]. The pore diameter can be adjusted to match the size of a given enzyme, while the pores can be ordered in different shapes, such as

hexagonal, cubic or spherical [80]. Moreover, the size of the MPS particles can be adjusted for different applications, in which micrometer-sized mesoporous particles (up to 5 μm) are mostly used in biocatalytic applications [81].

In general, most of the MPS materials are synthesized from an organic-inorganic self-assembly between a silica precursor (*i.e.* TEOS) and a block copolymer surfactant as a template for forming micelles, hexagonal or other types of surfactant assemblies in an aqueous solution or oil in water microemulsion. The silica precursor is hydrolyzed and polymerized in the water domain of the template to form an inorganic network which mirrors the template structure. After polymerization, hydrothermal treatment is performed on the formed silica network in order to increase cross-linking, as well as adjust the pore diameter and particle size. To finish, the organic template or surfactant is burnt away by calcination. The pore size of the materials can be tuned by changing the hydrothermal treatment [82, 83].

Several analytical techniques are employed to characterize the structure of the mesoporous materials. Scanning electron microscopy (SEM) is used to determine the morphology and the size of the MPS particles. Transmission electron microscopy (TEM) can be used as a supplementary to SEM for characterization of the local pore structure. Nitrogen sorption analysis can be used to measure the surface area, pore volume and pore size distribution in the MPS particles [84-86]. Thermogravimetric analysis can be applied to confirm that the surface is adequately functionalized, if any surface modification is performed. For a more detailed description of the synthesis of the MPS materials and the characterization methods used in this thesis, the reader is referred to references [53, 58, 59, 87].

2.2 Support properties

It is important to remember that enzymes can differ considerably in size, shape, isoelectric point, surface charge distribution and catalytic performance (See Table 1.1). Therefore, in the immobilization process the properties of the support (here, mesoporous silica), such as pore size, pore morphology and particle size should be considered as crucial factors to obtain an optimal fit where enzyme loading and catalytic function can be significantly improved [80, 88].

Moreover, the physico-chemical properties of the support surface including hydrophobicity and charge density may result in a different pore microenvironment for the enzyme compared to the bulk phase [57, 89-91].

2.2.1 Pore size and morphology

Pore size is one of the important properties of the mesoporous silica that affects enzyme immobilization. Choosing an ideal pore size in relation to the size of a given enzyme is extremely important, as it can result in either increased or decreased enzyme loading, stability and activity. The pores should be large enough for the enzyme to diffuse and also be protected from the surroundings. They cannot be too narrow as the enzyme may lose its flexibility, which would lead to a decrease in activity [12, 92]. Additionally, the enzymes may block the pore opening and in this case, the enzyme loading of the immobilization process would not be optimal [93, 94]. On the other hand, if the pore size is significantly larger than the enzyme, a high enzyme loading can be obtained, however, there is a higher probability that the enzyme may leak out from the pores during catalysis. Enzyme stability can be improved by employing an optimal pore size. For example, some enzymes can lose their activity as they are removed from their natural environment. These enzymes may require a narrower pore size compared to a relatively stable enzyme which sometimes leads to higher enzyme activity due to a beneficial conformational change of the enzyme [55, 95]. Another major factor concerning the choice of pore size is the mobility of the immobilized enzyme. If the pore size is too small, the mobility of the immobilized enzyme may be restricted, which may decrease the enzymatic activity. For example, Gustafsson *et al.* [53] showed that lipase with a 4.5 nm hydrodynamic radius exhibits the highest activity in 9 nm pore size of the mesoporous silica compared to when smaller pore sizes were used. In Paper II, it has been shown that the rotational mobility of lipase in the 9 nm pore diameter particles is higher compared to the similar particle with 6 nm pore diameter. It is noteworthy that having a higher mobility after confinement can be helpful to increase the possibility of the contact between the enzyme active site and the substrate [96, 97].

The morphology of the pores also affects the enzyme immobilization. Most mesoporous silica materials are classified according to pore structure. For example, SBA-15 (*Santa Barbara Amorphous-15*) and MCM-41 (*Mobil Composition of Matter*) are mesoporous silica particles with hexagonal pores, KIT-6 (*Korea Institute of Technology- 6*) and SBA-16 (*Santa Barbara Amorphous- 16*) with cubic pore geometries, while MCF (*Mesostructured Cellular Foams*) have spherical cellular pores and are extensively used in enzyme immobilization [74, 83, 92]. The cubic and foam structures are usually more beneficial for the immobilization due to the higher accessibility of the pores for the enzymes and thus the substrate. The hexagonal structures with long one-dimensional pores can hinder the diffusion of the enzymes into the deeper parts of the pores.

This may be the result of enzymes blocking the pore opening and thereby preventing the rest of the enzymes from penetrating the pore. The pore morphology of the most used silica materials, the SBA-15 and MCF particles, is schematically shown at the end of this Chapter.

2.2.2 Particle size

The size of the MPS particles can affect both the enzyme loading and activity. It is noteworthy that a unique particle size cannot be defined for mesostructured cellular foams (MCF), since MCF consists of a large number of silica cells that are agglomerated together. However, for particles with a hexagonal pore structure, such as SBA-15, the particle size is important. In smaller particles, the length of the pores is shorter, therefore, minimizing the empty space inside the pores, specifically in the co-immobilization of two enzymes. Moreover, shallower pores may improve the accessibility of the enzyme for the substrate. The substrate may be able to reach a larger relative amount of active sites within a certain time frame [77, 98].

2.2.3 Surface modification

The surfaces of mesoporous silica can be functionalized with organic groups (i.e. amines, thiols, phenols. Such surface modifications can improve the enzyme-support interaction, preventing the leakage of enzymes from the pores. Therefore, the immobilized enzymes inside the pores can experience higher stability. Furthermore, the surface modifications may change the orientation of the confined enzymes in a way that the active sites become more or less accessible to the substrate. These changes may result in improving or deteriorating the enzymatic function. Since enzymes are very complex biomolecules with different amino acid residues in the active site and on their outer surface, it is not simple to predict which functionalization, either hydrophilic or hydrophobic on the support material, can enhance the enzyme loading, activity and stability [69, 99].

At first sight, hydrophilic surfaces may seem more desirable, as most enzymes are hydrophilic and no concern arises regarding the enzyme conformational changes. However, due to the positively charged amine group in hydrophilic functionalization, the enzyme may be strongly adsorbed to the entrance of the pore and thus decreasing enzyme loading significantly [70, 100].

Even though the interaction between an enzyme and a hydrophobic surface can lead to the unfolding and inactivation of the enzyme [70], for some enzymes, such as lipases and alcohol dehydrogenase a higher activity is recorded [33, 90, 101]. One reason might be that the stability of the immobilized enzymes is controlled by an entropic effect. Upon immobilization the unfolded enzymes lose more entropy than the folded enzymes, resulting in higher stability and thus higher activity [90]. In addition, changes in the accessibility of the active site can lead to a higher catalytic activity of enzymes after immobilization on hydrophobic surfaces. For example, the structure of lipase makes the active site more accessible for the substrate nearby hydrophobic surfaces due to the hydrophobic pockets close to the active site. This effect between lipase and hydrophobic surfaces results in higher stability and activity of lipase in catalytic applications [102].

In the context of this thesis, mesoporous silica with two different types of hydrophobic functionalization are used; (*i*) octyltriethoxysilane (OC) with a long carbon chain, and (*ii*) 3-mercaptopropyltrimethoxysilane (MP) with a thiol group at the end of the carbon chain (Papers III-IV). The main reason for using hydrophobic surface in Paper III was to avoid the adsorption of the enzymes to the pore wall while the pore microviscosity was probed. Moreover, in Paper IV, a hydrophobic surface with thiol group was used, since Zezzi *et al.* [58] reported that immobilized FaldDH has a higher specific activity compared to the free enzyme and other types of organic groups, *i.e.* aminopropyltrienthoxysilane and octyltriethoxysilane which were employed for functionalization.

2.3 Choice of immobilization strategy

2.3.1 Covalent binding

Enzymes can be immobilized into mesoporous silica by covalent attachment (Figure 2.1a). In this method, the support material is usually modified with a chemically active surface that binds to specific functional and reactive groups on the enzymes *i.e.* amino, thiol or hydroxyl groups [103, 104]. As the enzyme is chemically bound to the support, the occurrence of enzyme leakage from the support decreases significantly during the reaction, which is one of the most important advantages of this strategy [63]. However, the enzyme can lose its flexibility through the covalent binding and also the enzyme conformation may change which may alter the enzyme activity, especially if the covalent bond is involved in or is close to an essential part of

the active site. Covalent binding of the enzyme to the silica might also block the pore entrances, affecting enzyme loading as a result [62, 105].

2.3.2 Physical adsorption

In physical adsorption a multitude of weak forces such as hydrogen bonds, van der Waals attraction, electrostatic forces and/or hydrophobic interactions are involved between the enzyme and the support surface (Figure 2.1b) [69, 93]. This method is usually considered one of the most robust methods and is frequently used in large-scale production. Since there is no chemical activation of the support, the risk of conformational changes of the enzyme is minimized. Therefore, the enzyme activity is typically retained or even increased after immobilization. The main drawback of this method is that the interactions are often weak, thus the enzyme can leak out of the support [68, 74]. To minimize enzyme leakage, it is important to correctly choose the material with respect to pore size for an optimized fit of the enzyme in the pores. The surface net charges on the enzyme and on the silica can be controlled by changing the pH of the solution. To have an attractive electrostatic interaction between enzyme and silica, a pH somewhere in between the point of zero charge (pzc) of silica (pzc ~2) and the isoelectric point (pI) of the specific enzyme should be chosen. At a pH above the pI of the enzyme or below the pzc of silica, both components have the same net charge, which leads to repulsive electrostatic forces. However, it is noteworthy that the enzyme net charge is not distributed evenly on the surface and there is a possibility that positively charged areas on the enzyme give rise to an electrostatic attraction between the enzyme and support, assuming that the overall charge above the pI of an enzyme is negative [63, 88].

In the context of this thesis, physical adsorption with no electrostatic attraction was applied as the most suitable immobilization strategy. Since the repulsive electrostatic forces between silica and enzyme prevent the enzyme from sticking to the pore wall, the microenvironment can be probed with high accuracy. Moreover, if the electrostatic attraction occurs in the system there is a chance that enzymes block the pore openings due to very strong binding between enzyme and support. Therefore, a higher enzyme loading may be achieved with the repulsive interaction.

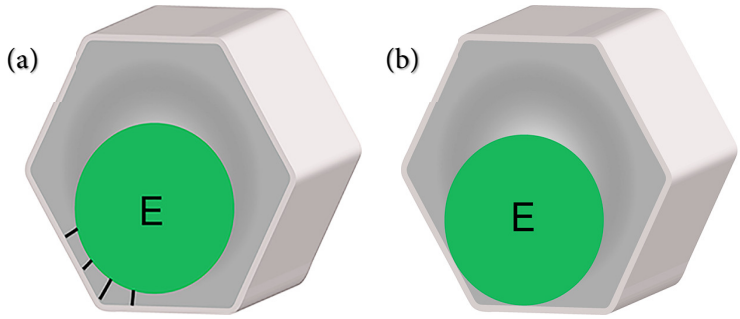

Figure 2.1. Schematic representation of (a) covalent binding and (b) physical adsorption of enzyme immobilization in mesoporous silica; an enzyme (E) in SBA-15 with hexagonal pore morphology.

2.4 Microenvironment inside the pores

It is clear that physical effects, such as the mobility and distribution of the immobilized enzyme as well as the pore microviscosity, are difficult to separate from biochemical effects inside the pores. Consequently, optimal immobilization conditions cannot be easily predicted. Furthermore, the environment inside the pores is not necessarily the same as in the bulk solution. Both the immobilization and the reaction conditions, including pH, viscosity, substrate concentration and activity may differ significantly from the conditions in the bulk [89, 100, 106, 107]. Therefore, it is important to characterize the microenvironment inside the pores in order to improve our understanding of how the combination of material properties (enzyme and support) and the immobilization conditions (temperature, pH, pressure) can be used to optimize the enzyme loading, stability and activity. For example, spectroscopic methods based on fluorescent dyes have been used to measure the pH inside the pores of MPS materials. In one approach, the pH probe SNARF-1 was attached to the silica walls of the particle pores [107] and in a reverse approach, the same pH probe was bound covalently to the proteins [57]. In the first approach, Yamaguchi *et al.* reported a more acidic pore environment than the bulk solution [107], but their approach needed a dense cover of amine groups on the pore surface which may alter the physico-chemical properties of the pore surface and the efficiency of enzyme immobilization. The second approach performed by Thörn *et al.* indicated that the pores in mesoporous silica provide a slightly buffering environment [57]. The latter approach has the advantage of monitoring the pH at the actual position of the enzyme in the pore as long as the dye does not affect the enzyme structure. It should be considered that the pH reported by a mobile enzyme-bound SNARF-1 is dependent on its radial distribution in the mesoporous silica pores. Therefore, the distribution of enzymes after

immobilization should be considered as another physical parameter which can influence the local microenvironment of immobilized enzymes. Matsuura *et al.* used labeled proteins and Förster resonance energy transfer (FRET) spectroscopy to investigate how pore size affects protein distances in a silica-based mesoporous material [106]. The results indicated that the distances between two proteins are highly dependent on the pore size; the smaller the pore size, the shorter the distance between the labeled proteins. In this thesis, the distribution of two co-immobilized enzymes in mesoporous silica particles was studied by using FRET. The effect of the concentration of the labeled-enzymes on the average distance and enzymatic activity was analyzed in detail (Paper IV). The characterization of the microenvironment that enzymes sense inside the porous materials is one of the main goal of this thesis and can be traced in all the appended papers.

2.5 Co-immobilization of enzymes for CO_2 reduction

An enzymatic cascade reaction is defined as a one-pot process that combines at least two enzymatic reactions involving several enzymes in concurrence. The efficiency of a cascade reaction is not only determined by the efficiency of the individual enzymes, but also by the transfer of reaction intermediates from one enzyme to the next. In nature, there are numerous biocatalytic cascade reactions which occur through different enzymes. If the enzymes involved in a cascade reaction are in close spatial proximity to one another, substrate channeling may lead to an increased overall rate of the reaction. In nature, this effect can be observed in cells [49, 108].

By mimicking nature, the co-immobilization of enzymes in various supports has become a high-interest area in enzyme immobilization studies since 1985 [11]. The co-immobilization of enzymes have several advantages which can be brought to industries, *i.e.* reducing the costs of production, decreasing the amount of chemicals and time used for product recovery, as well as minimizing the concentration of harmful or unstable compounds in reversible reactions [109]. Moreover, the co-immobilization of enzymes for a bio-multi-step reaction can be exploited in our life through different medical and environmental applications which make our life more eco-friendly with a higher standard. For example, immobilized multi-enzyme systems can be used in biosensors for the quantification of molecules which have biological interest, such as lactose, D-glucose and cholesterol [40, 41].

One of the highly desired environmental applications is the conversion of carbon dioxide (CO_2) to methanol (CH_3OH), which can be performed through a multi-enzymatic cascade reaction [8, 110, 111].

The reduction of CO_2 to CH_3OH is not a spontaneously reaction, or in a scientific word, it is not a thermodynamically favored cascade reaction in ambient conditions. Therefore, it is necessary to engineer the cascade reaction in terms of energy level [8]. Different approaches have been attempted to perform this reaction, such as using electrocatalysis, photocatalysis and biocatalysis. The biocatalytic conversion of CO_2 to CH_3OH is a more favorable approach as the other two methods demand excessive energy, specific equipment and low selectivity of substrate. In biocatalysis of CO_2 to CH_3OH, three enzymes are used: (*i*) formate dehydrogenase (FateDH) for the conversion of CO_2 to formate, (*ii*) formaldehyde dehydrogenase (FaldDH) for the reduction of formate to formaldehyde, and in the final step (*iii*) alcohol dehydrogenase (ADH) for the transformation of formaldehyde to methanol (Figure 2.2). Nicotinamide adenine dinucleotide (NADH) is used as the cofactor for all three enzymes.

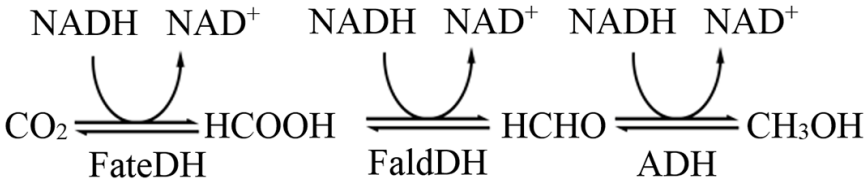

Figure 2.2. Schematic representation of the biocatalytic conversion of carbon dioxide to methanol through three steps: (i) conversion of carbon dioxide (CO_2) to formate (HCOOH), (ii) HCOOH to formaldehyde (HCHO), and (iii) HCHO to methanol (CH_3OH).

The kinetic parameters of the three enzymes are presented in Table 2.1, which shows the maximum rate of reaction at saturating substrate concentration (Vmax) as well as the substrate concentration at which the reaction rate is half of the maximum rate (Km). FateDH and FaldDH are more efficient in the reverse reaction (oxidation reaction) compared to the reduction reaction, which is needed for the conversion of CO2 to methanol. On the other hand, ADH can efficiently reduce formaldehyde to methanol. Therefore, to increase the yields of this enzymatic method, improvements to the first two steps are required. These improvements can be achieved by enzyme immobilization into or onto the surface of a support material. A number of studies have shown that, after immobilization, the cascade reaction leads not only

to higher catalytic efficiency but also to a higher enzyme stability, reusability, and a lower bioprocess costs [49, 56].

Table 2.1. Kinetic parameters of formate dehydrogenase, formaldehyde dehydrogenase and alcohol dehydrogenase [49, 112].

Enzyme	Reaction [a]	V_{max} [b] ($mM.min^{-1}$)	K_m [c] (mM)
Formate dehydrogenase (FateDH)	$CO_2 \rightarrow HCOOH$	0.002	30-50
	$HCOOH \rightarrow CO_2$	0.02	3.3
Formaldehyde dehydrogenase (FaldDH)	$HCOOH \rightarrow HCHO$	NA[d]	NA[d]
	$HCHO \rightarrow HCOOH$	0.01	0.06
Alcohol dehydrogenase (ADH)	$HCHO \rightarrow CH_3OH$	0.3	17.5
	$CH_3OH \rightarrow HCHO$	$0.5 \cdot 10^{-3}$	275

a. Reactions in red and black color indicate the reduction and oxidation reactions, respectively. Carbon dioxide: CO_2; Formate: HCOOH; Formaldehyde: HCHO; Methanol: CH_3OH.
b. V_{max}: The maximum rate of reaction at saturating substrate concentration
c. K_m: The substrate concentration at which the reaction rate is half of the maximum rate
d. NA: Not available

In Paper IV, the two enzymes FateDH and FaldDH were co-immobilized in mesoporous silica (different MCF particles in terms of surface functionalization). The enzymatic activity was investigated at different concentrations of the co-immobilized enzymes as well as the effect of the concentration on their distance.

2.6 Mesoporous silica used in the thesis

In order to obtain the optimum immobilization conditions, it is necessary to choose the suitable support for a given enzyme based on the relative pore/enzyme size. In this thesis, three different types of mesoporous silica materials were tailored with a variety of pore sizes and surface modification to probe the microenvironment inside the pores with better accuracy and also to characterize the behaviour of the enzymes.

Santa Barbara Amorphous material number 15 (SBA-15) is commonly used as immobilization supports for a variety of enzymes since first synthesized in 1998 by Zhao *et al.* [82]. SBA-15 with the pores arranged in a hexagonal symmetry, the pore size range and particle size can be tailored in a relatively broad range.

Hiroshima Mesoporous Materials (HMM) is a silica material consisting of small spherical particles first described by Yokoi *et al.* in 2006 [113]. The main properties of HMM are their very small particle size, around 40 nm (compared to 1-2 μm for SBA-15), and their non-

organized porous structure. The latter is the result of the method used for synthesis, which is an oil-in water emulsion consisting of water, octane, styrene and TEOS [87].

Siliceous mesostructured cellular foams (MCF) consist of ultra large pores, up to 40 nm in diameter, which are connected together through smaller windows of about 10 nm to 20 nm. The MCFs were introduced for the first time by Schmidt-Winkel *et al.*[83] and similarly to HMM particles, MCFs are synthesized in an oil in water emulsion. This silica material with cage-like structure has an additional advantage compared to SBA-15 and HMM. The windows through the pores create more space to host a higher amount of enzymes, and also the window size is always smaller than the size of the pore opening which makes the leakage diminished [58, 114].

In Papers I and II, SBA-15 (in different pore and particle sizes) and HMM (only one size) have been used as the supports for the given enzymes to study the translational and rotational mobility of enzymes during/after immobilization. The effect of varying particle size, pore diameter and enzyme hydrodynamic radius on the efficiency of enzyme immobilization was investigated.

MCF materials were used in Paper III together with SBA-15 to probe the pore microviscosity using enzyme-bound dye. The microviscosity changes were studied in different pore size, morphology and with using hydrophobic surface.

In Paper IV, the MCF materials used were well-tailored for the CO_2 reduction application. The pore size and the type of hydrophobic modification were, according to recent published papers [58, 59], the most suitable materials for obtaining a higher activity and stability.

In Paper V, the distribution and location of immobilized enzymes were visualized by TEM in different MCF and SBA-15. The efficiency of the different pore morphology was studied using stereology quantification.

The physical properties of SBA-15, HMM and MCF used in all the appended papers are summarized in Table 2.2, and Figure 2.3 shows the schematic illustration of pore morphology in mesoporous silica particles used in this thesis.

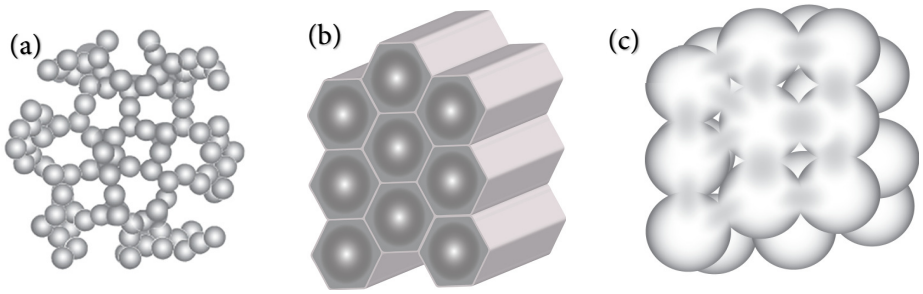

Figure 2.3. Schematic illustration of pore morphology in (a) HMM, (b) SBA-15, (c) MCF mesoporous silica particles.

Table 2.2. Physical properties of mesoporous silica used in the thesis.

Silica material	Pore diameter (nm)	Window diameter (nm)	Specific surface area ($m^2.g^{-1}$)	Specific pore volume ($cm^3.g^{-1}$)	Particle size (nm)	Hydrophobic modification	Paper
HMM	9.1	---	463	0.91	40	---	II
SBA-15	9.4	---	606	1.03	300	---	II
SBA-15	9.3	---	502	1.18	1000	---	I, II
SBA-15	8.9	---	554	1.17	2000	---	II, III
SBA-15	6.0	---	986	1.08	2000	---	II
MCF2	26.5	11.2	523	1.94	---	---	III
MCF2-OC	24.8	11.2	453	1.67	---	Octyl groups	III
MCF12	33.0	13.0	375	1.84	---	---	III
MCF12-OC	32.7	13.0	325	1.68	---	Octyl groups	III
MCF	32.8	11.3	612	2.45	---	---	IV
MCF-MP	32.9	11.3	527	2.27	---	Mercaptopropyl groups	IV
SBA-15	6.8	---	749	1.13	---	---	V
SBA-15	10.0	---	370	1.00	---	---	V
MCF	26.8	10.7	485	1.81	---	---	V

3 Theory and Methodology

The work presented in this thesis is based mainly on spectroscopic studies, therefore a brief introduction to photophysics is provided in this chapter, together with descriptions of the techniques used. First, the basic principles of the interaction between light and matter is outlined including absorption and fluorescence concepts. Second, the chromophores used in different absorption and fluorescence assays are briefly described. To conclude the chapter the microscopy technique used in this thesis, transmission electron microscopy (TEM) is described.

3.1 Light-Matter interaction

Electromagnetic radiation includes radiation from very low energy like radio waves to very high energy such as gamma rays. Spectroscopy is, according to the IUPAC Goldbook, defined as "the study of physical systems by the electromagnetic radiation with which they interact or that they produce". Here the physical systems we will be concerned with are molecules and the

electromagnetic radiation will be limited to the near-infrared (NIR), visible light and near or middle ultraviolet wavelength ranges.

A molecule can, as a consequence of quantum mechanics, only take on certain, discrete energy levels, and we distinguish between rotational, vibrational and electronic energy levels. This implies that there is a well-defined energy difference between each level, and a molecule in an initial state can get excited to a final state if it absorbs light with energy equal to the energy difference (ΔE) between the two states. This is known as Bohr´s frequency condition [115] and is given as

$$\Delta E = E_{Final} - E_{Initial} = h.\nu \tag{3.1}$$

where h is Planck's constant (h=6.626·10^{-34} J.s) and ν is the frequency of the light. Light is subject to the wave-particle duality and can be described either as individual particles, photons or as waves of energy[116]. The energy of a photon (E) can be quantified by Planck's equation:

$$E = h.\nu \tag{3.2}$$

where h is Planck's constant and ν is the frequency of the photon. If instead a wave description is used, light can be thought of as a harmonic wave of an oscillating electric and magnetic field which are perpendicular to each other and to the direction of propagation [117]. The wave is characterized by the frequency of the oscillating fields (ν), which in turn can be related to the wavelength (λ) through speed of light (c = 3·10^{8} m.s^{-1}):

$$\nu = \frac{c}{\lambda} \tag{3.3}$$

If the incoming light matches an energy difference within the molecule, and if the oscillating electric field of light with the correct wavelength creates an oscillation in the electron cloud of a molecule. With these two conditions the molecule can be excited from initial state to final state with a higher energy. This transition occurs with the highest efficiency if the electric field of the light is polarized parallel to the transition moment. This quantum property known as the transition dipole moment determines the magnitude of the probability of the electronic transition from the initial state to the final state [117]. Here, we will focus our attention on

transitions between different electronic states that can be induced by light in the visible and UV regions.

3.2 Photophysics

When a photon is absorbed by a molecule, the absorbed energy will lead to a re-arrangement of the electrons within the molecule, and put the molecule in a higher energy state which is referred to as an excited state. Commonly this state is a singlet state with paired electrons denoted S_n, or in the case of unpaired electrons, it is called a triplet state (T_n). Both types of excited states are numbered in a serial order based on their energy gap relative to the ground state, *i.e.* the first singlet excited state is called S_1. Each electronic state is also associated with a number of vibrational states, which are closer together in energy compared to the difference between two excited electronic states. Once an excited state is formed, it can be deactivated either through non-radiative transitions or radiative (emission of light) transitions. The different photophysical pathways can be visualized in a Jablonski diagram, Figure 3.1, which shows the different excitation and de-excitation processes occurring when a molecule interacts with light.

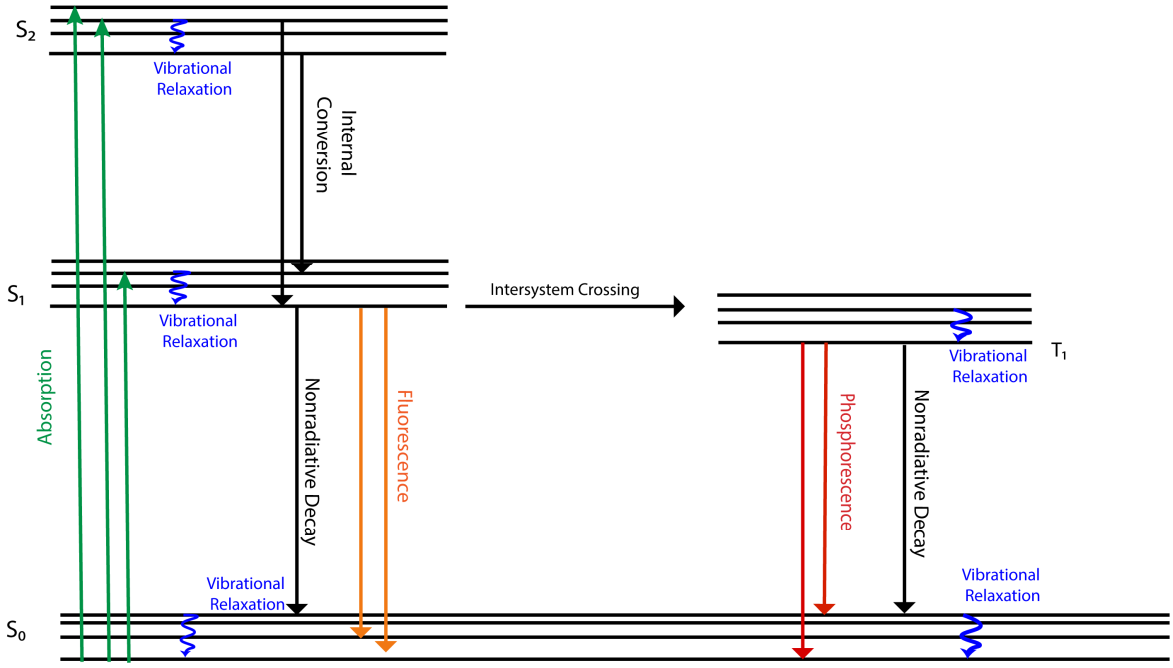

Figure 3.1. Jablonski diagram depicting different energetic transitions occurring in excited molecules.

The existence of vibrational states shows that for an excited molecule, there is a range of transitions that can be matched with Bohr's frequency conditions (Equation 3.1). The energy absorbed by the excited electron in S_1 can be distributed to different vibrational modes. The energy in these vibrations is quickly transferred to the surrounding environment by non-radiative transitions (vibrational relaxation), so that the molecule relaxes to the lowest vibrational state in S_1. According to Kasha's rule [118], relaxation to the lowest vibrational level of S_1 is faster than relaxation from S_1 to S_0. Therefore, emission from S_1 to S_0 will occur from the lowest vibrational level of S_1. The magnitude of the energy difference between absorption and fluorescence is referred to as the Stoke's shift. In some cases the molecule can relax via a process called inter-system crossing to a triplet state (Figure 3.1). Emission from this state to the ground state is called phosphorescence, but this process will not be further discussed in this thesis.

In addition to the wavelength, the intensity of the fluorescence is an important property of a fluorescent molecule. The intensity is dependent on the extinction coefficient of the molecule and on its fluorescence quantum yield (Φ_F) which is defined as the ratio between the number of photons emitted by a molecule as fluorescence and the amount of photons that is absorbed by the same molecule [16]. This relation can be described as:

$$\Phi_F = \frac{\text{Photons emitted}}{\text{Photons absorbed}} = \frac{\Gamma}{\Gamma + k_{nr}} \tag{3.4}$$

where Γ is the fluorescence rate constant and k_{nr} is the rate of non-radiative decay to the ground state (S_0). The fluorescence rate constant in the relationship represents the photons emitted while the sum of rate constants make up for all transitions. One way to measure the fluorescence quantum yield is using a reference substance with a known quantum yield (Φ_R),

$$\frac{\Phi}{\Phi_R} = \frac{I}{I_R} \cdot \frac{n^2}{n_R^2} \cdot \frac{A_R}{A} \tag{3.5}$$

where I is the integrated emission intensity, A is the absorbance at the excitation wavelength and n is the refractive index of the solvent in which the sample and reference is contained. R denotes the parameters corresponding to the reference compound. The product between the

quantum yield and the extinction coefficient is called the fluorescence brightness, higher brightness leads to better detection targets even with low concentration.

The fluorescence lifetime is another important photophysical property which is the average time the molecule spends in the excited state before emitting a photon. The lifetime is inversely proportional to the sum of rate constants involved in the transition from the excited state to the ground state [16]; the lifetime equation can be described as following:

$$\tau = \frac{1}{\Gamma + k_{nr}} \tag{3.6}$$

Absorption spectroscopy

An absorption spectrum is measured using a spectrophotometer which includes a light source, a monochromator and a detector (Figure 3.2). The monochromator selects a specific wavelength from the light, which then passes through the sample with an intensity (I_0). If the sample absorbs light of this wavelength, the intensity that is sensed by the detector (I) will be reduced compared to I_0. The absorption is dependent on the concentration (c) (the number of molecules), the path length (l) that the light travels within a sample (often in a quartz cuvette) and the extinction coefficient (ε) which is a factor that expresses the ability of the molecules to absorb light of a certain wavelength. This relation is described by Beer- Lambert law [119]:

$$A(\lambda) = \log \frac{I_0(\lambda)}{I(\lambda)} = \varepsilon c l \tag{3.7}$$

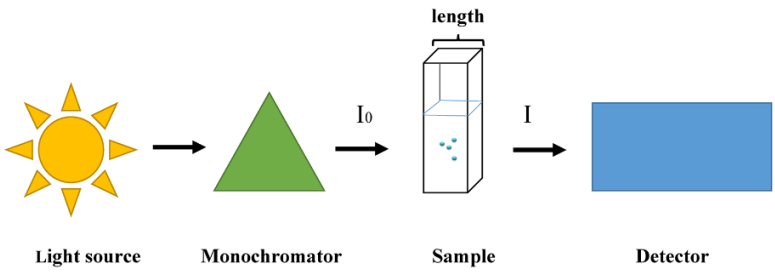

Figure 3.2. Schematic illustration showing a basic set-up of a spectrophotometer. The correct wavelength of the light (I_0) passes through the sample (I) with a defined path length (l) towards the detector.

Absorption spectroscopy is often used to determine the concentration of a sample with a known extinction coefficient (ε) [120, 121] and can also be used to monitor protein loading and pore filling (see Section 3.3).

Fluorescence spectroscopy

Fluorescence can be measured in general with two different techniques: Steady state and time-resolved. In steady state, the sample is excited with a continuous beam of light and the emission intensity is scanned over the wavelength range of interest. In time-resolved fluorescence the sample is exposed to a pulse of light where the pulse width is shorter than the decay time of the molecules in the sample. Once a population of molecules is excited with a radiation pulse, the initially excited population will decay over time to the ground state. Time-resolved measurement is a powerful analysis method to measure the lifetime of a fluorophore. The lifetime value is measured as a function of the rate constants depopulating the excited state. In other words, the lifetime value can be gained by studying the kinetics of the photophysical process.

It is noteworthy that a steady state measurement is simply an average of the time-resolved measurement over the intensity decay of the fluorescence. Therefore, much of the molecular information which can be taken from fluorescence can be lost during time averaging process. In this thesis, we took advantage of both techniques to characterize the pore microenvironment.

Steady state fluorescence can be monitored using a spectrofluorometer (fluorescence spectrometer) which is a common technique to record the emission and excitation spectra of a sample. Figure 3.3 shows the basic setup of a spectrofluorometer. This setup has a continuous beam of light (UV-visible light) that is directed through a monochromator used to select the correct radiation energy to excite the sample. The emission monochromator is scanned over the wavelength range of interest to collect the fluorescence spectrum. An excitation spectrum is measured in a similar way; however, this time the emission monochromator remains in a specific wavelength while scanning through the excitation energies. For many molecules, the excitation spectrum overlaps with the absorption spectrum. Also kinetic studies are possible where only one wavelength (monochromatic light) is used and the intensity of the fluorescence can be recorded over time. The main work performed in Paper I is based on this kind of kinetics measurement.

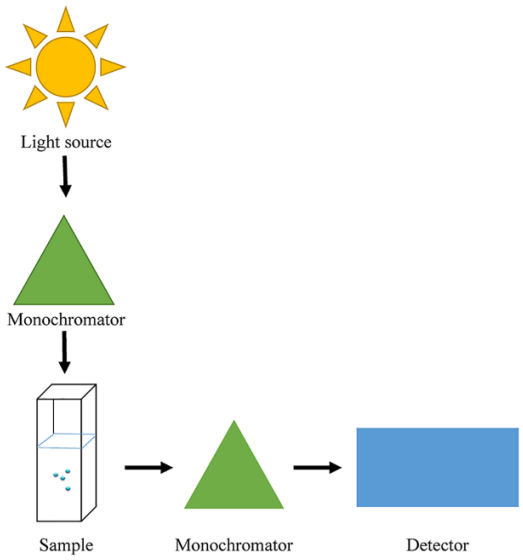

Figure 3.3. Schematic illustration showing a basic set-up of a spectrofluorometer. The correct wavelength of the light is selected by an excitation monochromator, led through the sample, then an emission monochromator and recorded by the detector.

The fluorescence lifetime is most commonly determined with the method called time correlated single photon counting (TCSPC). The principle is based on the proportionality between the probability of detecting a photon at a certain time after excitation and the fluorescence intensity at that time. A pulsed light source (laser) is used to excite the sample repeatedly and the time between excitation and the first photon reaching the detector is recorded (Figure 3.4). Every counted photon is collected in a channel with a specific time interval. Measurements are repeated until enough photons (often 10000 for statistical reasons) are counted in the top channel. To avoid artefacts it is important to ensure that it is impossible for two photons originating from the same pulse to reach the detector and there the count rate should be kept low. Finally, a histogram with the amount of photons counted per time interval, representing the fluorescence decay as a function of time, is constructed. The lifetime can be obtained by fitting the decay in the histogram to an exponential function. The instrument response function (IRF) is recorded, which represents the way the laser pulse is seen by the system. The IRF decay can be used in reconvolution fitting for having more accurate analysis of the measured decay. It should be noted that the emission intensity are measured in magic angle (54.7 °) as no polarization effect can be seen in this angle. The scattering effect of the MSPA particles is diminished.

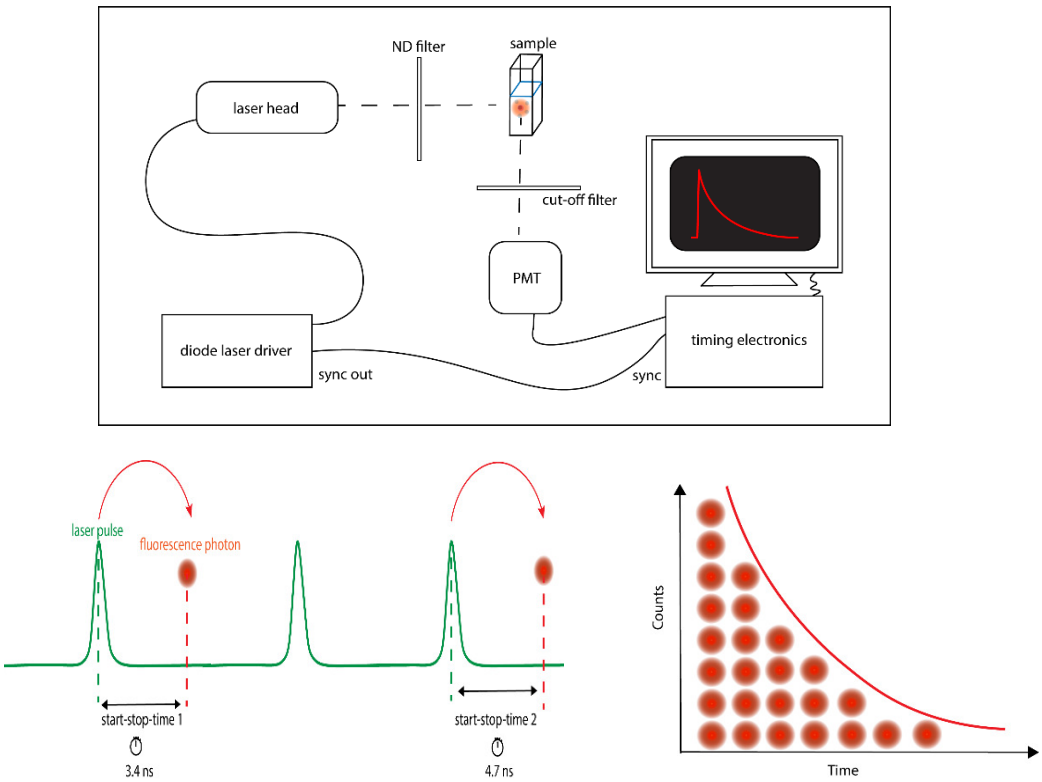

Figure 3.4. Schematic illustration showing a basic set-up of time correlated single photon counting (TCSPC).

Polarized fluorescence spectroscopy - anisotropy

When a fluorescent molecule is excited with polarized light, the resulting fluorescence emission is also polarized. However, the emitted light can be depolarized if the molecule rotates. The main cause of fluorescence depolarization is rotational diffusion of the fluorophore during its excited-state life. Therefore, by measuring the fluorescence depolarization the rotational mobility of a fluorophore can be determined. Fluorescence anisotropy measurements are made by exciting the fluorophore with polarized light and measuring the fluorescence intensity both parallel and perpendicular to the excitation polarization.

Figure 3.5 shows a fluorescence anisotropy spectroscopy setup with polarizers. Briefly, the light passes through an excitation polarizer that only allows light in one orientation to be transmitted, such as vertically oriented light. The light excites a fluorescent molecule in the sample and by rotation of the molecule, the orientation of the emitted light changes. By using an emission polarizer, the light with the same orientation as the excitation polarizer, vertical light can pass completely through the emission polarizer. If the light is perpendicular to the polarizer, it will be blocked.

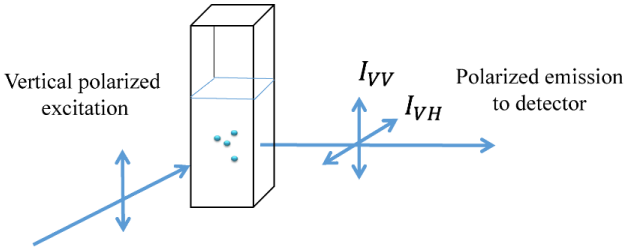

Figure 3.5. Schematic illustration showing a basic set-up of fluorescence anisotropy spectroscopy, where I_{XY} is the emitted intensity and the subscripts X and Y indicate the polarization directions of the excitation and emission light, respectively, with H and V referring to horizontal and vertical.

The anisotropy, *r*, is calculated from the intensities recorded with the emission polarizer arranged vertically (V) and horizontally (H), when the sample is excited with vertically polarized light. The G factor is the ratio of the sensitivities of the detection system for vertically and horizontally polarized light, which is measured using horizontally polarized excitation and correction factor for the instrument:

$$G = \frac{I_{HV}}{I_{HH}} \tag{3.8}$$

$$r = \frac{I_{VV} - GI_{VH}}{I_{VV} + 2GI_{VH}} \tag{3.9}$$

where I_{XY} is the emitted intensity and the subscripts X and Y indicate the polarization directions of the excitation and emission light, respectively; H and V referring to horizontal and vertical. When the sample is excited by linearly polarized light an average oriented excited population is generated. If the excited fluorescent molecules, fluorophores, are not allowed to move until they emit their energy, the emission will be polarized as well. This property is called fundamental anisotropy (r_0), it depends on the angle between the absorption and emission transition dipoles, β:

$$r_0 = \frac{2}{5}\left(\frac{3\cos^2\beta - 1}{2}\right) \tag{3.10}$$

The r_0 can be between -0.2 and 0.4, corresponding to an angle of 90° and 0°, respectively, between the absorption and emission transition dipole moments.

It is noteworthy that fluorescence anisotropy can be measured in both steady state and time-resolved techniques. In time resolved, the polarization plane of the fluorescence photon is determined by the actual orientation of the molecule at the moment of emission, shortly after the excitation. The time-resolved anisotropy *r(t)* will be considered as the kinetics of the process and it can be extracted from the decays of polarized emission components, using Equation 3.9. The TCSPC set-up can be used to measure time-resolved anisotropy by applying the excitation and emission polarizers to the set-up.

Absorption and fluorescence are powerful techniques that can be used to determine properties and monitor reactions and processes. The applications of absorption and steady state and time-resolved fluorescence spectroscopy used in this thesis are described below.

3.3 Photophysics in the thesis

3.3.1 Protein loading and pore filling in enzyme immobilization

A main property of an enzyme-particle system is the amount of immobilized enzyme per amount of particles. This value is usually reported as the mass of the immobilized enzyme per particle mass as called protein loading (P_{LD}) (mass of enzyme /mass of particle) [80, 95]. The most commonly used technique for measuring the amount of immobilized enzymes is an indirect method which consists of measuring the absorption of the solution surrounding the particles (supernatant). The particles are sedimented by centrifugation, the supernatant is separated and the amount of free enzymes (non-immobilized enzymes) is measured using absorption spectroscopy. However, this method cannot be completely suited, if the percentage of enzyme leakage from the particles is high during an enzyme-catalyzed reaction [122-125]. By using this indirect method, the degree of immobilization has been calculated in all papers of this thesis.

This P_{LD}-value cannot fully represent the actual amount of protein in the pores, since it depends on variations in pore volume of the particles. Therefore, a suitable parameter to describe protein concentration in the pores is pore filling (P_f) which is defined as the fraction of the pore volume that is occupied by the proteins [88]:

$$P_f = \frac{V_{prot}}{V_{pore}} = \frac{\frac{4\pi}{3} R_H^3 N_A P_{LD}}{M_W V_{pore}} \quad (3.11)$$

where the volume V_{prot} of (hydrated) protein is obtained from the hydrodynamic radius of the protein (R_H), protein loading (P_{LD}), Avogadro's number (N_A) the molecular weight of protein (M_w), and the V_{pore} is the specific pore volume per gram of particles which can be measured by nitrogen adsorption-desorption method. To calculate the number of proteins per particle (N_{prot}) the following equation can be used [88]:

$$N_{prot} = \frac{N_A P_{LD} \rho_{part} V_{part}}{M_W} \quad (3.12)$$

V_{part} is the average volume per particle estimated as a sphere with diameter (D) and ρ_{part} is the density of the (dry porous) particles calculated from the particle porosity Φ as

$$\rho_{part} = \rho_{silica}(1 - \Phi) = \rho_{silica} \frac{1 - V_{pore}}{V_{pore} + \rho_{silica}^{-1}} \quad (3.13)$$

where ρ_{silica} = 2.196 g cm^{-3} is the density of amorphous silica [88, 126]. ·

In all the papers of the thesis, the protein loading (P_{LD}) values were measured using absorption spectroscopy in order to calculate the degree of immobilization. In Paper II and Paper III, the pore filling of the samples (P_f) was calculated for more accurate comparison between different mesoporous silica.

3.3.2 Rotational mobility of free and immobilized enzymes

The fluorescence anisotropy of a fluorophore is used to measure the protein rotational mobility on the time scale of the fluorescence lifetime. Rotational mobility can be defined as correlation rotational time (the time it takes the protein to rotate by one radian) based on Perrin equation for a protein with lifetime (τ) as follows [16, 127]:

$$r = \frac{r_0}{1 + \frac{\tau}{\theta}} \tag{3.14}$$

where the rotational correlation time (θ) is related to the steady state anisotropy (r) and fundamental anisotropy (r_o). For a spherical protein with radius R, the rotation correlation time (θ) is given by [16]

$$\theta = \frac{\eta \frac{4}{3} \pi R^3}{k T} \tag{3.15}$$

where η is the solution viscosity, k is Boltzmann constant and T the temperature.

It should be noticed that in the system of proteins immobilized in porous particles, there is an additional process which is the rotation of the whole MPS particle This rotation can potentially affect the anisotropy based on Soleillet theory about depolarization [128], occurring with a rotational correlation time (θ_{part}). To what degree each process can affect the whole system is dependent on how strong proteins are immobilized into the particles. For example, in the case of a protein which is strongly adsorbed to the pore wall the rate of rotation will be zero relative to a coordinate system fixed to the particle, it means the rotational correlation time of protein goes to infinity ($\theta_{prot} = \infty$), but the protein may still rotate as a consequence of the rotation of the particle if it is fast enough. A more detailed interpretation can be found in the Paper II for the lipase immobilization in mesoporous silica.

3.3.3 Förster resonance energy transfer (FRET)

FRET is a process in which energy is transferred non-radiatively via long-range dipole-dipole coupling from an excited donor fluorophore to another molecule or acceptor which does not need to be fluorescent. To observe FRET between a fluorophore pair (donor-acceptor), there are few conditions that must be satisfied; (*i*) the fluorescence emission spectrum of the donor molecule must overlap the absorption spectrum of the acceptor chromophore, (*ii*) The two fluorophores (donor and acceptor) must be in the close proximity to one another (typically 1 nm to 10 nm), (*iii*) The transition dipole orientations of the donor and acceptor must be approximately parallel to each other [129, 130].

The transferred energy between two fluorophores is evaluated and presented by a direct measure of the fraction of photons absorbed by the donor that is transferred to an acceptor. It can be calculated as the ratio of the transfer rate (k_T) to the total decay rate of the donor,

$$E = \frac{k_T}{(\tau_D^{-1} + k_T)} \tag{3.16}$$

where τ_D is the lifetime of the donor in the absence of acceptor.

The transfer efficiency (E) can experimentally be measured using the relative fluorescence intensity of the donor in the absence (F_D) and presence of acceptor (F_{DA}), and also with time-resolved measurements by the relative lifetime of the donor in presence (τ_{DA}) and absence (τ_D) of the acceptor [16], as following

$$E = 1 - \frac{F_{DA}}{F_D} = 1 - \frac{\tau_{DA}}{\tau_D} \tag{3.17}$$

Since E depends on the inverse of the sixth power of the distance (r) between the two fluorophores (Equation 3.18), FRET has become the technique to study protein-protein interaction and to measure distances between fluorophores [131, 132]. R_0 is defined as the Förster distance and represents a characteristic parameter of every fluorophore pair defining the distance where the transfer efficiency is 50%.

$$E = \frac{R_0^6}{(R_0^6 + r^6)} \tag{3.18}$$

The Förster distance [133] depends on the overlap integral of the donor emission spectrum with the acceptor absorption spectrum and their mutual molecular orientation. The R_0 value is defined as following [102, 133]:

$$R_0 = 0.211(k^2 n^{-4} \Phi_D J(\lambda))^{1/6} \tag{3.19}$$

where Φ_D is the fluorescence quantum yield of the donor in the absence of the acceptor, $J(\lambda)$ is the spectral overlap integral between the normalized donor fluorescence and the acceptor excitation spectra, κ^2 is the dipole orientation factor between donor and acceptor transition moments and n is the effective refractive index. The unit of R_0 is based on Angstrom (Å).

Figure 3.6 represents the dependency between the energy transfer efficiency (E) on the distance between a fluorophore pair (r).

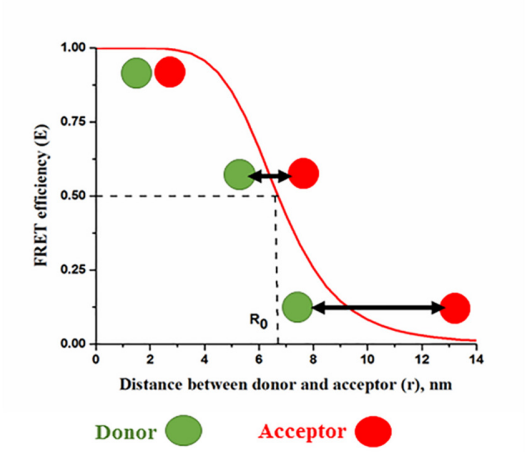

Figure 3.6. FRET efficiency vs the distance between donor and acceptor.

3.4 Chromophores

Spectroscopic techniques are used in order to investigate the structure of the molecules as well as their physical chemistry in different conditions. There are different absorbance and fluorescence assays *i.e.* Bradford or in general colorimetric assays [134-136], which can be used in spectroscopic studies. However, these assays are always based on either intrinsic protein chromophores or an extrinsic dye which can be attached to the enzyme covalently [137, 138]or non-covalently [139, 140].

3.4.1 Intrinsic or natural chromophores

Absorption. Protein chromophores are the peptide bonds and the aromatic amino acid residues, tyrosine, tryptophan and phenylalanine. The absorption spectrum of proteins is

characterized by two maxima, at 200 nm (peptide bonds) [141] and 280 nm (if the protein has aromatic residues) [16].

The absorption properties of the peptide bonds at 200 nm can be used to investigate the secondary structure using circular dichroism [142]. The molar absorptivity of a protein might be predicted for proteins with no tyrosine or tryptophan residues [143]. The protein concentration can be measured through absorption measurement of peptide bonds at 200 nm [144]. However, a number of other substances used in protein solution can absorb light in this range of wavelength such as alkenes or carbonyl compounds. Therefore, to obtain a reliable data at 200 nm the proteins must be purified to make them free of any other chemicals and also the buffers should be chosen carefully [145].

The maximum absorption at 280 nm is observed based on the aromatic amino acid residues and can be used for calculating the protein concentration using Beer-Lambert equation (Equation 3.7) [119]. This is a common and simple way of measuring the protein concentration. There is no limitation for using different buffers, since buffer components usually do not absorb light in this absorption range (Figure 3.7a). Moreover, the aromatic amino acid composition is an important factor for calculating the extinction coefficient (molar absorptivity) of each protein. The extinction coefficient of a protein can be determined experimentally by using solutions with known concentration or based on the amino acids data composition [120, 121]. A main drawback of this method is the nucleic acids contamination that can be present in biological samples. Since the nucleic acids can absorb light at 260 nm strongly they can interfere with the protein measurements. However, there is a way to calculate the protein/nucleic acid ratio and correct the nucleic acid contamination from the measurements [123, 146, 147].

Fluorescence. The intrinsic fluorescence of a folded protein is a mixture of the fluorescence from individual aromatic residues, phenylalanine (Phe), tyrosine (Tyr) and tryptophan (Trp). The maximum of emission spectra for proteins can be in a range of wavelength from 250 nm to 400 nm (starting with phenylalanine and ending with tryptophan) (Figure 3.7b). In steady state measurements, the peak can be seen at 350 nm, which shows that tryptophan has higher impact on the emission spectra. There is a possibility of peak shifting to longer wavelengths with changing polarity of the local environment of the residues due to solvent relaxation [16]. Fluorescence from aromatic residues gives valuable information about the structure, folding, binding interactions of proteins [16]. Furthermore, one of the main advantages of using

intrinsic fluorescence is that a native protein can be studied with no changing in its structure [148, 149].

Since Tryptophan (Trp) has the higher contribution in fluorescence measurements compared to phenylalanine and tyrosine in proteins, a large number of studies have been aimed to investigate the mobility and rotational freedom of tryptophan residues in various enzymes. By using this knowledge the mobility of the enzyme can be distinguished from the mobility of tryptophan residues [127, 149-152]. In Paper II, the rotational mobility of enzymes after confinement in mesoporous silica has been studied using absorption and fluorescence of the aromatic residues in lipase (MML) and bovine serum albumin (BSA).

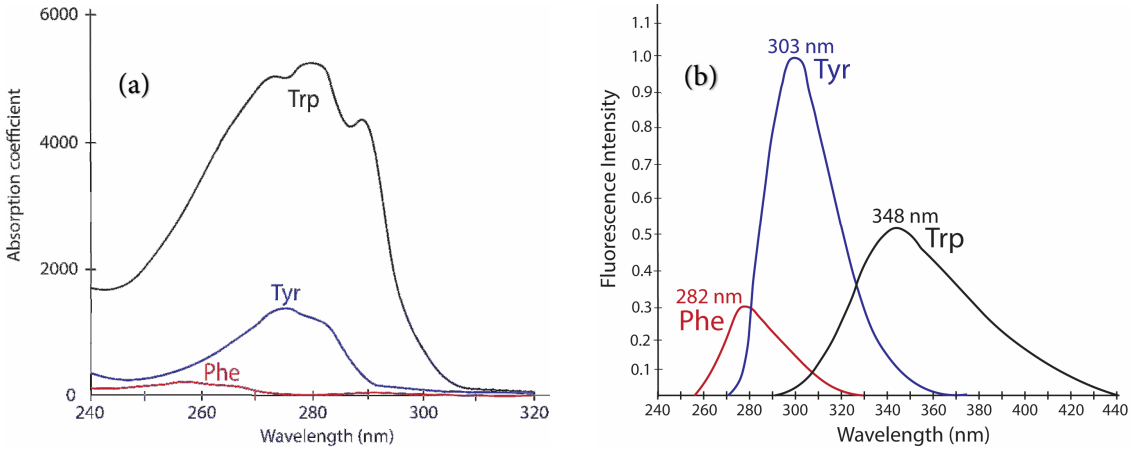

Figure. 3.7. (a) Absorption and (b) emission spectra of aromatic amino acid residues in proteins, Trp (Tryptophan), Tyr (Tyrosine), Phe (phenylalanine). Redrawn from principles of fluorescence spectroscopy 3rd edition by Lakowicz [16].

3.4.2 Extrinsic chromophores

Since most of the interesting molecules are non-fluorescent or in some cases the intrinsic fluorescence is not enough for a desired experiment *i.e.* DNA and lipids, fluorescence can be obtained by labeling the molecules with extrinsic chromophores. In early 1950, the first generation of extrinsic probes which can be attached to proteins was discovered, these probes could be excited in longer excitation wavelength compared to the aromatic residues of proteins. For example, Dansyl Chloride was introduced as an extrinsic dye by Gregorio Weber with excitation and emission wavelength at 350 nm and 520 nm, respectively [123, 153]. Today, many extrinsic probes (dyes) are available commercially with a specific sensitivity to micro-environmental changes [16]. The extrinsic probes can be attached to the enzymes either non-

covalently such as styryl dyes [154], ruthenium complexes [155] or covalently through the reaction with amino group on the enzyme such as SNARF-1[57].

Absorption. The spectrum absorption of the enzyme labeled with an extrinsic dye usually has two maxima, one at 280 nm which shows the maximum absorption of the enzyme per se and the second one is the wavelength for the maximum excitation of the dye. Based on the correction factor of the dye at 280 nm, the concentration of the enzyme can be calculated correctly. Moreover, the degree of labeling, *DOL*, (number of dyes per enzyme) can be reported based on the enzyme and dye concentration.

Fluorescence. One of the advantages of using extrinsic dyes is their sensitivity to the microenvironment based on their structure. In this thesis, three different extrinsic dyes have been used. Choosing a proper dye for enzyme immobilization in mesoporous silica can be challenging. It is better that the probe is bound to the protein covalently for making sure that the enzyme and dye experience the same local environment. Moreover, the probe should be negatively charged to prevent interactions with the negatively charged silica wall, and also have a high photostability.

In Paper I, epicocconone was used to monitor the immobilization process in real time based on being sensitive to microviscosity [156, 157]. This dye is only weakly fluorescent in water (emission at 420 nm) but becomes highly fluorescent (emission at 605 nm) in the presence of proteins. Epicocconone can be bound to the amine group of the protein covalently and it has a long Stokes' shift (almost 100 nm). Therefore, it is less affected by Rayleigh scattering and can be multiplexed with more common fluorescent dyes. It has been reported that the labeling of proteins with epicocconone can be dissociated and the stability of the labeling is pH dependent; the more acidic condition, the higher stability [158, 159].

The molecular structure and the excitation and emission spectra of epicocconone-attached BSA can be found in Figure 3.8, also Table 3.1 shows the spectral properties of this dye.

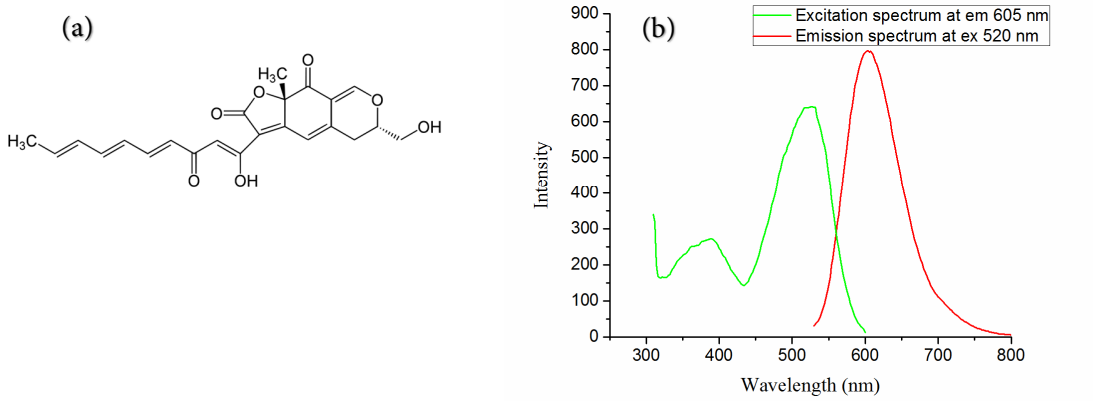

Figure 3.8. (a) Epicocconone molecular structure, (b) excitation and emission spectra of epicocconone attached BSA.

In Paper III and Paper IV, two different carbocyanine dyes, Sulfo-Cyanine3 NHS ester (denoted Cy3) and Sulfo-Cyanine5 NHS ester (denoted Cy5) were used, first as molecular rotors to measure the viscosity inside mesoporous silica and second as a donor-acceptor pair in the FRET study. The spectral properties of these two dyes can be found in Table 3.1 as well as the molecular structure in Figure 3.9.

Table 3.1. Spectral properties of epicocconone and the carbocyanine dyes

Fluorescent dye [a]	Ex [b] (nm)	Em [c] (nm)	Φ [d]	Ɛ [e] ($M^{-1}cm^{-1}$)	CF_{280} [f]	M_w [g] (Da)
Epico	520	605	0.21	11200	0.76	410
Cy3	550	565	0.1	162000	0.06	735.80
Cy5	650	665	0.2	271000	0.13	777.95

a. Epico: epicocconone; Cy3: Sulfo-cyanine3 NHS ester; Cy5: sulfo-cyanine5 NHS
b. Maximum excitation wavelength
c. Maximum emission wavelength
d. Fluorescence quantum yield in water; for Epico provided from [160], for the carbocyanine dyes provided by the supplier.
e. Extinction (molar absorption) coefficient at excitation wavelength; for Epico provided from [158], for the carbocyanine dyes provided by the supplier.
f. Correction factor at 280 nm wavelength for calculation degree of labeling; provided by the supplier
g. Molecular weight; for Epico provided from [160], for the carbocyanine dyes provided by the supplier.

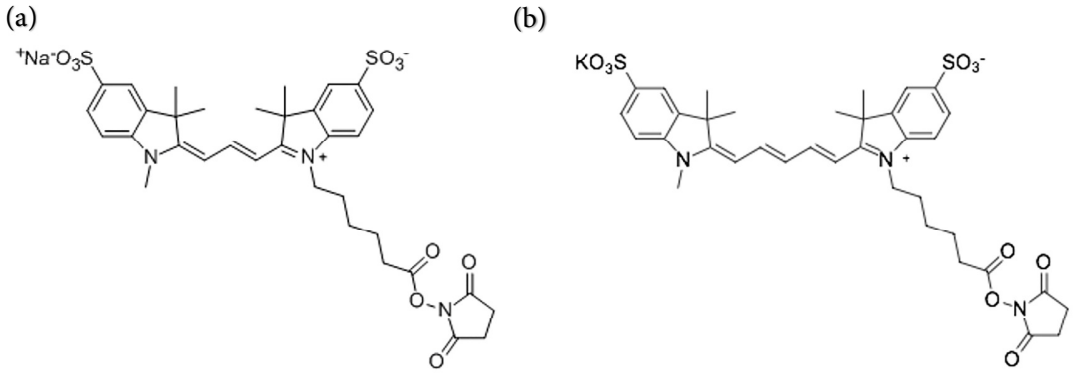

Figure 3.9. Molecular structure of (a) Cy3: Sulfo-Cyanine3 NHS ester,(b) Cy5: Sulfo-Cyanine5 NHS

Both Cy3 and Cy5 can be considered as fluorescent molecular rotors which are defined as sensors of microenvironmental changes. Their fluorescence (spectrum shape and intensity) can change if their rotation is restricted. It has been suggested that the change of fluorescence intensity is caused by the restriction of intramolecular rotational relaxation [161]. These two dyes are also well-known as a FRET pair, since the absorption spectrum of the Cy5 used as acceptor is overlapped with the fluorescence emission spectrum of the Cy3 used as donor, see Section 3.3 [129, 162].

These two dyes are photostable, negatively charge and can be bound covalently to the amine group of the protein through the activated NHS (N-hydroxysuccinimide) ester group. In Paper III and Paper IV, the degree of immobilization was determined indirectly by measuring the absorption of protein-attached Cy3 and Cy5 in the supernatant after the immobilization. The absorption spectra of Cy3, Cy5 and the enzyme, with the maximum of absorption at 550 nm, 650 nm and 280 nm, respectively, are well separated in the UV-visible region (Figure 3.10). The foundation of Paper III and Paper IV is based on the fluorescence spectra of the labeled enzymes which will be discussed in Chapter 5 and Chapter 6.

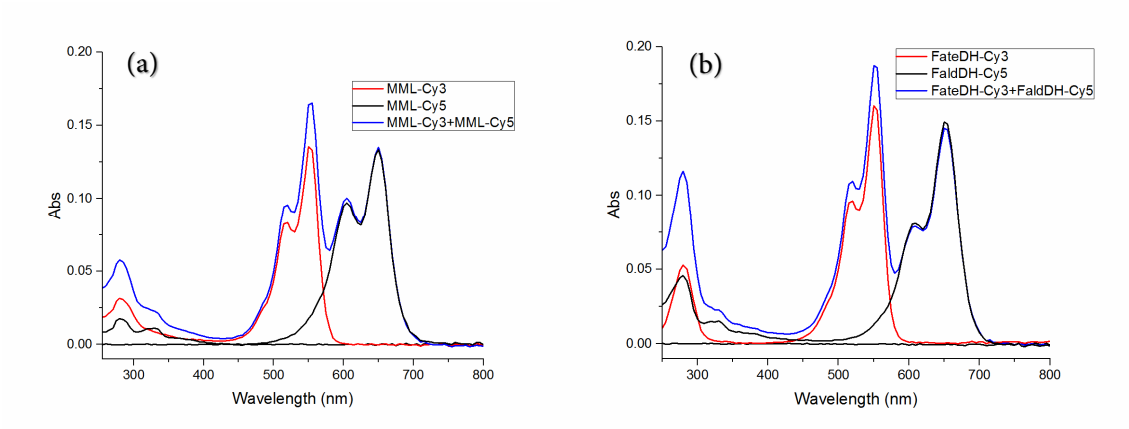

Figure 3.10. Absorption spectra of labeled enzymes, (a) MML-Cy3 and MML-Cy5 from Paper III, (b) Cy3-FateDH and Cy5-FaldDH from Paper IV; Individual samples (red and black lines), mixing of two labeled enzymes (blue line). The blue line is the same as the sum of the two other lines. The peak at 280 nm is the excitation wavelength for enzymes; excitation wavelength maximum at 550 nm related to Cy3; excitation wavelength maximum at 650 nm related to Cy5.

3.5 Transmission electron microscopy (TEM)

Transmission electron microscopy (TEM) is a microscope technique that utilizes electrons to visualize specimens with a magnification up to 10^6. It is possible to obtain a resolution in the range of 1 Å due to the short wavelength of electrons. An electron beam is accelerated in vacuum at high voltages through a thin sample. The image is obtained by focusing the electron beam onto the specimen (Figure 3.11). The objective lens situated below the sample together with several intermediate lenses forms the image from the transmitted electrons. Finally, the projector lens enlarges the image and projects it onto a fluorescent screen. Thicker regions in the sample scatter more electrons compared to thinner regions. Therefore, thicker regions with high scattering will appear darker on the screen than thinner regions. In this work, TEM microscopy was used together with immunogold staining to determine the distribution of immobilized enzymes in different mesoporous silica.

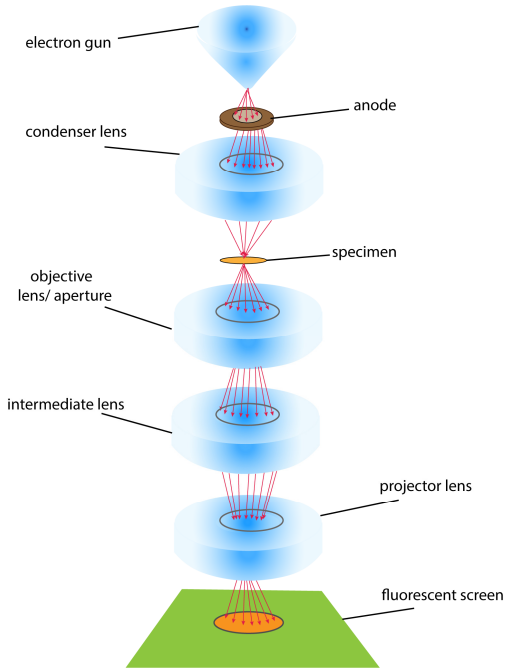

Figure 3.11. Transmission electron microscopy

3.5.1 Immunogold staining

Immunogold staining (IGS) is a staining technique often used in electron microscopy. In this staining technique, colloidal gold particles are most often attached to secondary antibodies, in sequence the secondary antibodies are attached to primary antibodies which are designed to

bind a specific antigen or enzyme (Figure 3.12). The size of gold particles used in this technique is usually between 5 nm to 20 nm in diameter. The gold nanoparticles have an excellent electron scattering property because of high electron density. Therefore, the electron beam cannot be transmitted through the gold particle and causes a high contrast such as dark spots in the TEM image. The two most widely used immunogold labeling techniques are the "pre-embedding" and "post-embedding" techniques. In Paper V, the post-embedding technique has been used which means that the staining is performed on the sample after resin embedding and sectioning the samples. To quantify the amount of immobilized enzymes in different mesoporous silica, stereology method was used. This method provides practical techniques for extracting quantitative information about a three-dimensional material from measurements made on two-dimensional planar sections of the material. This method is based on random, systematic sampling to provide unbiased and quantitative data [163]. It is noteworthy that in Paper V, all sample sections are considered as unbiased systematic random sampling. Since the sectioning was done from different regions of the sample, all the enzymes had the same chance of being in the section.

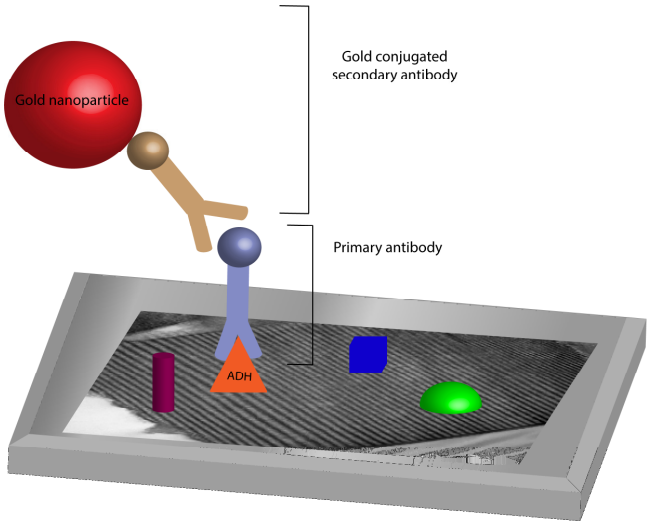

Figure.3.12. Schematic view of IGS preparation based primary antibody, secondary antibody conjugated gold nano particle

Original Work

In the second part of the thesis, the original work that constitutes the foundation for this thesis is summarized. Further details can be in the appended papers. A brief introduction to the scientific questions addressed is provided together with a summary of the results. Moreover, some unpublished results are included in order to provide a wider picture of the original work. Chapter 4 regards the studies on the dynamics of the enzyme immobilization, as published in Paper I and II including some unpublished results. Chapter 5 concerns the work on the characterization of the microenvironment of mesoporous silica particles, as discussed in Paper III. Finally, Chapter 6 summarizes the work on the distribution of enzymes after immobilization in mesoporous silica particles as described in Paper IV, V.

4 Dynamics of Enzyme Immobilization in Mesoporous Silica

In this chapter, the results of the main works in Paper I and II are presented. The main core of this chapter is the dynamics of enzyme immobilization, which includes the translational mobility of the enzymes while immobilizing into mesoporous silica particles through a real-time method, and also the rotational mobility of the enzymes after immobilization into mesoporous silica.

4.1 Real-time monitoring of enzyme immobilization into mesoporous silica

In the first part of my PhD, our main aim was to understand the mechanism of the enzyme immobilization. In other words, the aim was to investigate the mechanistic steps of enzyme transporting into the pores of the mesoporous silica materials. The most common methods used for monitoring the immobilization process are based on indirect methods. In these methods, the free enzymes in the solution surrounding the silica particles are studied, after the enzyme-particle suspension has been centrifuged. Although, this technique was performed to

monitor the kinetics of the immobilization [53, 88], there are a number of limitations that make the indirect method not very desirable for characterizing the immobilization mechanism. The most important limitation is the low time resolution because of the time consuming techniques used to measure the free enzyme concentration such as the Bradford method [122]. At that time, Thörn *et al.* reported that the enzyme immobilization in mesoporous silica can be monitored directly by using quartz crystal microbalance with dissipation monitoring (QCM-D) [164]. In the QCMD approach, the enzyme immobilization can be studied based on the changes of mass and viscoelastic properties of the silica materials adsorbed to a macroscopic surface. The study showed that a higher amount of enzymes are immobilized into mesoporous silica than into nonporous particles and onto a flat silica surface. This study and our eagerness to understand the mechanisms behind the immobilization were the main motivations to develop a direct method that can be used actually in samples with particle suspensions instead of flat silica films.

A large number of fluorescence spectroscopy studies have been performed to investigate the effect of immobilization on the behavior of the enzymes and their microenvironment [106, 107, 165, 166]. In some cases, the enzymes have been labeled with a fluorescent dye which is identified for a specific study. Therefore, in Paper I, we proposed a fluorescence assay to monitor the enzyme immobilization in real-time by taking advantage of fluorescence spectroscopy and epicocconone as the used dye. The immobilization of three different proteins, lipase (MML), bovine serum albumin (BSA), and glucose oxidase (GOX) into SBA-15 mesoporous silica particles with 9.3 nm pore diameter was monitored over time. The main reason to work with this size of pore and these enzymes was two studies that Gustafsson *et al.* performed previously. They reported that MML can have a higher activity, and higher stability can be seen for GOX in the MPS particles with 4.6 nm pore radius (R_{pore}) compared to other pore sizes [53, 167]. The proteins were labeled with the dye epicocconone which binds to amine groups of proteins forming a fluorescent product with excitation maxima at 390 nm and 520 nm and an emission maximum at 605 nm. The reader is referred to section 1.2.1, 2.6 and 3.4 for more details about physico-chemical properties of the materials.

The interaction between all three labeled proteins and the MPS particles (R_{pore} = 4.6 nm) were monitored in real time by measuring the emission intensity versus time at the emission maximum at 605 nm. In Figure 4.1, upper curves show the emission time profiles for the epicocconone-MML conjugate after particles were added at $t = 0$ min in three different SBA-15 concentrations. It is noteworthy that the SBA-15 particles were added after 10 min of

equilibrium time. The concentration of the proteins was kept constant, and only the silica particle concentrations were changed between 0.0018 and 0.360 g/l. The lower curve (black curve) in Figure 4.1 shows the intensity profile for the reference sample (no particles), when it is subjected to the same illumination as the samples containing particles. It is seen that the reference sample exhibits a steady decrease in intensity during the illumination due to bleaching of the dye.

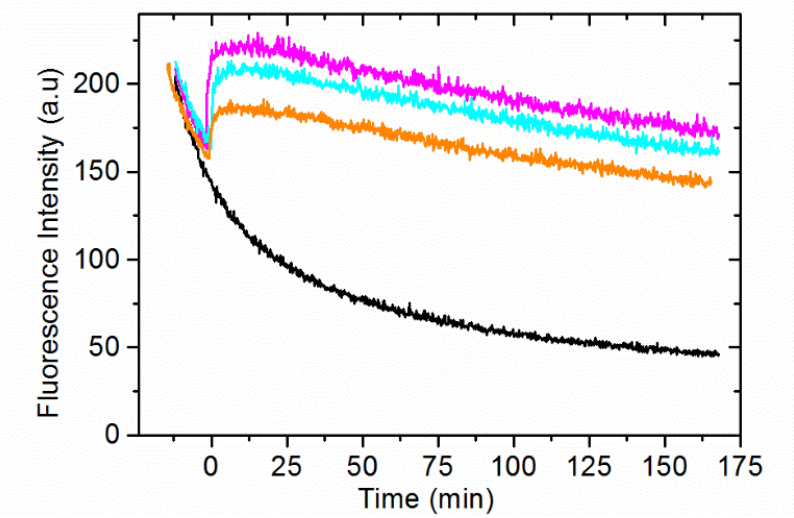

Figure 4.1. Raw data on the emission intensity time profiles after mixing the epicocconone–MML conjugate with the MPS particles at concentrations of 0.043 g/L (magenta, top decay), 0.036 g/L (cyan, second decay from top), 0.026 g/L (orange, third decay from top), and the reference conjugate sample with no particles (black, bottom decay). Particles were added at t = 0 min, emission wavelength: 605 nm; excitation at 520 nm.

4.1.1 Quantifying the kinetics of enzyme immobilization

To quantify the rate of enzyme immobilization for each protein, the recorded emission time profiles of the samples at 605 nm (Figure 4.1) were corrected for photochemical bleaching of the protein-dye conjugate by subtracting the corresponding intensity profile of the particle-free reference sample. We made the assumption that the bleaching processes are not affected by the presence of the particles.

The resulting intensity profiles *I(t)* were fitted to a single exponential growth function

$$I = I_o + A(1 - e^{-k't}) \qquad (4.1)$$

Where I_o is the intensity before the particles are added (defined as $t = 0$) and k' a (pseudo first order) rate constant.

Figure 4.2 shows the corrected time profiles obtained in this manner for MML at three different particle concentrations, using the data in Figure 4.1. In the upper panel of Figure 4.2, the black curves show the corrected data and the solid lines are the fits to a single exponential growth (as shown in Equation 4.1) with the 95% confidence interval for the fits (the dotted lines). The lower panel in Figure 4.2 shows the residuals between the corrected experimental data and the exponential fits. The values of the rate constant k' obtained from the fits in Figure 4.2 (0.10, 0.09 and 0.07 min^{-1} for 0.043, 0.036 and 0.026 g/l SBA-15, respectively) show that a higher SBA-15 concentration leads to a faster interaction with the proteins.

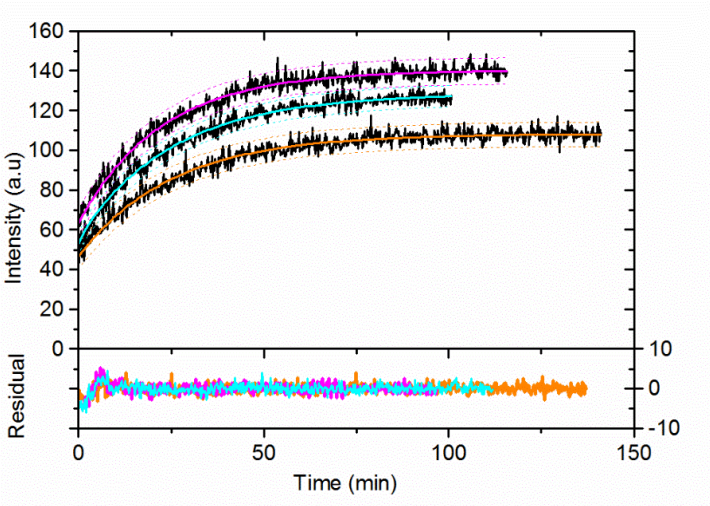

Figure 4.2. Bleaching-corrected emission intensity time profiles during immobilization of epicocconone–MML conjugate in the MPS particles and fitting to a single exponential growth model. Upper panel: Emission traces recorded at particle concentrations of 0.043 g/l (magenta, top decay), 0.036 g/l (cyan, middle decay), and 0.026 g/l (orange, bottom decay).

The full set of emission time profiles for the epicocconone conjugates with MML, BSA, and GOX in the presence of the particles at different concentrations was analyzed in the same manner. Figure 4.3 shows the fitted constants k' for all three proteins plotted versus the MPS particle concentration. The results confirm that the rate constant (k') increases with increasing particle concentrations for all three proteins. It should be mentioned that each data value in Figure 4.3 was obtained from the average of three independent experiments in each particle concentration.

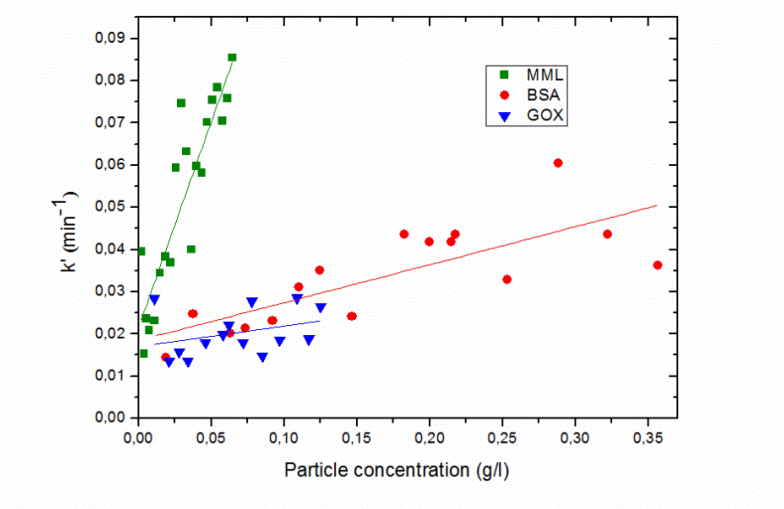

Figure 4.3. Pseudo-first-order rate constants k′ versus SBA-15 particle concentration for GOX (blue inverted triangles), BSA (red circles), and MML (green squares). Solid lines are least square linear fits.

4.1.2 Mechanism of enhanced emission intensity after adding the particles

The presence of the particles can change the fluorescence intensity of the dye in at least two ways, (*i*) the light scattering by the SBA-15 particles affects the fluorescence measurements, (*ii*) the quantum yield of the dye can be altered due to microenvironmental changes in the pores compared to the surrounding bulk solution. In general, the MPS particles scatter light according to Rayleigh [168] or Mie [169] theory depending on the particle size; when the particles are added both types of scattering are expected to reduce the detected emission. Firstly, the number of excitation events is reduced by the lower photon flux of excitation light, and secondly the emitted light may also be scattered and not reach the detector. Furthermore, scattering effects are expected to appear instantaneously when the MPS particles are added to the fluorescent sample, thus these effects cannot explain the slow rise over tens of minutes or longer that we observe. Therefore, a more likely explanation for the enhanced emission in Figure 4.2 is that it reflects a change in the fluorescence quantum yield of the dye when the labeled proteins interact with the particles. Importantly, a different microenvironment inside the MPS particles will affect the dye fluorescence when the epicocconone is brought inside the pores by the proteins (or possibly in contact with the external particle surface). It is noteworthy that the emission increase cannot be explained by the particles protecting the dye partially from bleaching because then the intensity should still decrease, albeit more slowly. Therefore, the increase in intensity with time most likely reflects an increased quantum yield due to the proteins interacting with the MPS particles.

Fluorescent dyes are in general sensitive to the local environment including its polarity, pH and microviscosity [16], which can be reflected in changes in spectral shape, emission intensity or both. Studies of epicocconone interacting with cyclodextrines [157] and surfactant assemblies [156] indicate that an enhanced local viscosity increases the emission intensity with unchanged spectral shape as we observe in the presence of the MPS particles, whereas polarity is reported to have no detectable effect on the fluorescence properties of epicocconone. Both experimental NMR studies [170] and theoretical simulations [171] showed that at least close to the pore wall the water molecules are slowed down by interactions with the silica surface. Therefore, an enhanced microviscosity upon immobilization can be expected and consequently the emission intensity of epicocconone increases.

4.1.3 Protein-particle interaction and the effect of the protein size

The main difference between the proteins studied in paper I is their size. There is a less significant difference in their isoelectric points (see Table 1.1, Chapter 1). In fact, all three proteins have a negative net charge at the pH 6 used in the immobilization experiments. Therefore, the binding to the negatively charged silica surface of the MPS particles probably is driven by a multitude of weaker hydrogen bonding. This leads us to assume that size rather than binding affinity is the most important difference between the three proteins. All three proteins have an approximate globular shape, and can be modeled as spheres with an effective radius equal to the hydrodynamic radius (R_H).

A second-order rate constant (k) for each protein was obtained from the solid line slopes in Figure 4.3. The k value for MML, BSA and GOX, respectively, was reported to be 0.97 ± 0.02, 0.09 ± 0.02, and 0.04 ± 0.02 $(g/l)^{-1}min^{-1}$.

Figure 4.4 shows how the rate constant k depends on the ratio of R_H/R_{pore} where R_{pore} is the average pore radius of the SBA-15 particles. It is seen that an increased protein size has a strong retarding effect on the immobilization with an approximately 25-fold lower rate for GOX compared to MML. The resulting values show that k decreases strongly with increasing protein size (See Figure 4.4). The derived second-order rate constant k varies with the protein hydrodynamic radius according to $k \sim R_H^{-4.70\pm0.01}$ which is stronger than expected for diffusion. The predicted scaling (k_d) is $k_d \sim R_H^{-1}$ if the reaction between protein and particles is under diffusion control (See Paper I for more details). The significant stronger scaling than R_H^{-1}

indicates that the rate limiting step at high particle concentrations is not the diffusional encounter between proteins and particles but more likely the entry into the pores.

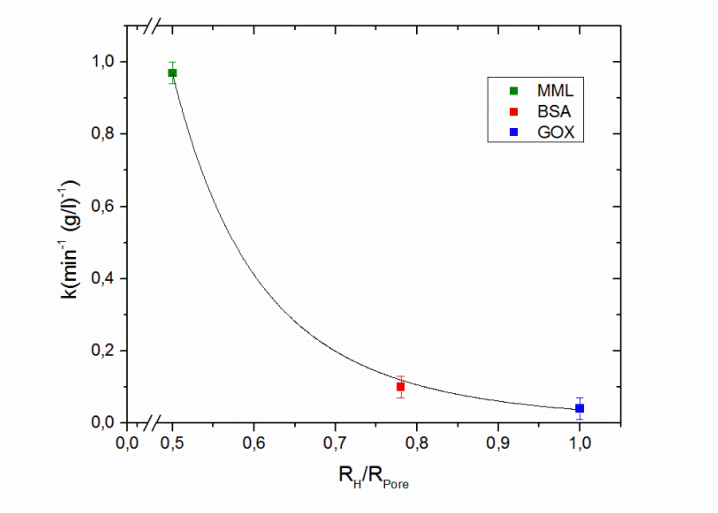

Figure 4.4. Plot of the second-order rate constant k versus the ratio between the hydrodynamic radii of the proteins (R_H) and the pore radius of the SBA-15 particles (R_{pore}). The values of k are from the fitted slopes in Figure 4.3; error bars are from the quality of the fits.

4.2 Rotational mobility of the enzymes after immobilization in mesoporous silica

The second part of the dynamics of the enzyme immobilization in the context of this thesis was directed to the rotational mobility of the confined enzymes. In other words, how the dynamics of proteins changes after they were localized in the mesoporous silica, either on the outer surface or inside the pores. Investigating the rotational mobility of immobilized proteins might seem like a contradiction at first. However, immobilization, here, means that the leakage into the external solution is prevented which sometimes referred to as encapsulation or confining enzymes in a solid materials. Therefore, the translational motion of proteins is restricted strongly but it does not mean that proteins cannot rotate inside the pores, depending on the mechanism and strength of the forces responsible for the immobilization. The non-translational motions of enzymes might be one of the reasons that give rise to the higher activity of the immobilized enzymes, because of small changes in the enzyme orientation and exposing the active site in a way that can be more accessible for the substrate [172, 173]. Therefore, I was convinced that the rotational mobility of the enzymes can be considered as an important factor for optimizing the immobilization process. To study the rotational mobility of the proteins, I utilized fluorescence anisotropy spectroscopy which is a powerful tool in biochemical research and medical analysis [174-178].

On the other hand, while I was designing the experiments, at the time I noticed that there was a lack of a systematic study about how protein size as well as pore and particle size can affect the degree of pore occupation by the immobilized enzymes. Therefore, the enzyme immobilization in terms of protein concentration as well as the rotational mobility in the different MPS particles was studied (Paper II).

In this study, two different proteins, lipase (MML) and bovine serum albumin (BSA), were immobilized individually in a set of five types of silica particles with different particles and pore sizes (See Table 2.2). The amount of bound protein (protein loading) of MML and BSA was measured using UV-Vis spectroscopy, and the actual protein concentrations in terms of volume fraction (pore filling) inside the pores of five different types of mesoporous silica particles were calculated (see Section 3.3). Moreover, under the same set of conditions fluorescence anisotropy spectroscopy was used to investigate the rotational dynamics of the confined proteins and compare with the rotation rates of the same proteins free in solution. The two sets of measurements are connected because the actual protein concentrations in the pores may affect the rotational motion of the immobilized proteins compared to the diluted protein samples which are used as particle-free references.

In contrast to Paper I [179], here the proteins have not been labeled with any dyes, instead I exploited the absorbance and fluorescence of intrinsic aromatic amino acids. The label-free approach avoids potential depolarization effects due to rotation of a dye attached to the protein by a flexible linker [79].

4.2.1 Protein loading and pore filling of the confined enzymes

Table 4.1 shows the measured protein loading (P_{LD}) values obtained for all the combinations of proteins and particles analyzed in this study, as well as pore filling (P_f) values and the average number of proteins per particle. The P_{LD} values are essentially constant for the four particle types with 4.6 nm pores. By comparing the two types of MPS-2000 particles, protein loading is considerably lower for the smaller pore size (3 nm), especially for the larger BSA where P_{LD} is 2.2 times lower than in the 4.6 nm pores for the same particle size.

Table 4.1. Protein loading, pore filling and average number of proteins per particle

		MML			BSA		
Particle type [a]	R_{por} [b] (nm)	P_{LD} [c] (μg/mg)	P_f [d]	N_{prot} [e]	P_{LD} [c] (μg/mg)	P_f [d]	N_{prot} [e]
MPS-40	4.5	288	0.284	133	336	0.604	75
MPS-300	4.7	300	0.261	$5.4 \cdot 10^4$	348	0.553	$3.0 \cdot 10^4$
MPS-1000	4.6	280	0.213	$1.7 \cdot 10^6$	340	0.472	$9.9 \cdot 10^5$
MPS-2000	4.5	284	0.218	$1.4 \cdot 10^7$	336	0.470	$7.9 \cdot 10^6$
MPS-2000	3.0	252	0.209	$1.3 \cdot 10^7$	152	0.230	$3.8 \cdot 10^6$

a. MPS-*D*, where *D* indicates average particle diameter in nm (see Table 2.2, Chapter 2)
b. Average pore radius (see Table 2.2, Chapter 2)
c. Protein loading (μg protein per mg of dry particles)
d. Pore filling (calculated based on Equation 3.11, Section 3.3)
e. Average number of proteins per particle (calculated based on Equation 3.12, Section 3.3)

The pore filling values show that for the particles with the larger pores, MML generally fills a significantly smaller fraction of the available pore volume (P_f = 20-30%) than the larger BSA (P_f = 50-60%). By contrast, in the case of the smaller pores both proteins occupy a similar fraction of the pore volume, 21-23%. The average number of bound proteins per particle (N_{prot}) was calculated to investigate how the proteins are distributed throughout the particles. The results show that for the smallest MPS-40 there is only approximately 100 proteins per particle on the average, and that N_{prot} increases strongly with increasing particle size.

Figure 4.5 shows a plot of the average number of proteins (N_{prot}) per particle (from Table 4.1) plotted versus particle diameter (D), and the strong increase shows that the larger particles accommodate many more proteins as expected. Importantly, the inset in Figure 4.5 shows that the number of protein per particle with the large pore radius 4.6 nm varies with the linear particle size D as $N_{prot} \sim D^{2.94\pm0.01}$ for MML and $N_{prot} \sim D^{2.95\pm0.01}$ for BSA. The near cubic scaling (*i.e.* proportionality to particle volume) supports that under our immobilization conditions both types of proteins are more or less evenly distributed inside the particles with the 4.6 nm pores. Notably, the particle-size dependence rules out that the proteins are adsorbed only to the external particle surface because then the expected scaling would be $N_{prot} \sim D^2$. In the case of particles with the same diameter but different pore sizes, the number of proteins per particle is lower for smaller pore sizes (Figure 4.5).

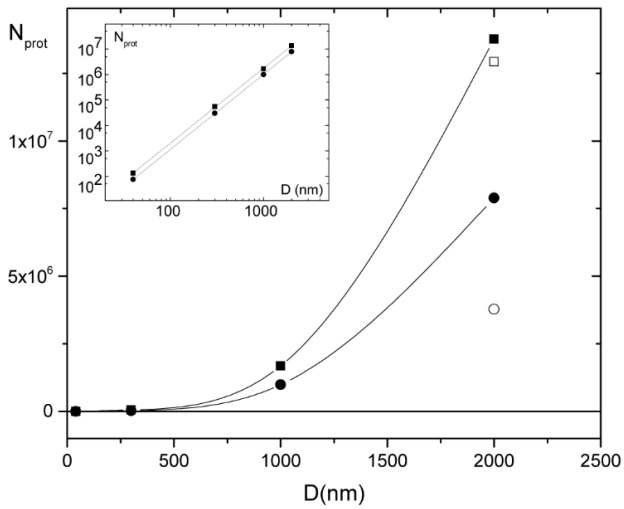

Figure 4.5. The average number of proteins per particle for MML (squares) and BSA (circles) versus the average particle diameter D. For pore radius 4.6±0.1 nm (solid; curves are guide to eye) and 3.0 nm (open). Inset: Double logarithmic plot for data with 4.6 nm pore radius where straight lines are least square linear fits giving slopes 2.94±0.02 for MML and 2.95±0.01 for BSA.

These results show that on a molecular level the effective number concentration of protein (pore filling, P_f) is very high under typical immobilization conditions, sometimes approaching close packing. Such crowded pores are likely to retard the transport of the substrate inside the pores. The results indicate that the enzymes are distributed essentially evenly throughout the particles. From a design point of view it is thus probably better to immobilize a certain amount of protein in a higher number of particles with smaller size, because substrate diffusion is expected to be slow to reach the enzymes at the bottom of long narrow pores.

4.2.2 Fluorescence anisotropy of the immobilized proteins

To investigate the rotational mobility, steady state anisotropy of free protein was measured and compared with the same protein when immobilized, either in two types of MPS-2000 particles with different average pore sizes or in four types of particles with varying diameter but essentially the same pore radius (4.6±0.1 nm), see Table 4.2.

The first observation is that in all the particles both MML and BSA exhibit an anisotropy in the presence of the particles which is significantly higher compared to the same enzyme in free solution. This observation indicates a slower protein rotation in the pores, but possibly also slower internal protein dynamics which also may affect the anisotropy. Secondly, for a given protein type the anisotropy in the MPS-2000 particles is higher in the smaller pores. Thirdly,

there is no obvious trend in the anisotropy values with particle size. Finally, free MML has a lower anisotropy than free BSA which is consistent with that the smaller MML rotates faster free in solution than BSA and in agreement with well-established results [149].

Table 4.2. Fluorescence anisotropy for free proteins and immobilized proteins in different particle type

		MML		BSA	
Particle type [a]	R_{pore} [c] (nm)	r [d]	θ_A [e] (ns)	r [d]	θ_A [e] (ns)
Free protein [b]	---	0.06	0.87	0.08	2.73
MPS-40	4.5	0.23	11.5	0.18	9.45
MPS-300	4.7	0.30	-----	0.27	56.70
MPS-1000	4.6	0.15	3.50	0.16	7.24
MPS-2000	4.5	0.17	4.58	0.18	9.45
MPS-2000	3.0	0.21	8.17	0.24	25.20

a. MPS-*D*, where *D* indicates average particle diameter in nm (see Table 2.2, Chapter 2)
b. Protein in buffer solution without particle
c. Average pore radius (see Table 2.2, Chapter 2)
d. Measured tryptophan steady state anisotropy. The uncertainty is ±0.01 as calculated from the variation between 3 to 4 independent experiments.
e. Apparent rotational correlation time calculated from anisotropy based on Equation.3.14, Section 3.3. The uncertainty is ±0.2ns from the variation between 3 to 4 independent experiments.

As previously mentioned, the anisotropy is monitored by tryptophan fluorescence and it reflects the rotational motion of the whole protein, but also the local motion of the tryptophan residues [127, 148, 150]. It is noteworthy that in the steady state anisotropy technique employed here these two contributions are convoluted into an apparent rotational correlation time (θ_A). The fact that θ_A is significantly larger in the pores than for free protein just reflects that one of those motions or both are retarded in the pores. Notably, the potential depolarizing effect of whole-particle rotation is negligible in the present study, because all studied particles are large enough to be viewed as non-rotating on the time scale of the tryptophan fluorescence lifetime [128, 149].

The maximum anisotropy in the system is $r = r_o = 0.3$, (the limiting anisotropy for tryptophan [149]) obtained for a protein which does not rotate in the pores (for instance due to pore wall adsorption) and does not exhibit any local tryptophan depolarizing motion. All the observed *r*-values (Table 4.2) are intermediate between the upper limit anisotropy (0.3) for fully adsorbed and rigid protein and the anisotropy value of respective protein when free in solution. This observation strongly indicates that both proteins do undergo some depolarizing motions inside the pores, and also that these motions are retarded compared to the free protein. This

interpretation is supported by the observation that the anisotropy is higher in the MPS-2000 with more narrow pores (3.0 nm) for a given protein, as expected since stronger confinement is likely to affect the motion more strongly.

4.2.3 Two different mechanisms of the enhanced protein anisotropy in the pores

The protein dynamics can be retarded after immobilization by two main mechanisms. One scenario could be due to the high protein concentration in the pores (Table 4.1). The retardation could then be caused by the same protein-protein hydrodynamic interactions in the pores. This kind of retardation was previously reported by Roosen-Runge *et al.*[180] for BSA motion in non-diluted solutions of free proteins (no particles).

On the other hand, for both MML and BSA the anisotropy is higher in the more narrow pores (Table 4.2) even though the pore filling is lower (Table 4.1). Therefore, the second possible mechanism is that the rotation is retarded by hydrodynamic interactions between the (individual) proteins and the pore wall. This retardation indeed is expected to be stronger in more narrow pores. Jones reported [181] theoretically that the rotation of a (single) spherical particle confined in a slit between two planar walls is stronger the narrower the gap, in agreement with that the anisotropy for both MML and BSA is higher in the more narrow pores (Table 4.2).

4.2.4 Time-resolved anisotropy of the immobilized proteins

The protein rotation is slower in the pores than outside the particle, as explained above, possibly because the protein-wall interactions can be more effective than protein-protein hydrodynamic interactions. Notably, a slowing down of internal protein dynamics may contribute to the increase in steady state anisotropy measured upon immobilization. Czeslik *et al.* have studied lysozyme and SNase bound to a planar silica/water interface using time resolved TIRF anisotropy measurements. The results have shown that a slow component corresponding to global protein motion (θ_{prot}) is the dominant contribution, but also that the correlation time for the internal motion (θ_{Trp}) can both decrease or increase after adsorption [182]. Therefore, time-resolved anisotropy would be an interesting extension for Paper II to investigate the effects of the immobilization on the local tryptophan residue motion in the MML and potential effects on its catalytic activity.

To satisfy my curiosity, time-resolved anisotropy of the enzyme (MML) immobilized in the same SBA-15 particles was measured as an extension of the study reported in Paper II. It should be mentioned that these data are unpublished and all the experiments were performed at laser lab in PicoQuant Company in Berlin. The MML enzyme was prepared and immobilized in the same MPS-2000 particles with two different pore dimeters (9 nm and 6 nm) using exactly the same procedure as described in Paper II. The light source was the powerful pulsed diode laser at 266 nm wavelength and the emission was recorded at 370 nm; a longer wavelength compared to the steady state measurement was used in order to avoid collecting the emission of tyrosine. It is noteworthy that the wavelength 295 nm usually is defined as the suitable wavelength in order to excite just tryptophan without exciting the two others aromatic residues in the protein. However, the emission decay was too weak when the sample was excited at 295 nm using pulsed LED (PLS), owing to high turbidity [16], see Section 3.4.

The decay of the fluorescence intensity could be fitted with three exponential in agreement with previous studies [148, 149]. Table 4.3 shows the lifetime (τ) values measured at magic angle (54.7°) and the rotational correlation time (θ_{Trp}) of each sample measured based on the anisotropy decays. The data reported here are the best fitting parameters obtained from commercial FluoFit software, patented by PicoQuant.

Table 4.3. Lifetime (τ) and rotational correlation time (θ_{Trp}) of tryptophan in free and immobilized MML

	MML		
	Free [a]	MPS-2000 [b]	MPS-2000 [b]
R_{pore} [c] (nm)	-------	9 nm	6 nm
τ_1 [d] (ns)	0.45	0.48	0.47
τ_2 [d] (ns)	2.35	3.00	2.80
τ_3 [d] (ns)	6.45	6.55	7.28
θ_{Trp} [e] (ns)	0.40	1.80	2.32
r [f]	0.07	0.12	0.18

a. Protein in buffer solution without particle
b. MPS-*D*, where *D* indicates average particle diameter in nm (see Table 2.2, Chapter 2)
c. Average pore radius (see Table 2.2, Chapter 2)
d. Measured tryptophan lifetime, the uncertainty is ±0.05 as calculated from the variation of 3 independent experiments.
e. Tryptophan rotational correlation time calculated from time-resolved anisotropy using FluoFit software. The uncertainty for MML is ±0.3 ns from the variation of 3 independent experiments.
f. Measured steady state anisotropy reported based on FluoFit software. The uncertainty is ±0.02 as calculated from the variation of 3 independent experiments.

As can be seen in Table 4.3, the lifetime of immobilized MML remains almost the same as free MML. The similar lifetimes of both free and immobilized enzymes show that the local environment of tryptophan residues has not changed significantly after immobilization in mesoporous silica. This observation suggests that the structure of the enzyme inside the mesoporous silica can experience the same local environment as the enzyme free in solution.

The rotational correlation time (θ_{Trp}) values of the free MML is shorter than the two other immobilized MML in mesoporous silica which is in agreement with the steady state measurements. However, the apparent rotational correlation time θ_A values calculated from steady state anisotropy are larger than the θ_{Trp} values of tryptophan.

The best fitting obtained from the time-resolved anisotropy measurements for MML shows only one θ value in each sample, therefore, the fraction of the overall rotation of the protein molecule (θ_{prot} in Equation 3.15) cannot be distinguished from the segmental motion of the tryptophan residues (θ_{Trp}). This could be explained by the fact that the proteins experience very high viscosity inside the mesoporous silica. As it has been explained in Paper II, the rotational correlation time of the global protein (θ_{prot}) is proportional to the viscosity of the solvent, see Equation 3.15. As will be shown in the next chapter of this thesis, the effective viscosity increases inside the mesoporous silica, at least 25 times higher than the viscosity experienced by free enzymes. Consequently, the θ_{prot} value increases significantly and becomes very long compared to a few nano second Trp lifetime, $\theta_{prot} >> \tau$, and based on Solleilet theory, the depolarization factor of the protein-rotation becomes unity, which means that the protein is viewed as non-rotating on the time scale of the tryptophan fluorescence lifetime [128, 149]. Moreover, we calculated that the fundamental anisotropy is lost by 83% associated fraction of tryptophan mobility and 17% by the mobility of global protein molecule in free MML sample. Therefore, it can be concluded that the rotation of tryptophan is the dominant in depolarizing motion in the study presented in Paper II. In this study, the associated fractional amplitudes of the Trp residues and the protein can be calculated only for the free MML sample, based on calculate θ_{prot} and measured θ_{Trp} from time-resolved anisotropy [127, 182]. This observation is in contrast with the conclusion that Czeslik *et al.* reported about the Trp residues in lysozyme and SNase adsorbed on a planar silica/water interface [182].

5 Microviscosity inside Mesoporous Silica

From a physical chemistry perspective, the microenvironment that the enzymes experience during or after the immobilization is one of the important factors that should be considered in the optimization of this process [90, 91]. This chapter focuses on the characterization of the microviscosity, which may be counted as one of the crucial parameters in the pores of mesoporous silica. The results that are presented here, are mainly based on Paper III. This paper was designed to answer two scientific questions which came up after Paper I and Paper II: (*i*) the effect of the microenvironment on the dynamics of the enzymes, (*ii*) better understanding of protein-protein interaction and protein-wall interaction.

The observations from Paper I and Paper II indicated that both dynamics, translation into the pores and rotation of the proteins inside the pores, are systematically slower when the protein and the pore are close in size. Such a dependence on the relative protein/pore-size is expected for simple steric reasons. However, both processes involve the motion of macromolecules in water, and therefore can be sensitive to the local viscosity of the solvent. The better understanding of such potential effects motivated me to measure directly the effective viscosity of the water sensed by the proteins inside the pores.

As previously mentioned, spectroscopic methods based on fluorescent dyes have been used to probe the microenvironment. For example, measuring the pH inside the pores of the MPS particles, where the results showed a buffering environment inside the pores compared to the bulk solution [57]. In Paper III, a viscosity-sensitive fluorescent dye was bound to the enzyme covalently. One of the advantages of using enzyme-bound fluorescent dyes is that the microenvironment is monitored at the actual position of the enzymes. Moreover, another possibility is that the effect of protein-protein interaction can be distinguished from protein-wall interaction more comprehensively.

5.1 Suitable dyes for probing the microenvironment

In Paper I, it has been shown that epicocconone covalently bound to the enzymes can be used to monitor the immobilization process in real time. In this method, the intensity variations could be measured over time and the fluorescence intensity of the dye increases as the enzymes interact with either the particle surfaces or the pores. It has been suggested that epicocconone can be introduced as a viscous-sensitive probe [156, 158, 159]. However, we were convinced that epicocconone cannot be considered as the most suitable dye for probing the microenvironment of the MPS particles due to its tendency for bleaching.

In Paper I, we showed that the epicocconone bleaching is a combination of a light-dependent process and a dark reaction. This interpretation was controlled by subjecting two identical samples of the free Epicocconone/GOX conjugate (no particles) to either continuous illumination, or to intermittent illumination in order to reduce the degree of light exposure (5 minutes off/1 minute on). The results in Figure 5.1 show that intermittent illumination indeed reduces the rate of intensity decay, which is consistent with that epicocconone is subjected to photo-bleaching. However, it is expected that the dye bleaching should be reduced by about 80% (the fraction 5/6 that the light is off), see green dashed line in Figure 5.1. These observations confirm the existence of two parallel bleaching mechanisms where one does not require light. Therefore, the nature of the dark-reaction bleaching needs to be better understood if the epicocconone dye is used as a viscous-sensitive probe. This interpretation encouraged me to look for a better probe in order to characterize microviscosity.

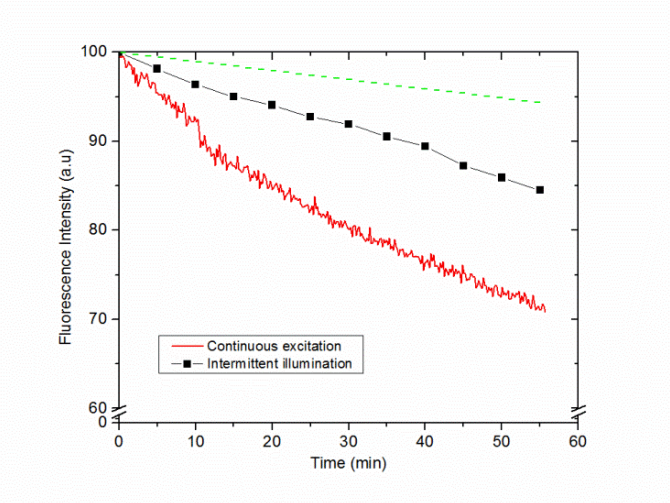

Figure 5.1. Effect of intermittent illumination on the epicocconone emission intensity. Two samples of epicocconone/GOX conjugate (without particles) were exposed to continuous excitation (red curve) and to intermittent illumination with light alternatingly off for 5 min and on for 1 min (black line connecting squares which indicate the time intervals of illumination). Dashed line corresponds to expected intensity decrease if bleaching is purely photo-induced (5/6 reduction of bleaching).

There are several types of fluorescent dyes which are sensitive to the microviscosity of the solvent, often based on the concept of molecular rotors which are slowed down by increasing viscosity [161, 183, 184]. However, it is a challenge to find a suitable fluorescent probe for measuring the viscosity of water inside the MPS particles. The chosen probe should be sensitive to the comparably low level of water viscosity since biocatalytic immobilization systems are applied mostly in aqueous environment. Also, it should be bound covalently to proteins to ensure that the viscosity is measured at the location of the immobilized proteins. The probe should preferably be negatively charged in order to minimize binding to the silica pore walls which carry a negative charge (point of zero charge = 2), and also it should be photo-stable.

5.1.1 Cy3 and Cy5 as fluorescent molecular rotors

Sulfo-cyanine3 NHS ester and sulfo-cyanine5 NHS ester, denoted in this thesis Cy3 and Cy5, respectively, were chosen as the viscous-probe since both are sensitive to viscosity, but to different extents. As can be seen in Figure 3.9, Cy3 and Cy5 differ only in the length of the polymethine chain linking two indole rings. It is well-established [185, 186] that carbocyanines with short polymethine chains (such as Cy3) photoisomerize in the first excited state more efficiently than the longer analogues (such as Cy5). Thus, it is expected that Cy3 is more sensitive than Cy5 to environmental factors such as temperature and local solvent viscosity [187]. Moreover, the relative rigidity of the molecule has important consequences for the

quantum yield of fluorescence, because internal conversion competes with fluorescence due to intermolecular motion in the excited states after photon absorption [16, 188]. Thus, as the viscosity of the solvent increases, molecular motion is slowed down and the quantum yield of fluorescence increases significantly.

Importantly, both dyes are negatively charged and hydrophilic with high photo-stability, and they can be bound covalently to the enzymes through amine groups of the protein which reacts with the ester group in the dyes. It should be noted that the two fluorescent probes, Cy3 and Cy5, were used in Paper III as a ratio pair.

5.2 A ratiometric method to measure microviscosity inside mesoporous silica

One of the techniques to measure viscosity in a complex system like living cells is to use a ratiometric method [188-190], since viscosity variations often are accompanied by changes in the polarity of the solvent. Therefore, a ratiometric method was used in Paper III for measuring the effective viscosity inside the pores, separately from potential polarity effects. This method is based on the ratio of the emission intensities (R) at the maximum emission wavelength of the two fluorescent rotors probes

$$\mathrm{R} = \frac{\mathrm{I_{Max}\ of\ Cy3\ at\ 565\ nm}}{\mathrm{I_{Max}\ of\ Cy5\ at\ 665\ nm}} \tag{5.1}$$

Where I_{max} is the emission intensity at the maximum emission wavelength. This ratiometric method was proposed previously by Luby-Phelps *et al.* [188] in order to measure the viscosity in the cytoplasm of living cells.

5.2.1 Two different strategies for labeling

In Paper III, the effective viscosity was measured at the position of the protein by covalently attaching Cy3 and Cy5 as the ratio pair to enzymes. In this ratiometric method, each enzyme should ideally carry both dyes. However, a potential drawback is that Förster resonance energy transfer (FRET) between the two dyes, while they are in close proximity affects the fluorescence spectra of the dye pair. The enzyme used here was lipase (MML) and its size is on the nanometer length scale, where FRET can be efficient. Therefore, two different strategies of dye labeling for the enzyme were investigated.

The first strategy is called “double labeling” in which each enzyme carries both dyes (Cy3 and Cy5), while in the second strategy “single labeling”, each enzyme carries either Cy3 or Cy5, and a 1:1 stoichiometric mixture of these two labeled enzymes were used in the ratio experiments.

The potential intensity-disturbing effect of FRET between Cy3 and Cy5 was controlled for both strategies. Figure 5.2a shows the emission spectra of free enzyme-dye conjugates (no particles) for the double labeled lipase (Cy3-MML-Cy5) and Figure 5.2b represents a 1:1 mixture of single- labeled lipase (Cy3-MML+Cy5-MML). Both spectra are compared with the individual emission spectra of labeled enzyme, Cy3-MML and Cy5-MML, respectively.

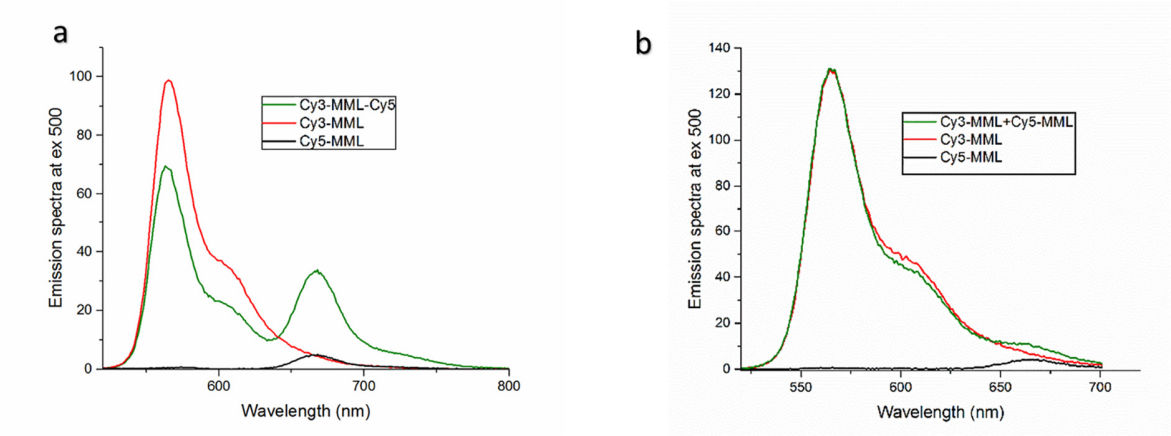

Figure 5.2. Steady state Förster resonance energy transfer for the two different strategies of labeling, compared to individual spectra for labeled proteins Cy3-MML (red) and Cy5-MML (black). a) Double-labeled lipase (Cy3-MML-Cy5; green curve) and b) a 1:1-mixture of single-labeled lipase (Cy3-MML+Cy5-MML; green curve). Phosphate buffer, pH 6 and particle free solution. Excitation at 500 nm, emission at 565 nm and 665 nm indicate Cy3 and Cy5, respectively.

As can be seen in Figure 5.2a, the emission spectrum of the double-labeled sample clearly deviates from the sum of the spectra of the individual labeled proteins. Especially, the emission of the Cy5-MML in double-labeled sample (centered at 665 nm, green line) is strongly increased compared to the individual Cy5-MML (black line). Secondly, the intensity in the emission of individual Cy3-MML (centered at 565 nm, red line) decreases significantly. Taken together these two observations strongly indicate an energy transfer from Cy3 to Cy5 when the dyes are sitting on the same enzyme. This observation is consistent with that the diameter of the MML-protein ($2R_H$ = 4.5 nm) is comparable to the Förster distance of the Cy3/Cy5-pair (R_o = 5.4 nm) [191]. Even though, it was not clear from the outset how strong this effect would be since the attachment of the dyes occurs randomly to the available lysine residues [192]. By contrast, Figure 5.2b shows that the emission spectra of the Cy3-MML+ Cy5-MML mixture

are almost identical to the sum of the spectra of the individual labeled proteins. This observation supports that FRET is negligible in the mixture of single-labeled enzyme (Cy3-MML+Cy5-MML) which made this approach promising for the purpose of this study in the single labelling approach. It should be noted that the situation may be different at the higher local protein concentrations in the pores after immobilization in the MPS particles.

5.2.2 Viscosity calibration curve for lipase bound Cy3 and Cy5

Before measuring the viscosity inside the mesoporous silica, a calibration curve was established for the emission intensity ratio *R* vs solvent viscosity for MML-attached dyes. This calibration curve was obtained by recording emission spectra for free lipase-attached dyes (no particles) in aqueous solutions with different concentrations of glycerol. The *R* values (see Equation 5.1) were calculated based on the emission spectrum for each sample at an excitation wavelength of 550 nm and 650 nm, respectively, for Cy3 and Cy5.

Figure 5.3 shows the fluorescence emission spectra of Cy3-MML+Cy5-MML in different aqueous mixtures with glycerol. The emission intensity increases with increasing glycerol concentration for both dyes, consistent with a viscosity increase, although the relative increase is larger for Cy3. Moreover, there is a red shift in the peak maximum of both dyes which indicates that both dyes are sensitive to other solvent effects as well, such as polarity. However, the red shift is larger for Cy5 (from 665 nm to 672 nm) compared to Cy3 (from 565 nm to 568 nm). The stronger intensity-effect of glycerol on Cy3 while Cy5 displays a stronger redshift is the basis for using the ratio method to separate viscosity and polarity effects.

It is noteworthy that the labeled enzymes retain their secondary structure even at the highest glycerol concentration based on the circular dichroism (CD) spectra of either Cy3-MML or Cy5-MML. This result is consistent with other studies which have investigated the effect of glycerol on protein folding and unfolding [193-195]. For more details about the CD result, the reader is referred to Paper III of this thesis.

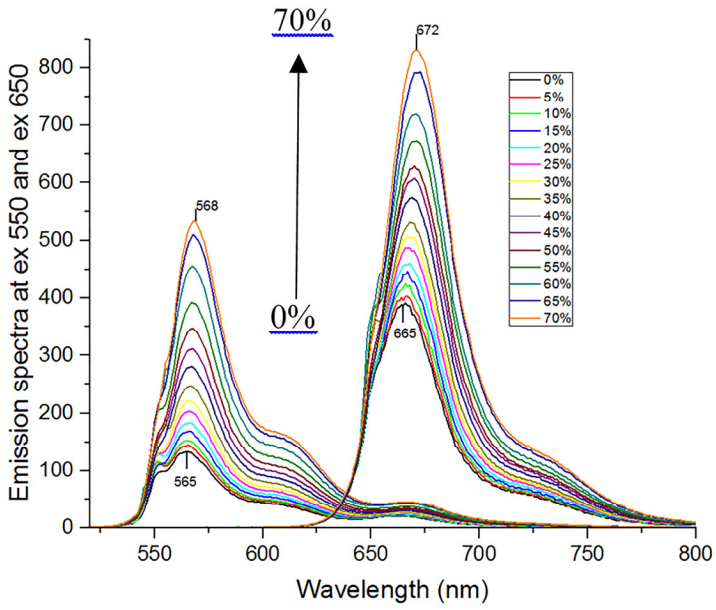

Figure 5.3. Fluorescence intensities of the mixture of single-labeled lipase (Cy3-MML+Cy5-MML) in different concentrations of glycerol (0-70% mass fraction of glycerol mixed with phosphate buffer). The Cy3 intensity maximum is at about 565 nm, and for Cy5 at about 665 nm. For both dyes the curve with lowest maximum corresponds to 0% glycerol (pure phosphate buffer), and both intensity maxima increase monotonously as the mass fraction of glycerol increases to 70%. Excitation wavelengths were 550 nm for Cy3-MML and 650 nm for Cy5-MML, respectively.

Figure 5.4 shows that the fluorescence intensity ratio (R) of Cy3-MML+Cy5-MML increases more than 2.3-fold in the studied viscosity range. The R-values fall essentially on a single master curve, which can be used as a calibration curve. The curve in Figure 5.4 is non-linear. A well-stablished format [183, 189, 190] for evaluating the data in calibration curves is the double logarithmic plot shown in the inset of Figure 5.4, where the approximately linear shape in the plot allows for extrapolation to high viscosities if necessary.

The validity of the calibration curve was controlled by measuring the intensity ratio R for the mixture of single-labeled (Cy3-MML+Cy5-MML) in an aqueous solution containing 40% ethanol (no glycerol). This aqueous solution has very similar viscosity (η = 2.34 cP) but distinctly different dielectric constant (ε_r = 63.3) compared to the aqueous solution with 30% glycerol (η = 2.26 cP, ε_r = 71.4) [188, 196, 197]. Therefore, these two samples (30% glycerol and 40% ethanol) should give the same R-values if the ratiometric method indeed reflects the viscosity of the solvent independently of its polarity, see red points in Figure 5.4.

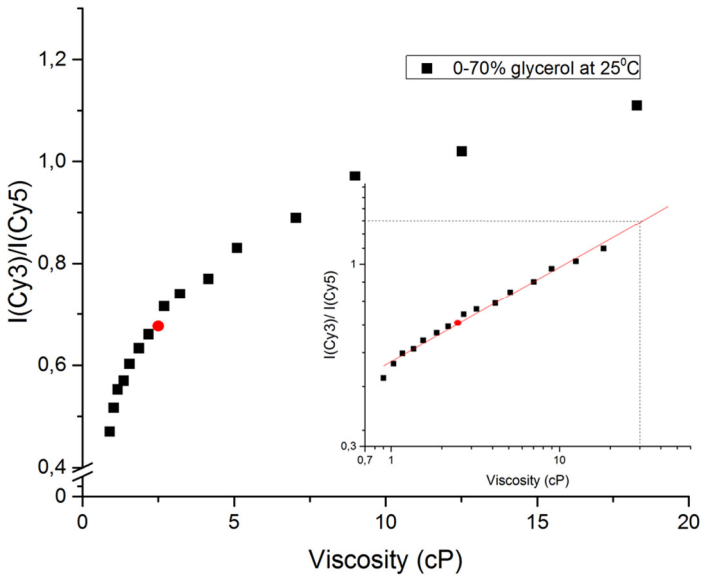

Figure 5.4. Calibration curve for intensity ratio R of the Cy3-MML+Cy5-MML sample vs viscosity (no particles). Black squares show the intensity ratio vs viscosity in aqueous solutions of glycerol between 0 and 70% in phosphate buffer. Red circle shows the intensity ratio in a control solvent with 40% ethanol in phosphate buffer (no glycerol; see main text). Inset shows log-log plot of the same data (black squares).

5.2.3 Effective viscosity inside mesoporous silica

In Paper III, The mixture of single-labeled lipase was immobilized into two different types of mesoporous silica particles, SBA-15 (Santa Barbara Amorphous-15) and MCF (Mesostructured Cellular Foam). These two types of mesoporous silica present different 3D-structure, pore architecture and size, see Section 2.6, Chapter 2. Additionally, the MCFs with octyl-functionalized surface were also used and compared to the unmodified MCFs. The reason of including the octyl-functionalized particles in this study is to alter the surface chemistry of the pore walls, and investigate the potential protein-wall interactions that may affect the effective viscosity measured through the ratiometric method.

The narrow pores of the MPS particles may increase the possibility of energy transfer (FRET) between the two dyes even in the Cy3-MML+Cy5-MML mixture approach, because the concentration of immobilized proteins can be very high in the pores as mentioned in Paper II [198]. To avoid such energy transfer after immobilization, the amount of protein added in the MPS particles was controlled. However, to make sure that there is no energy transfer in the immobilized samples, each sample was checked by using time-resolved fluorescence spectroscopy. The lack of FRET indicates that the individual enzymes are not packed close

enough in the pores to bring the Cy3 and Cy5 dyes within the Förster distance. Therefore, the calibration curve can be applied for the immobilized samples. It is worthy to mention that the interaction of enzyme attached Cy3 with pore walls was controlled by time-resolved anisotropy and no detectable interaction was reported which made the calibration curve valid for the immobilized samples. For more descriptive details, the reader is referred to Paper III.

To measure the effective viscosity inside the different mesoporous silica particles, the fluorescence intensity ratio of the Cy3-MML+Cy5-MML sample after immobilization was recorded exactly the same way as the calibration curve (Figure 5.3). The *R* values were corrected for the loaded dyes in each sample. Since the intensity ratio inside the MPS particles is sometimes higher than the highest ratio in calibration curve, a slight extrapolation was necessary to evaluate the viscosity. First the unmodified particles and then the OC-functionalized particles are discussed.

Table 5.1 shows the combined results of the *R*-values and the derived effective viscosity for the unmodified particles (SBA-15, MCF2, and MCF12). The results show that the effective viscosity inside the pores is considerably higher than in bulk water for SBA-15, MCF2 and MCF12 particles, and clearly decreases in the order of increasing pore size. The effect of pore size indicates that smaller pore sizes can confine the water more and the effective viscosity is higher. However, the pore filling obtained from different amount of the added protein can be another reason for a higher viscosity.

Table 5.1. Intensity ratio (R) and effective viscosity inside the different mesoporous silica particles[a]

	SBA-15 (8.9nm)[c]		MCF2 (26.5nm)[c]		MCF12 (33.0 nm)[c]	
Added protein[b]	R	Viscosity (cP)	R	Viscosity (cP)	R	Viscosity (cP)
20 µg/mg	1.33	31.3	1.23	23.4	1.20	21.4
40 µg/mg	1.39	36.1	1.27	26.3	1.22	22.7
60 µg/mg	1.48	46.4	1.35	32.4	1.30	28.2

a. Intensity ratio (R) and effective viscosity inside the different unmodified mesoporous silica particles, with ±0.01 and ±0.2 cP uncertainty, respectively.
b. Total amount of added protein per mg of silica particles.
c. Pore diameter of each silica particle (See Table 2.2, Chapter 2)

Viscosity in SBA-15 and MCF particles are approximately 40 and 30 times higher than water viscosity at 25 °C which is 0.89 cP. These measured viscosities can be compared with the viscosity and dynamics of water in silica porous materials with different pore size (from 100 nm to 2 nm) which have been reported earlier. Fukatsu *et al.* [199] have used proton NMR to investigate the mobility of water in the pores of mesoporous silica particles, in the same range

of pore diameters as investigated here. Interestingly, they reported that the molecular motions of adsorbed water are more restricted by confinement in pore size below 10 nm. The viscosity of pressure-driven flows in 200 nm wide channels is higher than in bulk water by a factor of 2.5 [200]. The dynamic properties of water molecules in silica particles with pore size in a few nm range (Vycor, MCM-41, SBA-15) have been studied by quasielastic neutron scattering (QENS) studies [201-203]. The QENS results indicated that the translational diffusion coefficient of water at room temperature is about a factor two lower than in bulk water, as supported by detailed molecular dynamics simulations [204, 205]. Moreover, strong retardation of water rotation (by a factor of about 8) in 2 nm pores has also been observed through the optical Kerr effect [206].

It is noteworthy that in Paper III, the molecular rotors which were attached to MML do not measure the viscosity of pure water in the pore, but the effective viscosity which the protein-bound probe experiences in the presence of the (single) protein. The effect of the protein itself on the water mobility in the pore may be important, because the protein is comparable in size to the pore radius and may disturb the flow-pattern of the water. Therefore, the average effective solvent viscosity experienced by the protein is better measured by a protein attached viscosity probe since the protein can probe the whole pore lumen.

In the OC-functionalized MCF materials (MCF2-OC and MCF12-OC), the energy transfer (FRET) between two dyes was observed even at the lowest added protein concentrations. Therefore, the effective viscosity values of the OC-modified MCF particles could not be reported properly. In Paper III, we showed that the hydrophobic surface modification with octyl groups increases the enzyme uptake in the MCF-particles by approximately a factor of 2 for a given amount of added protein. This observation is consistent with other studies regarding interaction between lipase and hydrophobic surfaces [96, 99, 101, 102]. In the presence of hydrophobic surfaces through a mechanism of action called interfacial activation, the enzyme can be adsorbed to the surface due to a hydrophobic pocket on their active sites [34, 207, 208]. The enzymes experience a less polar pore environment in the OC-functionalized particles. This conclusion was based on the observation that the emission peaks redshift (almost 3 nm) [209] compared to MCFs with no modification.

I have shown that the ratio-method could not be applied to evaluate the effective viscosity inside the OC-modified particles because of the presence of FRET. On the other hand, many studies have shown that activity and stability of the immobilized enzyme increase [101, 102], when immobilized on hydrophobic surfaces accompanied by a decrease in the mobility of

lipases [96, 97]. It could therefore be interesting to investigate with another method how the effective viscosity in the OC-modified particles changes. Interestingly, in a recent study Kubankova *et al.* reported that the fluorescence life time of Cy3 itself (no Cy5) can be used to estimate the microviscosity in blood clotting , if an appropriate calibration curve is established [187]. I have not measured such a calibration curve for our system, but a qualitative comparison between OC-modified and non-modified MCF-particles using the lifetimes of immobilized Cy3-MML suggested that the viscosity is higher after OC-modification.

5.2.4 Protein- protein and protein-wall interactions

In Paper II, we showed that enzyme immobilization under commonly used conditions may lead to high protein concentrations in the pores, with protein volume fractions of 20% or higher. Such a high protein concentration may lead to FRET between Cy3 and Cy5 even in the single labeling strategy, which would prevent the use of the ratiometric method. The relatively low amounts of added protein used in this study were chosen to avoid such energy transfer after protein immobilization. Table 5.2 shows the pore filling P_f (the fraction of the pore volume occupied by proteins) in the samples used Paper III.

Table 5.2 Calculated pore filling (P_f) in each sample[a]

	Pore filling **P_f** (%)				
Added protein[b]	SBA-15 (8.9nm)[c]	MCF2 (26.5nm)[c]	MCF12 (33.0nm)[c]	MCF2-OC (24.8nm)[c]	MCF12-OC (32.7nm)[c]
20µg/mg	0.37	0.37	0.41	0.81	0.88
40µg/mg	0.93	0.63	0.71	1.43	1.60
60µg/mg	1.18	0.92	1.25	2.00	2.36

a. Volume fraction protein (in %) in the pores, with ±0.05% uncertainty from 3 independent experiments..
b. Total amount of added protein per mg of silica particles.
c. Pore diameter of each silica particle (See Table 2.2, Chapter 2)

The total pore filling increases in each particle type when the amount of added protein is increased. Moreover, the pore fillings of the unmodified particles are comparatively insensitive to the particle type because pore volume (V_{pore}) of the SBA-15 particles is 60% smaller compared to the MCF particles (See Table 2.2, Chapter 2). The P_f values in the OC-modified particles are approximately twice as high as for the corresponding non-modified particle type at the same amount of added protein, which reflects the more efficient protein uptake in OC-modified particles in terms of pore occupancy.

Figure 5.5 summarizes the effective viscosity in the three different unmodified particles versus the pore filling values (P_f) by combining the data of Tables 5.1 and Table 5.2. It is seen that in all three particle types, the effective viscosity decreases with decreased pore filling and thus the immobilized protein concentration, revealing a protein-protein interaction effect on the measured viscosity, as expected.

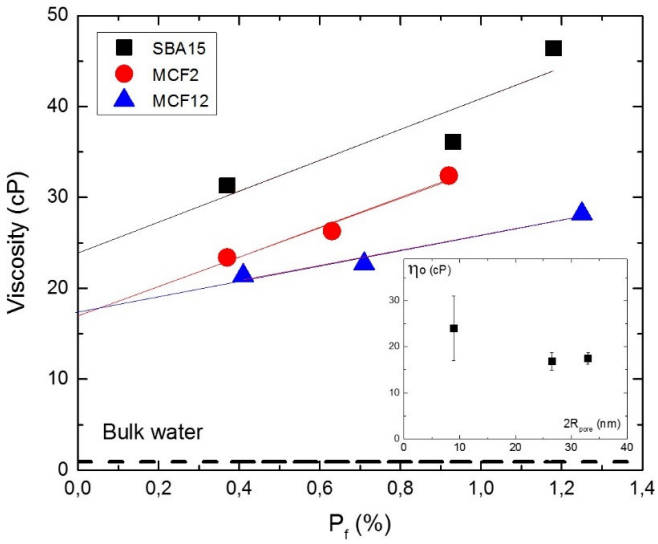

Figure 5.5. Effect of protein concentration on the effective viscosity in the pores. Plot of the viscosity data for the three particle types (Table 5.1) vs pore filling P_f (Table 5.2) for SBA15 (black squares), MCF2 (red circles) and MCF12 (blue triangles). Experimental uncertainties are indicated by symbol size. Dashed line corresponds to the viscosity of bulk water at 25°C. Straight lines are least square fits. The intercepts η_o (in cP) at P_f = 0 are 24±7cP (SBA15), 16.8±1.9cP (MCF2) and 17.5±1.3cP (MCF12). The inset shows η_o plotted vs. pore diameter (Table 2.2), with the uncertainties obtained from the linear fits.

The effective limiting viscosity (η_o) were obtained in the limit of infinite protein dilution in the pores (P_f = 0), as the intercepts of the fitted straight lines in Figure 5.5. The η_o values for SBA-15, MCF2 and MCF12 are 24±7, 16.8±1.9 and 17.5±1.3 cP, respectively. These values correspond to the effective viscosity sensed by a single protein in the pores since the effect of protein-protein interactions on the effective viscosity is removed by extrapolation to zero protein concentration.

It should be noted that the η_o in Figure 5.5 is higher than bulk water viscosity (dashed line in Figure 5.5) by a factor of approximately 27 in the SBA15 pores and 19 in both MCF-particle types. These enhancement factors indicate that confinement in the silica pores confers a considerable increase in the effective (pure) water viscosity, by approximately one order of magnitude. The inset of Figure 5.5 shows the values of η_o plotted versus pore diameter. In spite

of the substantial uncertainties, the plot indicates that the enhancement of the effective water viscosity is higher in more narrow pores, and levels off at a value of about 15 cP if the pores are larger than 20 nm in diameter.

The high value of η_o in the SBA-particles (Figure 5.5) supports our previous observation from the fluorescence anisotropy study of immobilized lipase and BSA in Paper II [198] that protein-wall interactions are more important rather than protein-protein hydrodynamic interactions in the retardation of protein rotation in the pore. The results here suggest that the protein-protein interaction effect is stronger in the pores than in bulk protein solution. In qualitative terms, the effective viscosity at 1.4% pore filling (P_f) of MML in the SBA-15 pores is doubled, to almost 50 cP (Figure 5.5) compared to η_o (24±7 cP), while the diffusion rate in the BSA experiments [180] is reduced by a factor of 2 compared to diffusion coefficient in dilute solution (D_o) only when the volume fraction of BSA has reached 10 %. A systematic comparison with theory will require more experiments with MCF particles.

6 Spatial Distribution of Immobilized Enzymes

In the second part of my PhD, the distribution and the location of the immobilized enzymes in mesoporous silica was studied in order to understand more about how these two factors can affect the catalytic efficiency of the enzymes. As discussed in Paper II, the enzymes are most likely distributed evenly throughout the SBA-15 particles with very high pore filling (P_f) values under typical immobilization conditions. Due to these high pore filing values, and the even distribution, the transport of the substrate inside the pores is likely to be retarded, and consequently, the catalytic efficiency of the enzyme might decrease. Therefore, to optimize the immobilization process for a specific application, it is crucial to identify the exact location and distribution of the immobilized enzymes in different MPS particles.

The core of this chapter is based on the original work presented in Paper IV and Paper V. In Paper IV, Förster resonance energy transfer (FRET) was used to study the distribution of two co-immobilized enzymes inside mesoporous silica, and how it can affect the catalytic efficiency of the enzymes. In Paper V, transmission electron microscopy with immunogold staining (TEM-IGS) was used to visualize the exact location, as well as to estimate the radial distribution and density, of the immobilized enzymes.

6.1 FRET study of co-immobilized enzymes in MCF particles

The conversion of CO_2 to formaldehyde as a part of the biocatalytic reduction of CO_2 to methanol was investigated in Paper IV. To produce formaldehyde from CO_2, two different enzymes; (*i*) formate dehydrogenase (FateDH), converting CO_2 to formate, and (*ii*) formaldehyde dehydrogenase (FaldDH), reducing formate to formaldehyde, are required. The use of enzymes free in solution is not very efficient for the CO_2 conversion, since the two enzymes are not sufficiently close to each other and the substrate channeling between the two enzymes is almost impossible. Hence, co-immobilization of these two enzymes in mesoporous silica is an interesting approach. Investigating the distance between the co-immobilized enzymes can be used to interpret the efficiency of the bioconversion. The biocatalytic cascade when CO_2 is converted to formaldehyde was explained in detail previously in Section 2.5, Chapter 2.

During the co-immobilization process, FateDH and FaldDH might compete to enter the pores or to adsorb on the outer/inner surface of mesoporous silica, which might influence the total amount of each enzyme that can be immobilized. In order to optimize the co-immobilization of FateDH and FaldDH, aiming for high reaction rates, two immobilization parameters were varied in the study; (*i*) enzyme concentration, and (*ii*) the order in which the enzymes were added and mixed with the host material. Furthermore, FRET was used in order to estimate the distance between the co-immobilized enzymes. FRET is a spectroscopic process in which an excited fluorophore (the donor) transfers its energy to a neighboring molecule (the acceptor) by non-radiative dipole-dipole interaction [16, 133].

The two enzymes, were labeled with the same carbocyanine dyes as used in Paper III; the FateDH enzyme with Sulfo-cyanine3 NHS ester (Cy3), and the FaldDH enzyme with Sulfo-cyanine5 NHS ester (Cy5). The labeled enzymes were used for two reasons; (*i*) to monitor the degree of immobilization of the two enzymes independently, and (*ii*) to determine the average distance between the two enzymes using FRET. Once labeled, the enzymes were co-immobilized into MCF particles with a pore diameter of approximately 33 nm, see Table 2.2, Chapter 2. Recently, Zezzi *et al.* reported that the activity of FaldDH increased by functionalizing the MCF surface with mercaptopropyl groups (MP), also observing a low enzyme leakage during the reaction [58]. Therefore, the MP-functionalized MCF particles were used for the co-immobilization of the two enzymes and compared with non-modified MCF.

6.1.1 Two co-immobilization methods: sequential vs simultaneous

To evaluate the order of adding and mixing the two enzymes with the host material, two approaches were used; (*i*) simultaneous co-immobilization, when the two enzymes were immobilized together (for 4h), and (*ii*) sequential co-immobilization, where FateDH was immobilized (for 2h) prior to the addition of FaldDH. It is noteworthy that the enzymes were co-immobilized in the unmodified MCF at a mass ratio of 1:15, (FateDH: FaldDH), aiming for a total enzyme loading of 150 $\mu g_{enzymes}$ per $mg_{support}$. This ratio was used since it was reported previously by Cazelles *et al.* [56] as the optimum ratio for the cascade reaction.

The degree of immobilization for each enzyme was determined separately using absorption spectroscopy, since the labeled enzymes (Cy3-FateDH and Cy5-FaldDH) have well separated absorption spectra in the visible region, with an absorption maximum at 550 nm for Cy3, and at 650 nm for Cy5, see Figure 3.10, Chapter 3.

Table 6.1 shows the degree of immobilization (percentage of the initial amount of each enzyme that were immobilized) for FateDH and FaldDH with the two different methods of co-immobilization, and the total amount of immobilized enzyme measured by absorption at 280 nm, both with and without the dye-labels.

Table 6.1. Degree of immobilization of each enzyme after co-immobilization in MCF using the concentration ratio FateDH: FaldDH = 1:15

Method	DOI Cy3-FateDH[a] (%)	DOI Cy5-FaldDH[a] (%)	Total amount of immobilized enzyme with labeling[b] (%)	Total amount of immobilized enzyme without labeling[b] (%)
Simultaneous	15	95	90	94
Sequential	95	95	95	95

a. Degree of immobilization (DOI) calculated from absorption of Cy3- and Cy5-labeled enzymes, respectively, in supernatant, as an average from 3 independent experiments, with the uncertainty of ± 5% calculated as half the maximum variation.
b. Calculated from absorption of total enzyme in the supernatant at 280 nm.

Simultaneous co-immobilization resulted in that only 15% of the added FateDH was immobilized, whereas 95% of the FaldDH was adsorbed into the support material. In contrast, the sequential method resulted in that 95% of both enzymes were co-immobilized. The low degree of immobilization of FateDH using simultaneous co-immobilization suggests that there is a higher selectivity of the FaldDH in adsorbing to the silica surface. Immobilized more favorably and in higher concentrations, FaldDH, which is a large enzyme (molecular dimensions of 8.6·8.6·19 nm) [51] would occupy the pores and partially block the windows of

the MCFs hindering FateDH (molecular dimensions of 5.3·6.8·10.9 nm) [210] to access the interior of the pores. Therefore, by co-immobilizing the enzymes sequentially, FateDH could enter the pores more efficiently, leading to a high degree of immobilization.

6.1.2 Estimation of the distance between the two co-immobilized enzymes

FRET measurements were performed with the aim to measure the distance between the two enzymes when they were co-immobilized in the MCF silica materials, in order to investigate to what extent, the enzyme-enzyme distance can affect the catalytic activity of the cascade. Experimentally, the output of FRET is presented as transfer efficiency (E). The E value depends on the inverse of the sixth power of the distance (r) between the two fluorophores, see Section 3.3, Chapter 3 for details.

The FRET efficiency was obtained from fluorescence lifetime measurements using time correlated single photon counting (TCSPC). The samples of co-immobilized enzymes, or free enzymes (no particles), were excited by a laser diode using an excitation source at 483 nm, where the donor Cy3 is excited, while the acceptor Cy5 has no absorption (See Figure 3.10, Chapter 3). Emission intensity time profiles were recorded at 565 nm, where the donor (Cy3) has its emission maximum. It is noteworthy that as a control experiment, the emission of each sample at 665 nm (the emission maximum of Cy5), was recorded with the same excitation source. This control experiment provided a proof of FRET in the samples with the donor in presence of the acceptor.

Figure 6.1 shows the emission intensity time profiles of the donor in absence of acceptor and the donor in presence of acceptor at two emission maximum wavelengths. The samples were co-immobilized in the MCF-MP particles with 1:15 ratio of the enzyme concertation. Since the lifetime values of both Cy3 and Cy5 are sensitive to the local environment [187], the spatial distribution of the two enzymes should be kept as similar as possible inside the pores during the lifetime measurements in the presence and absence of acceptor. To that end, Cy3-FateDH was co-immobilized with FaldDH in two ways, always keeping the amount of the enzymes the same. Either FaldDH was labelled with Cy5, denoted donor in presence of acceptor, or the FaldDH lacking the Cy5-label, which is referred as the sample with donor in absence of acceptor.

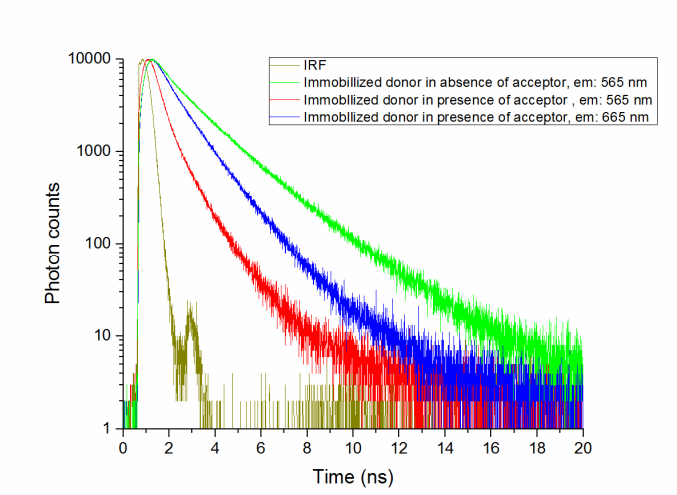

Figure 6.1. The emission intensity time profiles of the donor in absence of acceptor and the donor in presence of the acceptor at the emission maximum of 565 nm and 665 nm. The samples were co-immobilized in MCF-MP with 1:15 ratio of the concentration of the enzymes.

By fitting the intensity decays to mono, bi- or tri-exponential functions, the average lifetime of each sample was calculated. The efficiency of the energy transfer (*E)* between donor and acceptor was calculated from the measurements of lifetime values of the donor in presence and absence of the acceptor using Equation 3.17 (See Section 3.3, Chapter 3).

Table 6.2 shows the measured average lifetime values and calculated energy transfer efficiency of the free and co-immobilized enzymes in unmodified MCF and in MCF-MP at the three different mixing ratios used in the activity measurements. All values are average values ± maximum variation from 8 independent experiments for each sample. As seen in Table 6.2, there is no detectable FRET when the two enzymes are free in solution, which is consistent with a large distance between them in the dilute solutions at all three concentration ratios used. It can also be observed that immobilization increases the transfer efficiency significantly, to above 50% in several cases. Importantly, the *E* value is higher in MCF-MP than in MCF at a given mixing ratio. Furthermore, the FRET efficiency is the highest at the concentration ratio 1:15 for both MCF and MCF-MP, and decreases as the concentration of the two enzymes become more equal. Ideally, when different protein concentrations are compared, the fluorescence life times should be constant, but Table 6.2 shows a slight decrease in τ_D when the concentration of FateDH is increased, especially in the MCF particles. This is most likely due to self-quenching of the FateDH-bound Cy3 and means that the Förster radius R_0 is protein-concentration dependent.

Table 6.2. Life times and energy transfer efficiency of enzymes co-immobilized in MCF and MCF-MP at different enzyme concentration ratios.

	Free enzymes	MCF[a]			MCF-MP[a]		
Ratio[b]	all three ratios	1:15	1:3	1:1	1:15	1:3	1:1
τ_{DA} (ns)[c]	0.64±0.05	0.65±0.05	0.73±0.05	0.88±0.05	0.52±0.05	0.65±0.05	0.85±0.05
τ_{D} (ns)[d]	0.64±0.05	1.45±0.05	1.30±0.05	1.10±0.05	1.45±0.05	1.45±0.05	1.33±0.05
E[e]	0	0.56±0.02	0.44±0.02	0.20±0.02	0.64±0.02	0.55±0.02	0.36±0.02

a. Total protein loading 150 $mg_{enzymes} \cdot g_{support}^{-1}$.
b. Mixing ratio Cy3-FateDH: FaldDH-Cy5.
c. Average lifetime of donor (Cy3) in presence of acceptor (Cy5).
d. Average lifetime of donor (Cy3) in absence of acceptor (Cy5).
e. The transfer efficiency calculated from the average lifetime values using Equation 3.17.

It is noteworthy that the R_0 value for the Cy3/Cy5-pair under our conditions is approximately 6 nm in free solution which is in agreement with previous reports [162, 211]. However, after immobilization, the R_0 value can change due to two reasons: (*i*) possible self-quenching of Cy3 (due to high concentration of labeled protein in the pores) which could reduce the quantum yield of the donor, and (*ii*) enhancement the fluorescence intensity of donor due to high viscosity causing a higher quantum yield [187, 212]. After immobilization in MCF and MCF-MP, the R_0 value for each sample was calculated using Equation 3.19 to make sure that the values are close enough for comparison of the transfer efficiency values (Table 6.3).

Table 6.3. The calculated R0 (Förster distance) of donor after immobilization.

	MCF			MCF-MP		
Ratio	1:15	1:3	1:1	1:15	1:3	1:1
R_0	6.84±0.05	6.73±0.05	6.57±0.05	6.84±0.05	6.84±0.05	6.75±0.05

Table 6.3 shows that the calculated values of R_0 at different enzyme concentrations only vary between 6.6 and 6.8 nm. Since the maximum variation of 0.2 nm is much smaller than the pore diameter (33nm), the R_0 value was taken to be essentially constant when the transfer efficiency was compared at different enzyme concentrations.

When calculating R_0, the value $k^2 = 2/3$ for the dipole orientation factor was used, which assumes random orientation of the transition moments of the Cy3 and Cy5 chromophores. The assumption of free movement of the chromophores was supported by time-resolved anisotropy measurements on Cy3-FateDH in free solution and after immobilization, which also strongly supports that the donor dye does not adsorb to the silica wall since both dye and wall are negatively charged. For more details the reader is referred to Paper IV.

Our system is complex from a FRET point of view, since each Cy3-FateDH donor protein may be surrounded by several Cy5-FaldDH acceptors, and vice versa. Berney *et al.* [213] have used Monte Carlo simulations to study systems with multiple donors and acceptors, reporting suitable values for the number of donors per acceptor (R_{DA}) in FRET experiments. The reported number can have an effect on the mean distance between donors and acceptors. The R_{DA} values in the present study (number ratios 0.04, 0.17 and 0.53 for the mass mixing ratios 1:15, 1:3 and 1:1 respectively) partly covers the R_{DA} range 0.1-10 where the simulations indicated the highest sensitivity to donor-acceptor distance [213]. The energy transfer efficiency values in Table 6.2 are therefore suitable for discussing the distances at different enzyme concentrations, at least qualitatively. The higher E values in MCF-MP than in MCF reveal a shorter average distance between the Cy3-donor and the Cy5-acceptor, which can be interpreted qualitatively as the FateDH and FaldDH being closer on the average in the MCF-MP for a given mixing ratio. Similarly, it can be concluded that for a given particle type, they are closer for the optimal ratio of 1:15, compared to 1:3 and 1:1.

Equation 3.18 can be used to estimate the average distance (r) between FateDH and FaldDH from the FRET-efficiencies in Table 6.2 (taking into account that R_0 is essentially constant conditions in Paper IV), and the results are presented in Table 6.4.

Table 6.4. The calculated r (distance between two dyes) after immobilization.

	MCF			MCF-MP		
Ratio	1:15	1:3	1:1	1:15	1:3	1:1
r	6.58±0.05	7.20±0.05	8.30±0.05	6.20±0.05	6.61±0.05	7.45±0.05

It should be noted that the calculated r values are based on a single distance model between one donor and one acceptor fluorophore [16], so they are clearly complex averages for several reasons. In addition to that each Cy3-FateDH donor likely is surrounded by multiple Cy5-FaldDH acceptors, even for a single enzyme couple, the E-value reflects an average over several Cy3/Cy5-pairs, since each enzyme carries several dyes. Moreover, the exact location of Cy3 bound to FateDH and Cy5 bound to FaldDH are not known. Therefore, our comparison with

the results on catalytic activity will focus on the trends in the *E* values, rather than the actual values for the average distances. Still, one important conclusion can be drawn from the fact that the *r* values in Table 6.4 all are significantly smaller than the pore size (33nm). This observation, and the strong decrease in *E* vs *r* (Equation 3.18), indicates that the dominant contribution to the FRET in all immobilized cases studied here most likely are between enzymes that are located in the same pore.

6.1.3 The catalytic activity and distance between the two enzymes

The same procedure of co-immobilization was used for the activity measurement, except that the enzymes were not labeled with two dyes. Notably, Table 6.1 shows that the dye labels had no detectable effect on the degree of immobilization, at least in terms of the total protein uptake, so the activity measurements were most likely obtained at the same enzyme concentrations in the pores as the FRET results.

Figure 6.2 shows the specific catalytic activity in the three studied cases; (*i*) free in solution and sequentially co-immobilized in (*ii*) MCF and (*iii*) MCF-MP, respectively. For the mass ratio FateDH:FaldDH = 1:15, Figures 6.2a and 6.2b show that co-immobilization of the enzymes in MCF did not increase the yield of the cascade reaction significantly compared to the enzymes free in solution. In contrast, upon co-immobilization in MCF-MP the catalytic activity for formaldehyde formation increased about 4 times, as shown in Figure 6.2c. This improvement in the catalytic activity of the cascade reaction is very promising considering that these two catalytic reaction steps (reduction of CO_2 to formate and subsequent reduction of formate to formaldehyde) are the rate limiting steps for the overall conversion of CO_2 to methanol [56, 59, 214].

The trends in the transfer efficiencies in Table 6.2 exhibit a noteworthy correlation with the enzyme activity results in Figure 6.2. The higher the *E* value, (*i.e.* the shorter the average distance between the two enzymes), the higher the activity of the cascade reaction. This observation indicates that the cascade becomes more efficient when the two confined enzymes are closer to each other. The fact that no FRET was observed when the two enzymes are in free solution means that they exhibit no detectable tendency to aggregate, or otherwise, the Cy3 on one FateDH enzyme would come within the Förster distance (about 6 nm) from Cy5 on a nearby FaldDH, since both proteins are a few nm in size. This observation explains the lower catalytic activity of the enzymes when free in solution (Figure 6.2a), as well as supports that the

enhanced activity inside the particles is due to the forced proximity of the two enzymes upon immobilization.

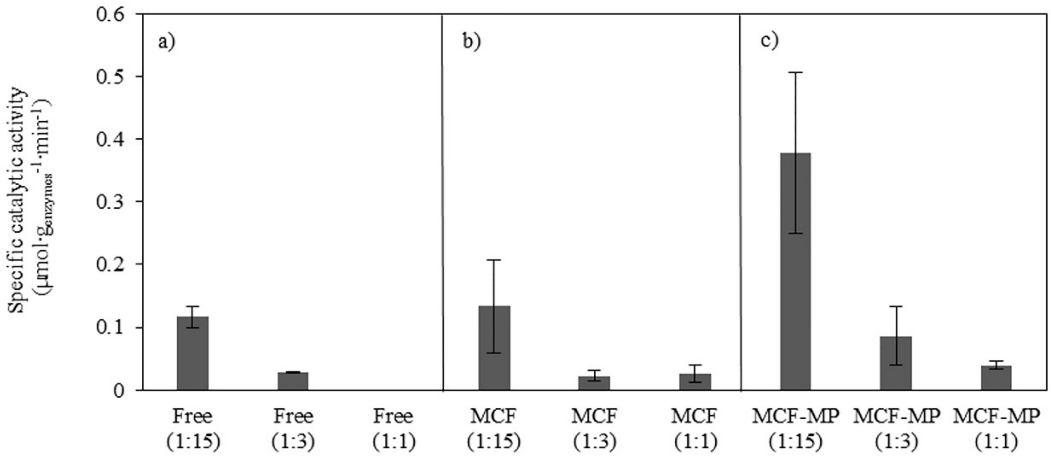

Figure 6.2. Specific activity of the cascade reaction using FateDH and FaldDH free in solution (a), and co-immobilized in MCF (b) and MCF-MP (c). The enzymes were co-immobilized using a sequential method. In parenthesis are the mass ratio of FateDH:FaldDH used in the reactions. Values are presented as means ± standard deviation (n=3).

It has been proposed [215] that distances smaller than approximately 10 nm between the catalytic sites of enzymes are required to promote substrate channeling, which potentially results in a higher efficiency of sequential reactions [215]. The FRET results presented here indeed indicate that the enzymes immobilized in MCF and MCF-MP are closer than 10 nm to each other, and also that the FaldDH enzyme, which is closest to a given FateDH, is located in the same pore. Such a situation would facilitate the transport of the formate-intermediate from FateDH to FaldDH. Secondly, the energy transfer is the highest when the enzymes are immobilized in the MCF-MP using a concentration ratio of 1:15 (FateDH:FaldDH), which also resulted in the highest catalytic activity. Finally, when the enzymes were co-immobilized in MCF, the energy transfer was smaller than in MCF-MP, which is consistent with the observation that the catalytic activity was not improved significantly in the non-modified particles. These results indicate that even though the enzymes are closer in the MCF than in free solution, the proximity is not high enough to efficiently promote substrate channeling as seems to occur when the enzymes are co-immobilized in MCF-MP.

6.2 TEM-IGS study of the immobilized enzymes

A common question for immobilization applications a common question is where the enzyme are localized, if the enzymes are only inside the pores after immobilization in the mesoporous materials, or if they are also subject to attachment on the outer surface of the silica particles. Previously, methods for monitoring the amount of immobilized enzymes in silica materials have been based on indirect methods, such as, UV absorption, fluorescence spectroscopy, Fourier Transform-Infrared Spectroscopy (FTIR) in order to quantify how much of the enzyme that remains in the surrounding solution [88, 179, 216-219]. However, at least until now, it has not been possible to distinguish the amount of enzymes on the external surface from the enzyme quantity inside the pores.

Microscopy techniques, used as direct methods, have been applied to visualize enzymes after immobilization into the MPS particles. Suh *et al.* have applied confocal laser scanning microscopy to observe the location and distribution of Cy5-labelled BSA in large mesoporous silica particles (150 μm) with varying pore size (2.2- 45 nm). The results showed that the proteins entered further into the pores with increasing pore size [220]. Furthermore, super-resolution microscopy (Stochastic Optical Reconstruction Microscopy, STORM) was recently used to monitor the penetration depth of different proteins in SBA-15 using different pore diameters. It was observed that the largest protein penetrates the porous support less, compared to two other smaller protein [94]. It should be noted that the highest resolution of the fluorescence setup at this time was 30 nm, while the size of the enzymes used in biocatalytic applications typically range between 4 to 12 nm, therefore, studying the exact location may not be possible using super resolution microscopy. In contrast, electron microscopy techniques have a typical resolution of 0.2 nm and hence can be a better choice to visualize the distribution and location of immobilized enzymes. Piras *et al.* [221] have developed a method using a combination of transmission electron microscopy and immunogold staining (TEM-IGS) to monitor the human lysozyme immobilized to SBA-15 particles. This method is based on a primary antibody specific for the protein in question, and a secondary antibody- conjugated gold nanoparticle which can be bound to the primary antibody. The results showed that the proteins are immobilized to both the external and internal surface of the SBA-15 particles.

In Paper V, the same procedure of the TEM-IGS method [221] was applied to visualize alcohol dehydrogenase (ADH) immobilized in three different silica materials, one MCF with 26.5 nm pore diameter, and two SBA-15 particles with 10 nm and 6.8 nm in pore diameters (see Table 2.2, Chapter 2). First, a qualitative comparison between the two types of mesoporous silica

(MCF and SBA-15) was performed. The main motivation was to show the effect of pore morphology on the protein uptake and if the pore structure can affect the activity efficiency of the enzymes. As has been discussed previously, the SBA-15 materials have a porous hexagonal array structure with a pore diameter less than 10 nm, whereas the MCF particles have spherical pores with connecting windows, and usually a pore dimeter larger than 10 nm [74, 83]. Secondly, the enzymes were immobilized into these silica materials with two different enzyme loadings, 150 and 300 (mg of enzyme per gram support), in order to study the distribution of immobilized enzymes in each silica material based on a stereology method. Moreover, the density and the radial distribution of the immobilized enzymes was investigated by using the image evaluation software ImageJ.

6.2.1 Qualitative comparison

The ADH loaded MPS particles, loading values of 150 and 300 mg of enzyme per gram support, as well as the control samples were imaged by TEM. However, for the qualitative comparison between different MPS particles, only the control sample and the loaded samples with 300 mg of enzyme per gram support will be discussed here. The morphology of the different silica materials (MCF and SBA-15) are compared in Figure 6.3a, Figure 6.4a and Figure 6.5a respectively. The spherical porosity of MCF in Figure 6.3a, is clearly visible, and can be compared with the typical hexagonal array of the pores and cylindrical parallel channels of SBA-15 (Figure 6.4a and 6.5a). However, the MCF windows cannot be observed in the TEM images. The presence and size of the window in MCF particles were measured using nitrogen sorption [83]. The TEM images of the control samples (Figures 6.3a, 6.4a, 6.5a) indicate the specificity of the labeling procedure since almost no gold particles are found, indicating very low unspecific binding.

Each black spot has a gold nanoparticle in the sample images (Figures 6.3b, 6.4b and 6.5b) can be associated with the presence of one alcohol dehydrogenase (ADH) molecule. Figure 6.3b shows the ADH loaded into MCF particles at two different degrees of enzyme loadings, as can be compared in Figure 6.4b and Figure 6.5b, displaying the ADH loaded into SBA-15-10 and SBA-15-6.8 particles, respectively. A larger number of gold nanoparticles can be seen in MCF (Figure 6.3b) as compared to the SBA-15 particles. The distribution of gold nanoparticles in the MCF images (Figures 6.3b) is more even, whereas the distribution of gold nanoparticles in the SBA-15 particles are restricted to the external surface (Figures 6.4b and 6.5b). The results are in agreement with previous observations [58, 59] were the MCF silica materials has been

reported as a better host material in biocatalytic applications. This since the enzymes can be more accessible for the substrate because of the uniform spherical pores, and that the enzymes are immobilized inside the pores. However, in the SBA-15 particles, with smaller hexagonal column morphology of the pores, the enzyme can block the opening of the pores and lower the amount of enzymes that might be immobilized. This is true for both types of SBA-15 particles used in this study, but especially for SBA-15-6.8 where it can be even more challenging due to the smaller pore diameter (6.8 nm) compared to the ADH enzyme (9.1 nm). In this case it is expected that the ADH molecules are immobilized more at the external surface. Clemments *et.al.* [94] have recently employed a mathematical model to reveal the penetration depth of immobilized proteins (the same size as ADH) into SBA-15 particles with a pore dimeter of 6nm using STORM super resolution microscopy. The results showed that the proteins cannot penetrate deeply into SBA-15, however, the penetration for proteins which are 10 times smaller than ADH was reported to penetrate 30% deeper. This result is in agreement with ours, with the ADH enzyme not being uniformly distributed on the SBA-15 particles in our study (Figure 6.4b and Figure 6.5b). It should be noted however that there are zones on the external surface with a higher labeling density and zones with lower density (internal surface).

It should be noted that the labeling procedure underestimates the number of immobilized enzymes, since the primary and secondary antibodies cannot bind effectively with all ADH immobilized, but only with those in the external top face of the ultra-section. Still, the number of ADH enzymes can be counted by using a stereology method, and compared with the obtained enzyme loadings in each MPS particle as it is used in biological applications [222, 223].

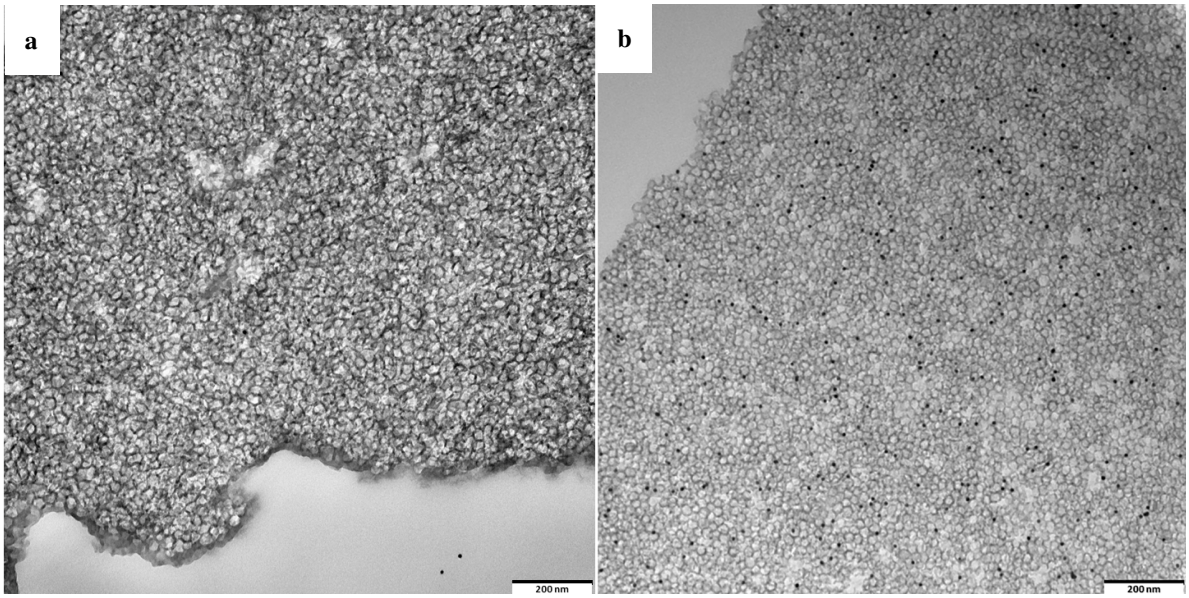

Figure 6.3. TEM images of immunogold labeling of MCF particles;(a) control sample (No ADH enzyme loaded) (b) with 300 $mg_{enzyme}.g_{support}^{-1}$ enzyme loading; scale bar 200nm.

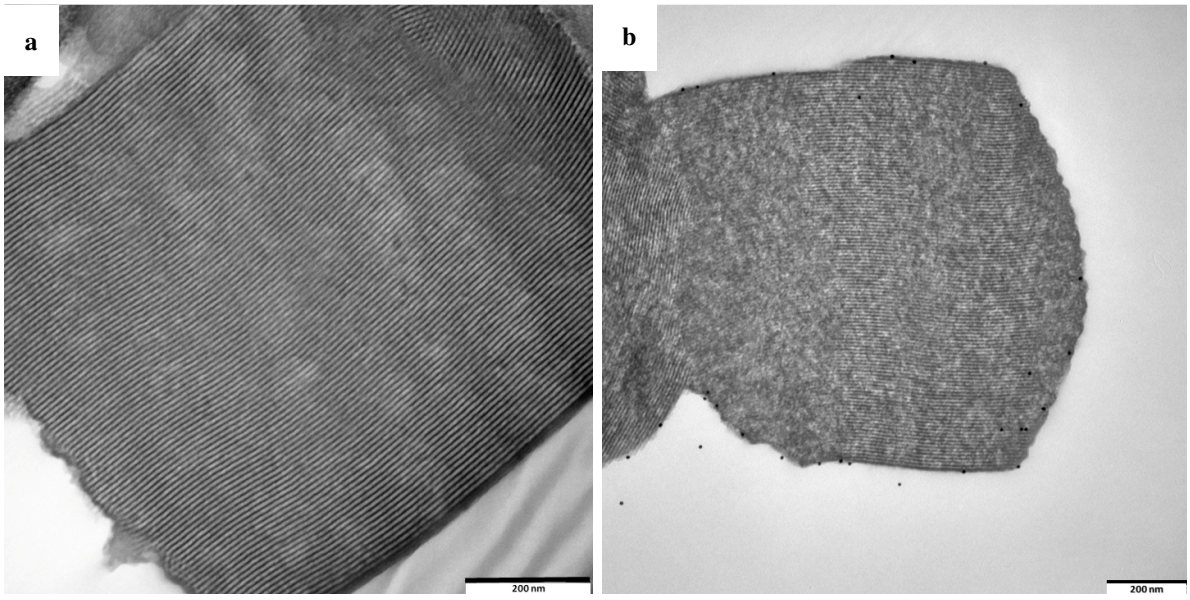

Figure 6.4. TEM images of immunogold labeling of SBA-15-10 particles; a) control sample (No ADH enzyme loaded) b) with 150 $mg_{enzyme}.g_{support}^{-1}$ enzyme loading; scale bar 200nm.

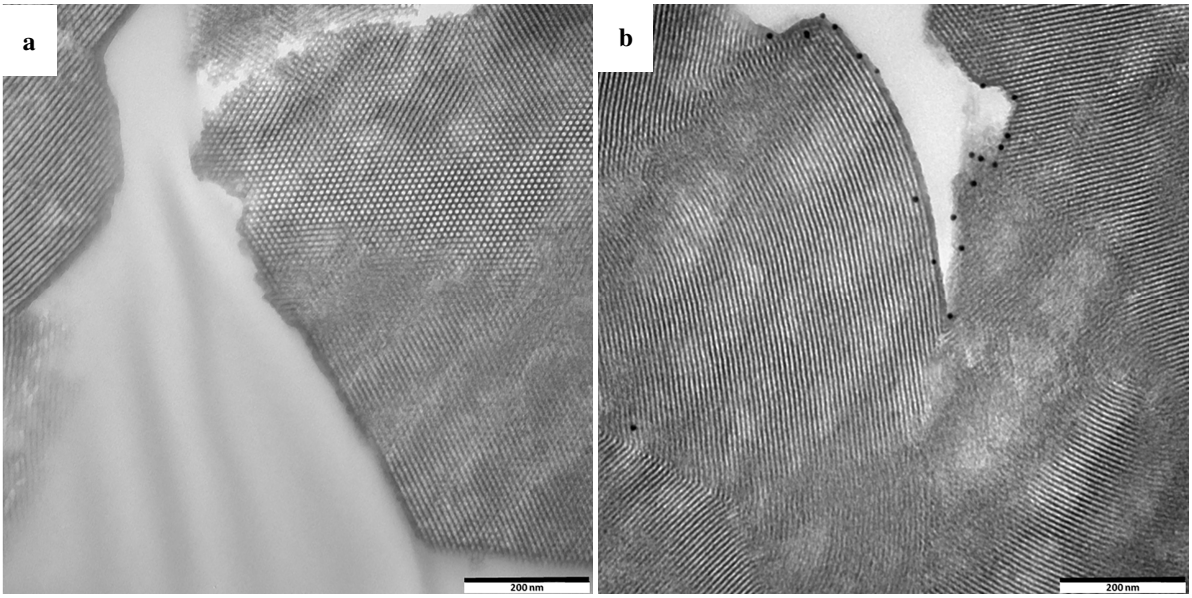

Figure 6.5. TEM images of immunogold labeling of SBA-15-6.8 particles; a) control sample (No ADH enzyme loaded) b) with 300 $mg_{enzyme} \cdot g_{support}^{-1}$ enzyme loading; scale bar 200nm.

6.2.2 Quantitative comparison

Alcohol dehydrogenase (ADH) was immobilized in the three different MPS using two enzyme loadings: 150 and 300 (mg enzyme per gram of support). Table 6.5 shows how the enzyme loadings obtained by the indirect method varied according to the MPS used.

In SBA-15-6.8 the small size of the pores in relation to the size of the enzyme (the hydrodynamic radius of ADH, R_H = 4.55 nm) restricts the access of the enzyme to the available pore volume, resulting in much lower enzyme loading. In SBA-15-10 a degree of immobilization of 93% was obtained for the loading of 150 $mg \cdot g^{-1}$. The mean pore size in this material is slightly bigger than the enzyme, however, it seems to be large enough for ADH to be immobilized inside the pores. As expected, for the enzyme loading of about 300 $mg \cdot g^{-1}$, only 240 $mg \cdot g^{-1}$ was immobilized (DOI: 80 %).

In contrast, when ADH was immobilized in the MCF support material the degree of immobilization was higher than 90 % at both enzyme loadings. The higher loadings of enzymes in MCF than in SBA-15-10, can be attributed to the higher porosity and the structure of the MCF. In the MCF the large pores can be more accessible to ADH, whereas in the SBA-15-10 the enzymes were immobilized close to the entrance of the long cylindrical pores, not penetrating inside of them and occupying the external surface of the silica.

Table 6.5. Degree of immobilization (DOI) of ADH in each silica material.

Support material	Enzyme loading expected (mgenzyme·gsupport^{-1})	Enzyme loading obtained (mgenzyme·gsupport^{-1})	DOI (%)
MCF	300	280	93
MCF	150	144	96
SBA-15-10	300	240	80
SBA-15-10	150	140	93
SBA-15-6.8	300	160	53
SBA-15-6.8	150	100	67

To estimate the number of immobilized enzymes in each silica material, a stereology method was applied in Paper V. To have an unbiased quantification, micrographs of the particle were taken at systematic positions with a random start. The magnification was chosen in a way that the gold-particles can be seen easily (*i.e.* x63000). A lattice grid, in this case square, with known mesh size 100 nm·100 nm was placed over the TEM image of the sample[224].

The number of gold labeled antibodies in a specific lattice square (10^4 nm) of each MPS sample was quantified and compared with protein loading values. The quantification values reported here are the mean value of 20 images of each sample. For details of the counting procedure see paper V.

As seen in Table 6.6, the number of the enzymes (N_{enzyme}) per unit area (10^4 nm) of the MCF particles are in the same direction and exhibits similar trends as the (indirectly) obtained enzyme loading values. For comparative reason, the ratio at the two enzyme loads was calculated for the particle densities (R_S), and the indirectly measured enzyme loading (R_E). For MCF the R_E-value (1.94) is surprisingly close to the R_S ratio (1.92). This observation suggests that the amount of enzyme immobilized into the MCF can be quantified both with indirect measurements through the supernatant, and direct microscopic observations.

In the SBA-15-10 and SBA15-6.8 particles, the stereology method gives a lower value for the R_s-value compared to the R_E-ratio. This result suggests that a certain amount of enzymes is immobilized at the outer surface which cannot be detected by TEM images properly because these enzymes are more easily removed by the particle washing. Especially in SBA-15-6.8, the internal immobilization of the enzyme is likely to be hindered because of the competition between the enzyme size (9.1 nm) and the pore diameter (6.8 nm), and thus a lower amount of the enzyme was immobilized into the pore compared with the MCF and SBA-15-10.

Table 6.6. Quantification of the enzymes immobilized in different MPS particles with stereology method in different expected enzyme loadings.

Support material	P_{LD} expected ($mg_{enzyme} \cdot g_{support}^{-1}$)	P_{LD} obtained ($mg_{enzyme} \cdot g_{support}^{-1}$) ±5	R_E	Density ($N_{enzyme}/10^4$ nm) ±0.2	R_S
MCF	300	280	1.94	1.48	1.92
MCF	150	144		0.77	
SBA-15-10	300	240	1.71	0.59	1.45
SBA-15-10	150	140		0.41	
SBA-15-6.8	300	160	1.6	0.33	1.32
SBA-15-6.8	150	100		0.25	

Finally, the radial distribution of the immobilized enzymes was estimated by using the software ImageJ. Figure 6.6 shows the immobilized ADH loaded in to MCF at 150 mg protein loading and with the radial grid used to evaluate the radial distribution. The distance between each layer is 100 nm and the area of each layer was calculated automatically based on a custom made macro (see Paper V for details). The number of immobilized enzymes (red spots in Figure 6.6) in each sample micrograph was counted and the density of immobilized enzymes in each layer was obtained. To compare the findings with the results from the stereology approached used above, the density is reported as number of enzymes per 10^4 nm^2. Figure 6.7 shows graphs of the radial distribution of the immobilized enzymes based on the density of gold nano-particle versus the distance from external surface to center

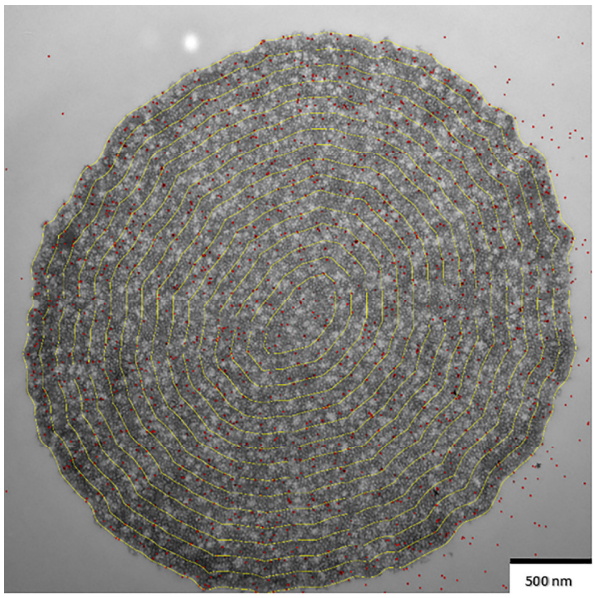

Figure 6.6. Overlay of the TEM image with the detected gold particles marked in red and the analyzed regions marked in yellow, MCF particle , at 150 mg $_{enzyme}$. $g_{support}^{-1}$, scale bar 500 nm

As seen in Figure 6.7, the density of the gold nanoparticles is the highest in the first 150 nm of each material. In the MCF particles, the density is seen to be almost constant up to 2000 nm from the surface. In contrast, both types of SBA-15 particles exhibits a monotonous decrease in the density as the distance from the surface increases. This observation shows that this particle type cannot be filled with enzymes probably due to the hexagonal and narrower pore morphology. Moreover, the results show that the enzymes cannot penetrate to the center of the SBA-15. Interestingly the decay of the density seems to be somewhat slower in SBA-15-10 (especially at the higher protein loading), consistent with the larger pore size compared to SBA-15-6.8.

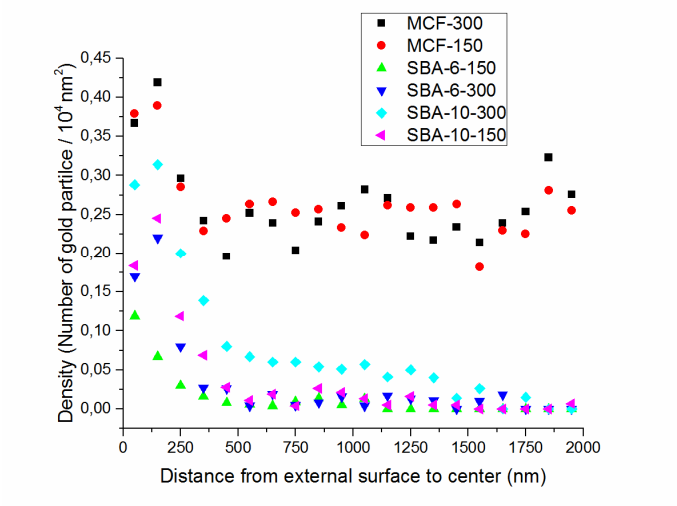

Figure 6.7. Penetration depth of the immoblized enzymes in to MPS particles, the data is obtained from 5 images per each material.

The results in Figure 6.7 show that the MCF particles have an even distribution inside the particles, probably due to its more open pore morphology and may therefore function more efficient for biocatalysis. Secondly, the results demonstrated how the stereology method can be used for quantification of the immobilized enzymes based on the results from the TEM-IGS.

Concluding Remarks

The main purpose of this thesis was to further understand the mechanism of enzyme immobilization in mesoporous silica particles and also optimizing the immobilization process. Characterization of the microenvironment inside the MPS particles was performed by using enzyme-attached dyes. The work has mainly been conducted through spectroscopy techniques, but in the last paper, transmission electron microscopy was combined.

In efforts to understand the mechanistic steps of immobilization process, the dynamics of enzyme immobilization was studied. A fluorescence assay was developed to monitor translational dynamics of epicocconone labeled enzymes in real time while they are immobilizing into the MPS particles. In Paper I, three enzymes different in size, but comparable with the given pore size, were studied. The results showed that the size of enzyme can strongly affect the translational dynamics. The rate of immobilization was also quantified for each enzyme; the larger the enzyme, the slower the rate of immobilization. We also showed that epicocconone used in this study has high degree of bleaching, both photo-bleaching and

through a dark reaction. The nature of the dark reaction needs to be better understood to improve the use of epicocconone in fluorescence spectroscopy.

As a continuation to Paper I, the rotational dynamics of the confined enzymes was studied in Paper II using the intrinsic amino acid residues. Fluorescence anisotropy spectroscopy, steady state and time-resolved, was exploited, in order to answer to what extent the rotational mobility of the global enzyme can be restricted after immobilization. The results showed that the rotational mobility of the confined enzyme is retarded compared to the enzyme free in solution, but that the enzymes still are mobile. This retardation is higher in the MPS particles with smaller pore size. The retardation of protein rotation was investigated by two mechanisms of either protein-protein or protein-wall hydrodynamic interactions. This study showed that the latter mechanism probably has stronger effect on the retardation of the enzyme rotation. The results from time-resolved anisotropy showed that tryptophan rotational mobility is dominant depolarization mechanism after immobilization and the global enzyme mobility is highly restricted.

In order to probe the microenvironment inside the MPS particles, two carbocyanine dyes (Cy3 and Cy5) in a ratiometric method were used in Paper III. The carbocyanine dyes used in this study are molecular rotors, meaning they are sensitive to viscosity, and also photo-stable as a suitable alternative to epicocconone. The microviscosity that the enzyme experience inside the MPS particles was measured. In this study mesoporous silica different in pore morphology and surface modification were used. The results showed that Cy3 and Cy5 are a good pair of protein-bound dyes to measure viscosity independently of other solvent effects such as polarity, if the two dyes are attached to different proteins. The intensity ratio calibration curve is more sensitive at low levels of viscosity and may require some extrapolation if the viscosity is much higher than in bulk water. The effective microviscosity is higher inside the MPS particles with smaller pore size for a given enzyme. The effective viscosity inside the MPS particles with the hydrophobic surface modification cannot be reported with this method because of the presence of FRET in the ratiometric method. The main reason may be the high pore filling of the enzyme in the modified particles.

The distribution of the enzymes inside mesoporous silica particles was studied by using two techniques, FRET (Paper IV) and TEM-IGS (Paper V). Paper IV showed that the specific activity of the cascade reaction using FateDH and FaldDH is 4 times higher when the enzymes are co-immobilized in the MCF particles with hydrophobic modification than in MCF without modification or free in solution. This result was in accordance with energy transfer efficiency

values from the FRET measurements, which suggests that the higher cascade efficiency is most likely because the two enzymes are closer to each other and in the same pore, meaning that the probability of direct substrate transfer between FateDH and FaldDH increases. Moreover, FRET measurement free in solution showed that there is no attractive interaction between the two enzymes, so the enhancement of catalytic activity in the particle pores is due to sterically forced proximity of the cascade participants. These findings can be used for a better understanding of immobilized enzyme cascades in general, and be applied in further optimization of biomimetic systems used to convert CO_2 to methanol. In order to improve the FRET measurement of the co-immobilized enzymes in mesoporous silica particles, the degree of labeling should be reduced to one cyanine dye per protein.

Finally the location of the immobilized enzymes was visualized using transmission electron microscopy and immunogold staining in Paper V. In this study two types of MPS particles are used with two different pore morphology, spherical and hexagonal. The quantification of the number of immobilized enzymes was discussed based on two different methods, stereology-based quantitative analysis of TEM images and indirect spectroscopic measurement of the amount of non-bound enzyme in the solution surrounding the particles. The results show that not only the size of the pores in the MPS particles is an important factor, but the morphology of the pores also plays a crucial role in optimizing the enzyme immobilization.

The work in this thesis shows that the size of the enzyme, the surface modification of the support and the pore morphology of the mesoporous silica can be crucial factors for obtaining higher enzyme activity, stability and loading. Moreover, measuring the effective viscosity in the MPS particles supports the idea that the protein-protein and protein-wall hydrodynamics interactions are two mechanisms involved in the retardation of the enzyme dynamics. The results of this thesis can be applied to optimize enzyme immobilization systems and to better design the immobilization process in biocatalytic applications.

Acknowledgements

This thesis is the summary of my PhD, a five-year journey. It wouldn't have been possible without the support of many people who deserve my deepest gratitude for their help and encouragement:

My advisor, **Björn Åkerman,** for your support, patience and always being available to answer my questions, for being a perfect teacher and educating me as a scientist. Thank you for encouraging me in a timely manner that lead me to complete my journey smoothly. I could not have asked for a better supervisor.

My co-advisor, **Anders Palmqvist,** for your scientific visions which helped me to enrich my research work.

My extra, unofficial supervisor, **Maria Abrahamsson,** for inviting me warmly to your Monday journals club. Thank you for your never-ending support (especially in the last two months) in science and non-science.

The members of SUPRA Enzyme Cluster, **Lisbeth Olsson, Cyrielle Bonzom, Milene Zezzi** along with **Anders** and **Björn** for fruitful discussions about enzyme immobilization.

Joakim Andreasson and **Marcus Wilhelmsson** for your guidance and scientific discussions about quenching and FRET, your pedagogical skills are wonderful.

Nina Kann, Bo Albinsson, **Per Lincoln**, **Jerker Mårtensson**, for your constructive feedbacks.

Sandra Rocha for always taking your time and proof reading my thesis. Your outstanding help and support during my PhD were heart-warming.

Milene Zezzi for always being energetic, positive. Thank you for the wonderful and fun days in the lab.

Nils Carlsson and **Kassam Abdel Mallek** for generously handing the "Paper I" project to me. A special thanks to Nils for teaching me optical spectroscopy in the very first six months of my PhD, you were always ready to help me in the lab, even though at the time you were writing your own thesis.

Massimo Micaroni for teaching me how to work with TEM patiently, **Hendrik Deschout** for helping me with MacroImage. A special thanks to **Center for Cellular Imaging (CCI)** in **Sahlgrenska academy** for providing a very professional service.

Frank Birke, **Eugeny Ermilov**, **Christian Oelsner** for accepting me warmly in **PicoQuant lab**, Berlin.

Gunilla Saethe, Anna Molander, Lotta Pettersson for your excellent administrative support.

My wonderful colleagues and friends:

Rita (*Roz*) and **Damir (*The Rock*)** for always being ready for Fika, no matter where (which floor!)! *The waffle lover* miss you guys every day at work!

Ville and Sangamesh, for being the best officemates, cheering me up with your sense of humour every day, and you guys will have my word that the common area will be given back to you soon! **Ville,** your care and support were priceless when I was writing this thesis!

Beautiful ladies in *Candy Office*, **Betul, Vandana and Elin** for kindly offering me candies, chocolates, cookies; without you guys, writing this thesis could have been bitter! I'm still touched by your support in the last few months. A special thanks to **Betul** and **Vandana** for keeping company with me during weekends when I was in the office; you are wonderful!

Dasha for spreading your positive energy every day, especially on Monday mornings and convincing me to dance Salsa!; **Kubra** for always being so kind and your beautiful words; **Sara** for being so nice and always ready to help with chemical ordering and many other things, even carrying my desk!; **Gerard** for being caring and proof reading my thesis; **Lynga** for being so helpful during my teaching time and for our joyful chats in corridors!; **Lu Lu** for being a very good story teller especially in the electrophoresis

lab!; **Istvan** for taking my random questions about proteins and also introducing me to the benefits of Irish coffee!; **Kumar** for our famous discussion about how to defence!; **Ranjeet** for always saving me in the lab!; **Gaowa, Fredrik, Cassandra, Valeria** for the Monday journals club and one special thanks to **Cassandra** for kindly proof reading my thesis; **Moa** and **Anders** for always answering my never-ending questions about FRET!.

To all my colleagues, present and past, in 5th floor and MC2: **Jesper, David, Louise, Maria MD, Magnus, Jocce, Lena, Amir, Anna M, Bella, Nesrine, Emelie, Yuanmo, Fredrik W, Tony, Nikola, Niklas, Robin, Jens, Laura, Hilda, Alena, Sune and many, many more.**

Hoda and Tobias for making beautiful memories, for all gatherings and Fika on Friday nights and discussing the gravity! **Hoda** having you close as a friend is amazing, thanks for cheering me up with cooking Persian food!

Mehrnaz, Mazdak for calling me ***Adrian's aunt*** officially, the way you supported me during the last few weeks was priceless. **Mehrnaz** thanks for being such a good friend and **Adrian** your smiles are magical.

Mahna for 15 years of friendship and always being a there to listen; no matter how far apart we are, you are always the first person to count on.

Elham and **Safa** for always being supportive; **Safa** you are not just my brother-in-law, you are my one and only brother; **Elham**, my beautiful sister, thanks for showing me how to be strong and not to give up even those moments that life is not colourful.

Shaghayegh, my lovely sister, for showing me how to raise tall like a "One" and not being a "Zero".

My parents: **Pooran and Seyed Ebrahim,** for your trust and endless love. Your passion of life is outstanding, thanks for showing me that every morning is a new day for being a better person and living the day to the fullest.

Sam, my bestie, for believing in me as a PhD, even at the time that I was writing my master thesis! Thanks for your care, support and love during the last 5 years.

Pegah S. Nabavi Zadeh, May 2018

Bibliography

1. Bernal, J.D., *The Physical Basis of Life.* Proceedings of the Physical Society. Section B, 1949. **62**(10): p. 597.

2. Andrew, P.B., *J D Bernal: the sage of science.* Journal of Physics: Conference Series, 2007. **57**(1): p. 61.

3. Armstrong, E.F., *Enzymes: A Discovery and its Consequences.* Nature, 1933. **131**: p. 535.

4. Blake, C.C.F., et al., *Structure of Hen Egg-White Lysozyme: A Three-dimensional Fourier Synthesis at 2 Å Resolution.* Nature, 1965. **206**: p. 757.

5. Kirk, O., T.V. Borchert, and C.C. Fuglsang, *Industrial enzyme applications.* Curr Opin Biotechnol, 2002. **13**(4): p. 345-51.

6. Kim, J., H. Jia, and P. Wang, *Challenges in biocatalysis for enzyme-based biofuel cells.* Biotechnology Advances, 2006. **24**(3): p. 296-308.

7. Malhotra, B.D. and A. Chaubey, *Biosensors for clinical diagnostics industry.* Sensors and Actuators B: Chemical, 2003. **91**(1): p. 117-127.

8. Xu, S.-w., et al., *Efficient Conversion of CO2 to Methanol Catalyzed by Three Dehydrogenases Co-encapsulated in an Alginate−Silica (ALG−SiO2) Hybrid Gel.* Industrial & Engineering Chemistry Research, 2006. **45**(13): p. 4567-4573.

9. Ahuja, S.K., G.M. Ferreira, and A.R. Moreira, *Utilization of enzymes for environmental applications.* Crit Rev Biotechnol, 2004. **24**(2-3): p. 125-54.

10. Koeller, K.M. and C.-H. Wong, *Enzymes for chemical synthesis.* Nature, 2001. **409**: p. 232.

11. Beatriz M. Brena, F.B.-V., *Immobilization of Enzymes and Cells* in *Methods in Biotechnology*, J.M. Guisan, Editor. 2006, Humana Press.

12. Datta, S., L.R. Christena, and Y.R.S. Rajaram, *Enzyme immobilization: an overview on techniques and support materials.* 3 Biotech, 2013. **3**(1): p. 1-9.

13. Reshmi, R., G. Sanjay, and S. Sugunan, *Enhanced activity and stability of α-amylase immobilized on alumina.* Catalysis Communications, 2006. **7**(7): p. 460-465.

14. Wang, P., et al., *Enzyme stabilization by covalent binding in nanoporous sol-gel glass for nonaqueous biocatalysis.* Biotechnology and Bioengineering, 2001. **74**(3): p. 249-255.

15. Jameson, D.M., *Perspectives on Fluorescence; A Tribute to Gregorio Weber*, ed. M. Hof. 2016, Springer International Publishing Switzerland: Springer, Cham.

16. Lakowicz, J.R., *Principles of Fluorescence Spectroscopy*. 3rd ed. 2006, Baltimor, USA: Springer.

17. Horowitz, N.H., *One-gene-one-enzyme: remembering biochemical genetics.* Protein Science : A Publication of the Protein Society, 1995. **4**(5): p. 1017-1019.

18. Wagner, I. and H. Musso, *New Naturally Occurring Amino Acids.* Angewandte Chemie International Edition in English, 1983. **22**(11): p. 816-828.

19. Alberts B, J.A., Lewis J, et al, *Molecular Biology of the Cell*. 4th ed. 2002: New York: Garland Science.

20. Pauling, L., R.B. Corey, and H.R. Branson, *The structure of proteins: Two hydrogen-bonded helical configurations of the polypeptide chain.* Proceedings of the National Academy of Sciences, 1951. **37**(4).

21. Lehninger, A., D. Nelson, and M. Cox, *Lehninger Principles of Biochemistry*. 2008: W. H. Freeman.

22. Berg, J.M., J.L. Tymoczko, and L. Stryer, *Biochemistry*. 2002: W.H. Freeman.

23. Monnier, J., et al., *Hydrocracking gas oils from synthetic crude with mixed pillared clay-alumina supported catalysts*, in *New Frontiers in Catalysis, Pt C*, L. Guczi, F. Solymosi, and P. Tetenyi, Editors. 1993, Elsevier Science Publ B V: Amsterdam. p. 1943-1946.

24. Allen, M.R. and T.F. Stocker, *Impact of delay in reducing carbon dioxide emissions.* Nature Climate Change, 2013. **4**.

25. Smith, K.M., *Single Electron Transfer Reactions in the Synthetic Organometallic Chemistry of First-Row Transition Metals.* Organometallics, 2005. **24**(5): p. 778-784.

26. Brown, N.J., et al., *From Organometallic Zinc and Copper Complexes to Highly Active Colloidal Catalysts for the Conversion of CO2 to Methanol.* ACS Catalysis, 2015. **5**(5): p. 2895-2902.

27. Dibenedetto, A., A. Angelini, and P. Stufano, *Use of carbon dioxide as feedstock for chemicals and fuels: homogeneous and heterogeneous catalysis.* Journal of Chemical Technology & Biotechnology, 2014. **89**(3).

28. Vilian, A.T.E., et al., *Immobilization of myoglobin on Au nanoparticle-decorated carbon nanotube/polytyramine composite as a mediator-free H2O2 and nitrite biosensor.* Scientific Reports, 2015. **5**.

29. Henard, C.A., et al., *Bioconversion of methane to lactate by an obligate methanotrophic bacterium.* Scientific Reports, 2016. **6**.

30. Wang, C., et al., *An enhanced chemiluminescence bioplatform by confining glucose oxidase in hollow calcium carbonate particles.* Scientific Reports, 2016. **6**.

31. Long, Y., et al., *Ultrasensitive Visual Detection of HIV DNA Biomarkers via a Multi-amplification Nanoplatform.* Scientific Reports, 2016. **6**.

32. Sharma, R., Y. Chisti, and U.C. Banerjee, *Production, purification, characterization, and applications of lipases.* Biotechnology Advances, 2001. **19**(8): p. 627-662.

33. van Tilbeurgh, H., et al., *Interfacial activation of the lipase–procolipase complex by mixed micelles revealed by X-ray crystallography.* Nature, 1993. **362**

34. Brzozowski, A.M., et al., *A model for interfacial activation in lipases from the structure of a fungal lipase-inhibitor complex.* Nature, 1991. **351**(6326): p. 491-494.

35. Brady, L., et al., *A serine protease triad forms the catalytic centre of a triacylglycerol lipase.* Nature, 1990. **343**: p. 767.

36. Brzozowski, A.M., et al., *Structure and molecular-model refinement of rhizomucor-miehei triacylglyceride lipase - a case-study of the use of simulated annealing in partial model refinement.* Acta crystallographica section b-structural science, 1992. **48**: p. 307-319.

37. Bankar, S.B., et al., *Glucose oxidase — An overview.* Biotechnology Advances, 2009. **27**(4): p. 489-501.

38. Wong, C.M., K.H. Wong, and X.D. Chen, *Glucose oxidase: natural occurrence, function, properties and industrial applications.* Applied Microbiology and Biotechnology, 2008. **78**(6): p. 927-938.

39. Wilson, R. and A.P.F. Turner, *Glucose oxidase: an ideal enzyme.* Biosensors and Bioelectronics, 1992. **7**(3): p. 165-185.

40. Kim, S.-H., et al., *Enzyme-based glucose biosensor using a dye couple system.* Dyes and Pigments, 2001. **49**(2): p. 103-108.

41. Lin, Y., et al., *Glucose Biosensors Based on Carbon Nanotube Nanoelectrode Ensembles.* Nano Letters, 2004. **4**(2): p. 191-195.

42. Wohlfahrt, G., et al., *1.8 and 1.9 A resolution structures of the Penicillium amagasakiense and Aspergillus niger glucose oxidases as a basis for modelling substrate complexes.* Acta Crystallogr D Biol Crystallogr, 1999. **55**(Pt 5): p. 969-77.

43. Brown, J.R., *Structure of bovine serum-albumin.* Federation Proceedings, 1975. **34**(3): p. 591-591.

44. Huang, B.X., H.Y. Kim, and C. Dass, *Probing three-dimensional structure of bovine serum albumin by chemical cross-linking and mass spectrometry.* Journal of the American Society for Mass Spectrometry, 2004. **15**(8): p. 1237-1247.

45. Engvall, E. and P. Perlmann, *Enzyme-linked immunosorbent assay, elisa .3. quantitation of specific antibodies by enzyme-labeled anti-immunoglobulin in antigen-coated tubes.* Journal of Immunology, 1972. **109**(1).

46. Majorek, K.A., et al., *Structural and immunologic characterization of bovine, horse, and rabbit serum albumins.* Molecular Immunology, 2012. **52**(3): p. 174-182.

47. LABROU, N.E. and D.J. RIGDEN, *Active-site characterization of Candida boidinii formate dehydrogenase.* Biochemical Journal, 2001. **354**(2): p. 455-463.

48. Schirwitz, K., A. Schmidt, and V.S. Lamzin, *High-resolution structures of formate dehydrogenase from Candida boidinii.* Protein Science : A Publication of the Protein Society, 2007. **16**(6): p. 1146-1156.

49. Luo, J., et al., *Cascade catalysis in membranes with enzyme immobilization for multienzymatic conversion of CO2 to methanol.* New Biotechnology, 2015. **32**(3): p. 319-327.

50. Liao, Y., et al., *Structure of formaldehyde dehydrogenase from Pseudomonas aeruginosa: the binary complex with the cofactor NAD(+).* Acta Crystallographica Section F, 2013. **69**(Pt 9): p. 967-972.

51. Tanaka, N., et al., *Crystal structure of formaldehyde dehydrogenase from Pseudomonas putida: the structural origin of the tightly bound cofactor in nicotinoprotein dehydrogenases.* J Mol Biol, 2002. **324**(3): p. 519-33.

52. Raj, S.B., S. Ramaswamy, and B.V. Plapp, *Yeast Alcohol Dehydrogenase Structure and Catalysis.* Biochemistry, 2014. **53**(36): p. 5791-5803.

53. Gustafsson, H., C. Thorn, and K. Holmberg, *A comparison of lipase and trypsin encapsulated in mesoporous materials with varying pore sizes and pH conditions.* Colloids Surf. B 2011. **87**(2): p. 464-71.

54. Hirayama, K., et al., *Rapid confirmation and revision of the primary structure of bovine serum albumin by ESIMS and Frit-FAB LC/MS.* Biochem Biophys Res Commun, 1990. **173**(2): p. 639-46.

55. Lei, C., et al., *Enzyme specific activity in functionalized nanoporous supports.* Nano.IOP, 2008. **19**(12).

56. Cazelles, R., et al., *Reduction of CO2 to methanol by a polyenzymatic system encapsulated in phospholipids-silica nanocapsules.* New Journal of Chemistry, 2013. **37**(11): p. 3721-3730.

57. Thorn, C., et al., *A method to measure pH inside mesoporous particles using protein-bound SNARF1 fluorescent probe.* Micropor Mesopor Mat, 2013. **165**: p. 240-246.

58. Zezzi do Valle Gomes, M. and A.E.C. Palmqvist, *Immobilization of formaldehyde dehydrogenase in tailored siliceous mesostructured cellular foams and evaluation of its activity for conversion of formate to formaldehyde.* Colloids and Surfaces B: Biointerfaces, 2018. **163**: p. 41-46.

59. Zezzi do Valle Gomes, M. and A.E.C. Palmqvist, *Influence of operating conditions and immobilization on activity of alcohol dehydrogenase for the conversion of formaldehyde to methanol.* New Journal of Chemistry, 2017.

60. Zoldak, G., et al., *Irreversible thermal denaturation of glucose oxidase from Aspergillus niger is the transition to the denatured state with residual structure.* J Biol Chem, 2004. **279**(46): p. 47601-9.

61. Kuchler, A., et al., *Enzymatic reactions in confined environments.* Nat Nanotechnol, 2016. **11**(5): p. 409-20.

62. Tran, D.N. and K.J. Balkus, *Perspective of Recent Progress in Immobilization of Enzymes.* ACS Catalysis, 2011. **1**(8): p. 956-968.

63. Mohamad, N.R., et al., *An overview of technologies for immobilization of enzymes and surface analysis techniques for immobilized enzymes.* Biotechnol Biotechnol Equip, 2015. **29**(2): p. 205-220.

64. Pierre, A.C., *The sol-gel encapsulation of enzymes.* Biocatalysis and Biotransformation, 2004. **22**(3): p. 145-170.

65. Sheldon, R.A., *Cross-linked enzyme aggregates (CLEAs): stable and recyclable biocatalysts.* Biochem Soc Trans, 2007. **35**(Pt 6): p. 1583-7.

66. Bunger, A.P., X. Zhang, and R.G. Jeffrey, *Parameters Affecting the Interaction Among Closely Spaced Hydraulic Fractures.* 2012.

67. Zhang, D.-H., L.-X. Yuwen, and L.-J. Peng, *Parameters Affecting the Performance of Immobilized Enzyme.* Journal of Chemistry, 2013. **2013**.

68. Zhou, Z. and M. Hartmann, *Progress in enzyme immobilization in ordered mesoporous materials and related applications.* Chem Soc Rev, 2013. **42**(9): p. 3894-912.

69. Fried, D.I., F.J. Brieler, and M. Fröba, *Designing Inorganic Porous Materials for Enzyme Adsorption and Applications in Biocatalysis.* ChemCatChem, 2013. **5**(4): p. 862-884.

70. Talbert, J.N. and J.M. Goddard, *Enzymes on material surfaces.* Colloids and Surfaces B: Biointerfaces, 2012. **93**: p. 8-19.

71. Slowing, II, et al., *Mesoporous silica nanoparticles as controlled release drug delivery and gene transfection carriers.* Advanced Drug Delivery Reviews, 2008. **60**(11): p. 1278-1288.

72. Rouquerol, J., et al., *Recommendations for the characterization of porous solids (Technical Report)*, in *Pure and Applied Chemistry*. 1994. p. 1739.

73. Rouquerol, J., et al., *Guidelines for the Characterization of Porous Solids*, in *Studies in Surface Science and Catalysis*, J. Rouquerol, et al., 1994, Elsevier. p. 1-9.

74. Hudson, S., J. Cooney, and E. Magner, *Proteins in mesoporous silicates.* Angew Chem Int Ed Engl, 2008. **47**(45): p. 8582-94.

75. Deng, W., et al., *Characterization of mesoporous alumina molecular sieves synthesized by nonionic templating.* Microporous and Mesoporous Materials, 2002. **52**(3): p. 169-177.

76. Antonelli, D.M. and J.Y. Ying, *Synthesis of hexagonally packed mesoporous TiO2 by a modified sol–gel method.* Angewandte Chemie International Edition in English, 1995. **34**(18): p. 2014-2017.

77. Hudson, S., et al., *Methodology for the immobilization of enzymes onto mesoporous materials.* Journal of Physical Chemistry B, 2005. **109**(41): p. 19496-19506.

78. Chen, B., et al., *Heated proteins are still active in a functionalized nanoporous support.* Small, 2013. **9**(13): p. 2228-32.

79. Chen, B., et al., *Probing mechanisms for enzymatic activity enhancement of organophosphorus hydrolase in functionalized mesoporous silica.* Biochem Biophys Res Commun, 2009. **390**(4): p. 1177-81.

80. Lee, C.H., T.S. Lin, and C.Y. Mou, *Mesoporous materials for encapsulating enzymes.* Nano Today, 2009. **4**(2): p. 165-179.

81. Giraldo, L.F., et al., *Mesoporous silica applications.* Macromolecular Symposia, 2007. **258**(1): p. 129-141.

82. Zhao, D.Y., et al., *Triblock copolymer syntheses of mesoporous silica with periodic 50 to 300 angstrom pores.* Science, 1998. **279**(5350): p. 548-552.

83. Schmidt-Winkel, P., et al., *Microemulsion templating of siliceous mesostructured cellular foams with well-defined ultralarge mesopores.* Chemistry of Materials, 2000. **12**(3): p. 686-696.

84. Lukens, W.W., et al., *Evaluating pore sizes in mesoporous materials: a simplified standard adsorption method and a simplified broekhoff–de boer method.* Langmuir, 1999. **15**(16): p. 5403-5409.

85. Brunauer, S., P.H. Emmett, and E. Teller, *Adsorption of gases in multimolecular layers.* Journal of the American Chemical Society, 1938. **60**(2): p. 309-319.

86. Barrett, E.P., L.G. Joyner, and P.P. Halenda, *The determination of pore volume and area distributions in porous substances. i. computations from nitrogen isotherms.* Journal of the American Chemical Society, 1951. **73**(1): p. 373-380.

87. Gustafsson, H., et al., *Immobilization of lipase from Mucor miehei and Rhizopus oryzae into mesoporous silica--the effect of varied particle size and morphology.* Colloids Surf. B 2012. **100**(0): p. 22-30.

88. Carlsson, N., et al., *Enzymes immobilized in mesoporous silica: a physical-chemical perspective.* Adv Colloid Interface Sci, 2014. **205**: p. 339-60.

89. Yamaguchi, A., et al., *Microviscosity of supercooled water confined within aminopropyl-modified mesoporous silica as studied by time-resolved fluorescence spectroscopy.* Analytical Sciences, 2012. **28**(11): p. 1065-1070.

90. Radhakrishna, M., et al., *Stability of proteins inside a hydrophobic cavity.* Langmuir, 2013. **29**(28): p. 8922-8.

91. Radhakrishna, M., et al., *Stability of proteins inside a hydrophobic cavity.* Langmuir, 2013. **29**(28): p. 8922-8928.

92. Díaz, J.F. and K.J. Balkus, *Enzyme immobilization in MCM-41 molecular sieve.* Journal of Molecular Catalysis B: Enzymatic, 1996. **2**(2): p. 115-126.

93. Yang, J., et al., *Adsorption of lysozyme and trypsin onto mesoporous silica materials*, in *Studies in Surface Science and Catalysis*, S.-E. Park, et al., Editors. 2003, Elsevier. p. 775-778.

94. Clemments, A.M., P. Botella, and C.C. Landry, *Spatial mapping of protein adsorption on mesoporous silica nanoparticles by stochastic optical reconstruction microscopy.* Journal of the American Chemical Society, 2017. **139**(11): p. 3978-3981.

95. Lei, C., et al., *Characterization of functionalized nanoporous supports for protein confinement.* Nanotechnology, 2006. **17**(22): p. 5531-8.

96. Sonesson, A.W., et al., *Adsorption and mobility of a lipase at a hydrophobic surface in the presence of surfactants.* Langmuir, 2006. **22**(13): p. 5810-5817.

97. Sonesson, A.W., et al., *Mobility of thermomyces lanuginosus lipase on a trimyristin substrate surface.* langmuir, 2007. **23**(5): p. 2706-2713.

98. Fan, J., et al., *Rapid and high-capacity immobilization of enzymes based on mesoporous silicas with controlled morphologies.* Chemical Communications, 2003(17): p. 2140-2141.

99. Fried, D.I., et al., *Influence of the hydrophilic-hydrophobic contrast of porous surfaces on the enzymatic performance.* Journal of Materials Chemistry B, 2015. **3**(11): p. 2341-2349.

100. Tu, J., et al., *Mesoporous silica nanoparticles with large pores for the encapsulation and release of proteins.* ACS Applied Materials & Interfaces, 2016. **8**(47): p. 32211-32219.

101. Fernandez-Lafuente, R., et al., *Immobilization of lipases by selective adsorption on hydrophobic supports.* Chemistry and Physics of Lipids, 1998. **93**(1–2): p. 185-197.

102. Manoel, E.A., et al., *Immobilization of lipases on hydrophobic supports involves the open form of the enzyme.* Enzyme and Microbial Technology, 2015. **71**(Supplement C): p. 53-57.

103. Heredia, K.L., et al., *Synthesis of heterotelechelic polymers for conjugation of two different proteins.* macromolecules, 2009. **42**(7): p. 2360-2367.

104. Grotzky, A., et al., *A fluorescently labeled dendronized polymer–enzyme conjugate carrying multiple copies of two different types of active enzymes.* Journal of the American Chemical Society, 2012. **134**(28): p. 11392-11395.

105. Jia, F., B. Narasimhan, and S. Mallapragada, *Materials-based strategies for multi-enzyme immobilization and co-localization: A review.* Biotechnology and Bioengineering, 2014. **111**(2): p. 209-222.

106. Matsuura, S.-i., et al., *Encapsulation of fluorescent proteins in folded-sheet mesoporous materials: Effect of pore size on energy-transfer efficiency.* Microporous and Mesoporous Materials, 2010. **131**(1–3): p. 245-251.

107. Yamaguchi, A., et al., *Acid-base equilibria inside amine-functionalized mesoporous silica.* Anal Chem, 2011. **83**(8): p. 2939-46.

108. Zhang, Y.H., *Substrate channeling and enzyme complexes for biotechnological applications.* Biotechnol Adv, 2011. **29**(6): p. 715-25.

109. Ricca, E., B. Brucher, and J.H. Schrittwieser, *Multi-enzymatic cascade reactions: overview and perspectives.* Advanced Synthesis & Catalysis, 2011. **353**(13): p. 2239-2262.

110. Obert, R. and B.C. Dave, *Enzymatic conversion of carbon dioxide to methanol: enhanced methanol production in silica sol−gel matrices.* Journal of the American Chemical Society, 1999. **121**(51): p. 12192-12193.

111. Sun, Q., et al., *Green and efficient conversion of co2 to methanol by biomimetic coimmobilization of three dehydrogenases in protamine-templated titania.* Industrial & Engineering Chemistry Research, 2009. **48**(9): p. 4210-4215.

112. Ruschig, U., et al., *CO2 reduction to formate by NADH catalysed by formate dehydrogenase from Pseudomonas oxalaticus.* Eur J Biochem, 1976. **70**(2): p. 325-30.

113. Yokoi, T., et al., *Periodic arrangement of silica nanospheres assisted by amino acids.* Journal of the American Chemical Society, 2006. **128**(42): p. 13664-13665.

114. Russo, P.A., et al., *Tailoring the surface chemistry of mesocellular foams for protein adsorption.* Colloids and Surfaces A: Physicochemical and Engineering Aspects, 2011. **386**(1): p. 25-35.

115. Bohr, N., *I. On the constitution of atoms and molecules.* Philosophical Magazine Series 6, 1913. **26**(151): p. 1-25.

116. Broglie, L.d., *XXXV. A tentative theory of light quanta.* Philosophical Magazine Series 6, 1924. **47**(278): p. 446-458.

117. Hecht, E., *Optics (4th Edition)*. 2001: Addison Wesley.

118. Kasha, M., *Characterization of electronic transitions in complex molecules.* Discussions of the Faraday Society, 1950. **9**(0): p. 14-19.

119. Swinehart, D.F., *The Beer-Lambert law.* Journal of Chemical Education, 1962. **39**(7): p. 333.

120. Gill, S.C. and P.H. von Hippel, *Calculation of protein extinction coefficients from amino acid sequence data.* Anal Biochem, 1989. **182**(2): p. 319-26.

121. Pace, C.N., et al., *How to measure and predict the molar absorption coefficient of a protein.* Protein Sci, 1995. **4**(11): p. 2411-23.

122. Bradford, M.M., *A rapid and sensitive method for the quantitation of microgram quantities of protein utilizing the principle of protein-dye binding.* Anal Biochem, 1976. **72**: p. 248-54.

123. Lowry, O.H., et al., *Protein measurement with the Folin phenol reagent.* J Biol Chem, 1951. **193**(1): p. 265-75.

124. Qiu, H.J., et al., *Immobilization of laccase on nanoporous gold: comparative studies on the immobilization strategies and the particle size effects.* Journal of Physical Chemistry C, 2009. **113**(6): p. 2521-2525.

125. Zheng, Y., et al., *Mussel-inspired surface capping and pore filling to confer mesoporous silica with high loading and enhanced stability of enzyme.* Microporous and Mesoporous Materials, 2012. **152**: p. 122-127.

126. Haynes, W.M. and D.R. Lide, *CRC handbook of chemistry and physics : a ready-reference book of chemical and physical data.* 2011, Boca Raton, Fla.: CRC Press.

127. Lakowicz, J.R., et al., *Rotational freedom of tryptophan residues in proteins and peptides.* ACS. Biochem, 1983. **22**(8): p. 1741-52.

128. Soleillet, P., *Sur les parametres caractérisant la polarisation partielle de la lumiere dans les phénomenes de fluorescence*. Ann.Phys.Biol.Med. 1929: Ann.Phys.Biol.Med.

129. Roy, R., S. Hohng, and T. Ha, *A practical guide to single-molecule FRET.* Nature Methods, 2008. **5**: p. 507.

130. Ishikawa-Ankerhold, H.C., R. Ankerhold, and G.P.C. Drummen, *Advanced fluorescence microscopy techniques—FRAP, FLIP, FLAP, FRET and FLIM.* Molecules, 2012. **17**(4): p. 4047.

131. Clegg, R.M., *Fluorescence resonance energy transfer.* Current Opinion in Biotechnology, 1995. **6**(1): p. 103-110.

132. Stryer, L. and R.P. Haugland, *Energy transfer: a spectroscopic ruler.* Proceedings of the National Academy of Sciences of the United States of America, 1967. **58**(2): p. 719-726.

133. Förster, T., *Zwischenmolekulare energiewanderung und fluoreszenz.* Annalen der Physik, 1948. **437**(1-2): p. 55-75.

134. Noble, J.E. and M.J.A. Bailey, *Quantitation of Protein*, in *Guide to Protein Purification, Second Edition*, R.R. Burgess and M.P. Deutscher, Editors. 2009, Elsevier Academic Press Inc: San Diego. p. 73-95.

135. Sapan, C.V., R.L. Lundblad, and N.C. Price, *Colorimetric protein assay techniques.* Biotechnology and Applied Biochemistry, 1999. **29**: p. 99-108.

136. Zor, T. and Z. Seliger, *Linearization of the bradford protein assay increases its sensitivity: Theoretical and experimental studies.* Analytical Biochemistry, 1996. **236**(2): p. 302-308.

137. Keppler, A., et al., *A general method for the covalent labeling of fusion proteins with small molecules in vivo.* Nature Biotechnology, 2003. **21**(1): p. 86-89.

138. Beatty, K.E., et al., *Selective dye-labeling of newly synthesized proteins in bacterial cells.* Journal of the American Chemical Society, 2005. **127**(41): p. 14150-14151.

139. Nakazumi, H., et al., *Red luminescent squarylium dyes for noncovalent HSA labeling.* Chemistry Letters, 2003. **32**(9): p. 804-805.

140. Moody, E.D., P.J. Viskari, and C.L. Colyer, *Non-covalent labeling of human serum albumin with indocyanine green: a study by capillary electrophoresis with diode laser-induced fluorescence detection.* Journal of Chromatography B, 1999. **729**(1-2): p. 55-64.

141. Sheehan, J.C. and G.P. Hess, *A new method of forming peptide bonds.* Journal of the American Chemical Society, 1955. **77**(4): p. 1067-1068.

142. Nordén, B., *Applications of linear Dichroism Spectroscopy.* Applied Spectroscopy Reviews, 1978. **14**(2): p. 157-248.

143. Anthis, N.J. and G.M. Clore, *Sequence-specific determination of protein and peptide concentrations by absorbance at 205 nm.* Protein Science : A Publication of the Protein Society, 2013. **22**(6): p. 851-858.

144. Stoscheck, C.M., *[6] Quantitation of protein*, in *Methods in Enzymology*, M.P. Deutscher, Editor. 1990, Academic Press. p. 50-68.

145. Goldfarb, A.R., *Absorption spectrum of the peptide bond. II. Influence of chain length.* J Biol Chem, 1953. **201**(1): p. 317-20.

146. Warburg, O. and W. Christian, *Insulation and Crystalisation of the Fermenting Process of Enolase.* Biochem Z, 1942. **310**(6): p. 384 - 421.

147. *Measuring protein concentration in the presence of nucleic acids by a280/a260: the method of warburg and christian.* CSH Protoc, 2006. **2006**(1).

148. Nishimoto, E., et al., *Internal motion of lysozyme studied by time-resolved fluorescence depolarization of tryptophan residues.* ACS Biochem, 1998. **37**(16): p. 5599-607.

149. Lakowicz, J.R., G. Freshwater, and G. Weber, *Nanosecond segmental mobilities of tryptophan residues in proteins observed by lifetime-resolved fluorescence anisotropies.* Biophys J, 1980. **32**(1): p. 591-601.

150. Graupner, M., et al., *Molecular dynamics of microbial lipases as determined from their intrinsic tryptophan fluorescence.* Biophys. J . 1999. **77**(1): p. 493-504.

151. Nishimoto, E., et al., *Internal motion of lysozyme studied by time-resolved fluorescence depolarization of tryptophan residues.* Biochemistry, 1998. **37**(16): p. 5599-5607.

152. Ruggiero, A.J, et al., *Subpicosecond fluorescence anisotropy studies of tryptophan in water.* J. Am. Chem. Soc., 1990. **112**.

153. Weber, G. and D.J. Laurence, *Fluorescent indicators of adsorption in aqueous solution and on the solid phase.* Biochem J, 1954. **56**(325th Meeting): p. xxxi.

154. Zubkov, M.V., et al., *Determination of total protein content of bacterial cells by SYPRO staining and flow cytometry.* Appl Environ Microbiol, 1999. **65**(7): p. 3251-7.

155. Berggren, K., et al., *A luminescent ruthenium complex for ultrasensitive detection of proteins immobilized on membrane supports.* Anal Biochem, 1999. **276**(2): p. 129-43.

156. Panda, D., S. Khatua, and A. Datta, *Enhanced fluorescence of epicocconone in surfactant assemblies as a consequence of depth-dependent microviscosity.* Journal of Physical Chemistry B, 2007. **111**(7): p. 1648-1656.

157. Burai, T.N., D. Panda, and A. Datta, *Fluorescence enhancement of epicocconone in its complexes with cyclodextrins.* Chemical Physics Letters, 2008. **455**(1-3): p. 42-46.

158. Coghlan, D.R., J.A. Mackintosh, and P. Karuso, *Mechanism of reversible fluorescent staining of protein with epicocconone.* Organic Letters, 2005. **7**(12): p. 2401-2404.

159. Bell, P.J.L. and P. Karuso, *Epicocconone, A novel fluorescent compound from the fungus epicoccum nigrum.* Journal of the American Chemical Society, 2003. **125**(31): p. 9304-9305.

160. Schapman, D., et al., *Characterization of fluorescent synthetic epicocconone-based dye through advanced light microscopies for live cell imaging applications.* Dyes and Pigments, 2017. **141**: p. 394-405.

161. Haidekker, M.A. and E.A. Theodorakis, *Environment-sensitive behavior of fluorescent molecular rotors.* Journal of Biological Engineering, 2010. **4**: p. 11-11.

162. Hohng, S., C. Joo, and T. Ha, *Single-molecule three-color FRET.* Biophysical Journal, 2004. **87**(2): p. 1328-1337.

163. Lucocq, J., *Quantitation of gold labeling and estimation of labeling efficiency with a stereological counting method.* Journal of Histochemistry & Cytochemistry, 1992. **40**(12): p. 1929-1936.

164. Thorn, C., H. Gustafsson, and L. Olsson, *QCM-D as a method for monitoring enzyme immobilization in mesoporous silica particles.* Microporous Mesoporous Mater., 2013. **176**: p. 71-77.

165. Tsien, R.Y., *The green fluorescent protein.* Annu Rev Biochem, 1998. **67**: p. 509-44.

166. Chalfie, M., *Green fluorescent protein.* Photochemistry and Photobiology, 1995. **62**(4): p. 651-656.

167. Gustafsson, H., et al., *Co-immobilization of enzymes with the help of a dendronized polymer and mesoporous silica nanoparticles.* Journal of Materials Chemistry B, 2015. **3**(30): p. 6174-6184.

168. Strutt, J.W., *LVIII. On the scattering of light by small particles.* Philosophical Magazine Series 4, 1871. **41**(275): p. 447-454.

169. Mie, G., *Beiträge zur Optik trüber Medien, speziell kolloidaler Metallösungen.* Annalen der Physik, 1908. **330**(3): p. 377-445.

170. Grunberg, B., et al., *Hydrogen bonding of water confined in mesoporous silica MCM-41 and SBA-15 studied by 1H solid-state NMR.* ChemPubSocEurope, 2004. **10**(22): p. 5689-96.

171. Shirono, K. and H. Daiguji, *Molecular simulation of the phase behavior of water confined in silica nanopores.* Journal of Physical Chemistry C, 2007. **111**(22): p. 7938-7946.

172. Damjanovich, S., B. Somogyi, and G.R. Welch, *Protein fluctuation and enzyme activity.* Journal of Theoretical Biology, 1983. **105**(1): p. 25-33.

173. Thorn, C., H. Gustafsson, and L. Olsson, *Immobilization of feruloyl esterases in mesoporous materials leads to improved transesterification yield.* J. Mol. Catal. B: Enzym., 2011. **72**(1-2): p. 57-64.

174. Jameson, D.M. and J.A. Ross, *Fluorescence polarization/anisotropy in diagnostics and imaging.* Chem Rev, 2010. **110**(5): p. 2685-708.

175. Tros, M., et al., *Picosecond orientational dynamics of water in living cells.* Nature Communications, 2017. **8**(1): p. 904.

176. Fernandes, D.D., et al., *Characterization of fluorescein arsenical hairpin (FlAsH) as a probe for single-molecule fluorescence spectroscopy.* Scientific Reports, 2017. **7**(1): p. 13063.

177. Fernandes, C.A.H., et al., *Biophysical studies suggest a new structural arrangement of crotoxin and provide insights into its toxic mechanism.* Scientific Reports, 2017. **7**: p. 43885.

178. Vinegoni, C., et al., *Measurement of drug-target engagement in live cells by two-photon fluorescence anisotropy imaging.* Nature Protocols, 2017. **12**: p. 1472.

179. Nabavi Zadeh, P.S., et al., *A fluorescence spectroscopy assay for real-time monitoring of enzyme immobilization into mesoporous silica particles.* Anal Biochem, 2015. **476**: p. 51-8.

180. Roosen-Runge, F., et al., *Protein self-diffusion in crowded solutions.* Proc Natl Acad Sci U S A, 2011. **108**(29): p. 11815-20.

181. Jones, R.B., *Rotational diffusion of colloidal particles near confining walls.* J Chem Phys, 2005. **123**(16): p. 164705.

182. Czeslik, C., et al., *Reorientational dynamics of enzymes adsorbed on quartz: a temperature-dependent time-resolved TIRF anisotropy study.* Biophys J, 2003. **84**(4): p. 2533-41.

183. Kuimova, M.K., et al., *Molecular rotor measures viscosity of live cells via fluorescence lifetime imaging.* Journal of the American Chemical Society, 2008. **130**(21): p. 6672-6673.

184. Haidekker, M.A. and E.A. Theodorakis, *Molecular rotors-fluorescent biosensors for viscosity and flow.* Organic & Biomolecular Chemistry, 2007. **5**(11): p. 1669-1678.

185. Lerner, E., et al., *A quantitative theoretical framework for protein-induced fluorescence enhancement–Förster-type resonance energy transfer (PIFE-FRET).* The Journal of Physical Chemistry B, 2016. **120**(26): p. 6401-6410.

186. Sanborn, M.E., et al., *Fluorescence properties and photophysics of the sulfoindocyanine cy3 linked covalently to DNA.* The Journal of Physical Chemistry B, 2007. **111**(37): p. 11064-11074.

187. Kubánková, M., et al., *Probing supramolecular protein assembly using covalently attached fluorescent molecular rotors.* Biomaterials, 2017. **139**(Supplement C): p. 195-201.

188. Luby-Phelps, K., et al., *A novel fluorescence ratiometric method confirms the low solvent viscosity of the cytoplasm.* Biophysical Journal, 1993. **65**(1): p. 236-242.

189. Kuimova, M.K., et al., *Imaging intracellular viscosity of a single cell during photoinduced cell death.* Nat Chem, 2009. **1**(1): p. 69-73.

190. Haidekker, M.A., et al., *A ratiometric fluorescent viscosity sensor.* Journal of the American Chemical Society, 2006. **128**(2): p. 398-399.

191. Sabanayagam, C.R., J.S. Eid, and A. Meller, *Long time scale blinking kinetics of cyanine fluorophores conjugated to DNA and its effect on Förster resonance energy transfer.* The Journal of Chemical Physics, 2005. **123**(22): p. 224708.

192. Boel, E., et al., *Rhizomucor miehei triglyceride lipase is synthesized as a precursor.* Lipids, 1988. **23**(7): p. 701-706.

193. Giudicelli, H. and J. Boyer, *Effects of glycerol on human adipose tissue triglyceride lipase activity.* J Lipid Res, 1973. **14**(5): p. 592-5.

194. Ou, W., et al., *Effects of glycerol in the refolding and unfolding of creatine kinase.* Tsinghua Science and Technology, 2002. **7**(4): p. 352-362.

195. Rariy, R.V. and A.M. Klibanov, *Correct protein folding in glycerol.* Proceedings of the National Academy of Sciences, 1997. **94**(25): p. 13520-13523.

196. OBERSTAK, J.B.S.A.H.E., *Viscosity of glycerol and its aqueous solutions* Industrial and Engineering Chemistry 1951. **43**(9): p. 2117-2120.

197. Timmermans, J., *The physico-chemical constants of binary systems in concentrated solutions. .* Interscience, 1960. **4**.

198. Nabavi Zadeh, P.S. and B. Åkerman, *Immobilization of enzymes in mesoporous silica particles: protein concentration and rotational mobility in the pores.* The Journal of Physical Chemistry B, 2017. **121**(12): p. 2575-2583.

199. Fukatsu, Y., et al., *Temperature and size effects on structural and dynamical properties of water confined in 1 - 10 nm-scale pores using proton nmr spectroscopy.* Analytical sciences : the international journal of the Japan Society for Analytical Chemistry, 2017. **33**(8): p. 903-909.

200. Li, L., et al., *Viscosity and Wetting Property of Water Confined in Extended Nanospace Simultaneously Measured from Highly-Pressurized Meniscus Motion.* The Journal of Physical Chemistry Letters, 2012. **3**(17): p. 2447-2452.

201. Takahara, S., et al., *Neutron Scattering Study on Dynamics of Water Molecules in MCM-41. 2. Determination of Translational Diffusion Coefficient.* The Journal of Physical Chemistry B, 2005. **109**(22): p. 11231-11239.

202. Takahara, S., et al., *Neutron Scattering Study on Dynamics of Water Molecules in MCM-41.* The Journal of Physical Chemistry B, 1999. **103**(28): p. 5814-5819.

203. Faraone, A., et al., *Translational and rotational dynamics of water in mesoporous silica materials: MCM-41-S and MCM-48-S.* The Journal of Chemical Physics, 2003. **119**(7): p. 3963-3971.

204. Romero-Vargas Castrillón, S., et al., *Effect of Surface Polarity on the Structure and Dynamics of Water in Nanoscale Confinement.* The Journal of Physical Chemistry B, 2009. **113**(5): p. 1438-1446.

205. Milischuk, A.A. and B.M. Ladanyi, *Structure and dynamics of water confined in silica nanopores.* The Journal of Chemical Physics, 2011. **135**(17): p. 174709.

206. Scodinu, A. and J.T. Fourkas, *Comparison of the Orientational Dynamics of Water Confined in Hydrophobic and Hydrophilic Nanopores.* The Journal of Physical Chemistry B, 2002. **106**(40): p. 10292-10295.

207. Kim, K.K., et al., *The crystal structure of a triacylglycerol lipase from Pseudomonas cepacia reveals a highly open conformation in the absence of a bound inhibitor.* Structure, 1997. **5**(2): p. 173-185.

208. Cygler, M. and J.D. Schrag, *Structure and conformational flexibility of Candida rugosa lipase1.* Biochimica et Biophysica Acta (BBA) - Molecular and Cell Biology of Lipids, 1999. **1441**(2–3): p. 205-214.

209. Carlsson, N., et al., *Diamond Cubic Phase of Monoolein and Water as an Amphiphilic Matrix for Electrophoresis of Oligonucleotides.* The Journal of Physical Chemistry B, 2005. **109**(39): p. 18628-18636.

210. Guo, Q., et al., *Structural and Kinetic Studies of Formate Dehydrogenase from Candida boidinii.* Biochemistry, 2016. **55**(19): p. 2760-2771.

211. Sun, Y., et al., *Bioinspired optofluidic FRET lasers via DNA scaffolds.* Proceedings of the National Academy of Sciences, 2010. **107**(37): p. 16039-16042.

212. Zadeh, P.S.N., et al., *Measuring viscosity iside mesoporous silica using protein bound molecular rotor probe.* Submitted for publication, 2018.

213. Berney, C. and G. Danuser, *FRET or No FRET: A Quantitative Comparison.* Biophysical Journal, 2003. **84**(6): p. 3992-4010.

214. Luo, J.Q., et al., *Cascade catalysis in membranes with enzyme immobilization for multi-enzymatic conversion of CO2 to methanol.* New Biotechnology, 2015. **32**(3): p. 319-327.

215. Wheeldon, I., et al., *Substrate channelling as an approach to cascade reactions.* Nature Chemistry, 2016. **8**(4): p. 299-309.

216. Secundo, F., G. Barletta, and G. Mazzola, *Role of methoxypolyethylene glycol on the hydration, activity, conformation and dynamic properties of a lipase in a dry film.* Biotechnology and Bioengineering, 2008. **101**(2): p. 255-262.

217. KONG, J. and S. YU, *Fourier Transform Infrared Spectroscopic Analysis of Protein Secondary Structures.* Acta Biochimica et Biophysica Sinica, 2007. **39**(8): p. 549-559.

218. Lei, L., et al., *Study on immobilization of lipase onto magnetic microspheres with epoxy groups.* Journal of Magnetism and Magnetic Materials, 2009. **321**(4): p. 252-258.

219. Lee, D.-G., et al., *Immobilization of lipase on hydrophobic nano-sized magnetite particles.* Journal of Molecular Catalysis B: Enzymatic, 2009. **57**(1): p. 62-66.

220. Suh, C.W., et al., *Analysis of protein adsorption characteristics to nano-pore silica particles by using confocal laser scanning microscopy.* J Biotechnol, 2004. **112**(3): p. 267-77.

221. Piras, M., et al., *3D vision of human lysozyme adsorbed onto a SBA-15 nanostructured matrix.* Chemical Communications, 2011. **47**(26): p. 7338-7340.

222. Herculano-Houzel, S., et al., *How to count cells: the advantages and disadvantages of the isotropic fractionator compared with stereology.* Cell and tissue research, 2015. **360**(1): p. 29-42.

223. von Bartheld, C.S. and F.S. Wouters, *Quantitative Techniques for Imaging Cells and Tissues.* Cell and tissue research, 2015. **360**(1): p. 1-4.

224. Lucocq, J., *Quantitation of gold labelling and antigens in immunolabelled ultrathin sections.* Journal of Anatomy, 1994. **184**(Pt 1): p. 1-13.